Biomimetic Micro/nano-Structured Surfaces: A Potential Tool for Tuning of Adhesion and Friction

by

Hamed Shahsavan

A thesis
presented to the University of Waterloo
in fulfillment of the
thesis requirement for the degree of
Master of Applied Science
in
Chemical Engineering - Nanotechnology

Waterloo, Ontario, Canada, 2012

AUTHOR'S DECLARATION

I hereby declare that I am the sole author of this thesis. This is a true copy of the thesis, including any required final revisions, as accepted by my examiners.

I understand that my thesis may be made electronically available to the public.

Abstract

Effects of biomimetic micro-patterning of polymeric materials on their interfacial properties were studied experimentally. Micropillars of PDMS and SU-8 epoxy were fabricated through soft lithography and UV lithography techniques, respectively. PDMS pillars were topped by thin terminal films of the same material through dipping method with different thicknesses and viscosities. Adhesion and frictional properties of biomimetic microstructures were examined in two modes of contact, i.e. laid and conformal contact. In the first mode of contact, i.e. laid contact, the contact between adhesive and adherent is laid on top of the micro-protrusions or is in contact with side wall of micropillars. Adhesion properties of the smooth and patterned PDMS were characterized through micro-indentation test. Moreover, the friction properties of the smooth PDMS sample and PDMS micropillars with different aspect ratios were examined in unidirectional friction testing. JKR theory of continuum contact mechanics was utilized to interpret the obtained data. To study the effect of second mode of contact, peeling behaviour of a conformal contact between solidified liquid PDMS and SU-8 micropillars was monitored. Kendall's model of elastic peeling was used to interpret the peeling data. It was found that patterning of the materials would decrease the real area of contact and accordingly adhesion and friction to the mating surface. Termination of the micropillars with a thin layer of the same material result in increment of adhesion as reduction of the real contact area could be compensated and the compliance of the near surface increases. Elastic energy dissipation as a result of enhanced compliance and crack trapping and crack propagation instabilities are the main reasons behind increment of adhesion of thin film terminated structures. Viscoelasticity of the terminal thin film remarkably increased the adhesion as a result of coupling mentioned mechanisms and viscoelastic loss on the surface. Decline of the overall friction could be tailored through use of different aspect ratios. Higher aspect ratios pillars show higher friction comparing to lower aspect ratio pillars. 550 folds enhancement of adhesion was observed for peeling of the PDMS tape from rigid micropillars with aspect ratio ranging from 0 to 6. It is concluded that for the lower aspect ratio micropillars, the elastic energy dissipation is playing the key role in adhesion enhancement. This role shifts toward side-wall friction during separation by increase in aspect ratio. These all give in hand a versatile tool to control and fine tune the interfacial properties of materials, whether they are concerned with adhesion or friction.

Acknowledgements

I would like to wholeheartedly express my gratitude and sincere to my research supervisor, Professor Boxin Zhao, for his persistent inspiration, guidance, and support. In one hand, his honest, kind, and flexible personality allowed me to work without any tension and learn without constraint. On the other hand, his disciplined working style and elucidatory advises taught me work attitude. I am indebted to him as he gave me opportunity to work on a multidisciplinary and cutting-edge research project. By this, I benefited from communication with modern society of science and technology, which is crucial for my career endeavors.

I would like to thank Dr. Amir. Ahmad Saghiri from Zeiss Co. , my dear cousin, for his constructive guidance in fabrication of SU-8 microstructures. More importantly, I am delighted to have him in my side whenever I need someone to consult with.

I am very grateful to Professor Bo Cui, Electrical and Computer Engineering Department at University of Waterloo, for his productive discussions on different nano- and microfabrication techniques. He familiarized me with a great deal of new concepts in fabrication and solid state devices whether it was in our consulting hours or his class.

I thank Professor Michael Tam, Chemical Engineering Department at University of Waterloo as one of the external evaluators of my thesis.

My special thanks and sincere is for two best friends of mine. A “kind brother” is the only word could describe Madjid to me. Not only was he a supporting brother, but also a teacher during these two years.

I would like to thank my lab mates for their help, useful suggestions, and cheer up during the period I was working with them.

Dedication

There exist no words or expressions being capable of portraying beauty of my parents' love, patience, and care. They mean everything to me. Thanks to my beloved sister Sareh. No one could be this much sweet and nice as she is. Thanks to my twin brother Hamid as he is helping mom and dad in my absence. And I thank Hossein, my brother in law, for his presence and care.

Table of Contents

List of Figures

List of Tables

Chapter 1
Introduction

All atoms adhere with considerable force [1]. However, how could we consider a world in which all components are stuck together and how could we justify free motions frequently observed in our daily life? Although the adhesion is a result of the inherent attractive nature of molecules or atoms on the surface of the materials, it does not convey exactly the same meaning as intermolecular or inter-atomic forces does. In fact, intermolecular surface forces are forces that are always present when two bodies are brought together, while adhesion or adhesive forces are those hold two bodies together [2]. Intermolecular forces can be the source of adhesion of the materials if two mating surfaces are ideally in contact. That is, both of them should be atomically smooth, extremely rigid, and chemically homogenous on the surface. However, non ideality is always present in practice and hinders the perfect intermolecular interaction between surfaces.

In addition to the atomic and intermolecular approach to adhesion, there are other approaches from different disciplines concerning with adhesion. Contact mechanics and fracture mechanics are two major fields addressing the events taking place in attachment and detachment of materials. As a result, effect of several mechanical and physical parameters on strength and toughness of an interface have been investigated. These trials, together with the principles of intermolecular interactions, have led scientists and industrialists to fine tune the adhesive, wetting, and frictional properties of different surfaces in disparate applications.

Conventional adhesives usually are in liquid or liquid like state of material and most often bond to the mating materials through two methods: 1) they make chemical bonds hard to break ; 2) or they take advantage of viscoelastic energy losses during the detachment. Liquid like adhesives are capable of making intimate contact with the mating surfaces, and usually are functional after solidification. The mechanisms of action for such adhesives have been discussed later in this manuscript. Further, liquid like materials such as viscoelastic materials with very low modulus of elasticity are usually employed in cases where the liquid like adhesives could not be used. Such viscoelastic materials also could be spread in shape of very thin films on the surface of other rigid elastic materials. Pressure Sensitive Adhesives (PSA) are the main example of this category of adhesives.

Conventional chemical and wet adhesives suffer from several disadvantages, such as proneness to absorb contamination, cohesive failure in detachment, weak functionality in harsh environments, and bio-incompatibility. Therefore, their use is inherently impeded in such applications that require repeatability, functionality in harsh environments, or compatibility to bio-interfaces.

Nowadays, interdisciplinary approach to resolve technological challenges is a common practice. Further, as technology gears toward miniaturized structures and applications, nanotechnology has been recognized as an effective interdisciplinary tool to tackle these challenges. For example, the emerging field of biomimetic adhesives has been introduced to resolve the ongoing issues for the functionality of adhesives. Learnt from the nature, scientists have been trying to mimic the effective interfacial properties of biological systems in synthetic structures. These trials address both adhesive and anti-adhesive properties found in biological systems.

The objective of this thesis is to introduce and experimentally examine the potential role of biomimetic structures in fine-tuning of the interfacial properties of materials, whether they are related to adhesion, friction, and wetting. The thesis is composed of 7 chapters. General information about the field and current status and demands is highlighted in chapter 1 as introduction. In chapter 2, we recapitalize the basic principles of adhesion and wetting for common smooth surfaces. In chapter 3, interfacial properties of the biological systems will be discussed and gecko adhesive system is introduced as the most promising prototype to be mimicked. In the following, fabrication methods of biomimetic synthetic structures would be elaborated. In chapter 4, we have introduced our recent results in fabrication of a new class of biomimetic adhesive utilizing principles of both biomimetic dry adhesives and conventional viscoelastic adhesives. A new approach to exploit frictional properties of the biomimetic microstructures have been experimentally explained in chapter 5. In chapter 6, a novel class of adhesives has been developed by introduction of conformal contact through biomimetic microstructured surfaces. Finally, the conclusions and future trend in the field has been discussed in chapter 7. The content in chapter 2 and 3 has been reformatted in a new manuscript to be published as a feature article in Macromolecular and materials Engineering journal. Chapter 4 and 5 are research chapters formatted to two journal manuscripts for publication and they are going to be submitted soon. Chapter 6 is a research chapter which has been already published in Langmuir and cited as reference [82] in this thesis.

Chapter 2
Conventional understanding of adhesion and wetting

In this section we recapitalize the principles behind two concepts of intermolecular forces and adhesive forces between liquid/solid and solid/solid pair contacts. The common mechanisms resulting in the disparity between intermolecular forces and adhesive forces are briefly discussed in terms of ideal and non-ideal adhesion. The non-ideality of the contact between two mating materials , i.e. surface roughness, surface compliance, and chemical heterogeneity, would be elaborated as a versatile tool for tuning and understanding of the interfacial phenomena, such as adhesion, wetting, and friction.

2.1 Thermodynamic and intermolecular principles of adhesion and wetting

The free energy change required for creation or destruction of a unit area of surface of a material is referred to surface free energy of that material, denoted by $\boldsymbol{\gamma_i = \frac{\partial E}{\partial A}}$. Unit of this parameter is J.m^{-2}. For liquids, this parameter commonly is called surface tension and denoted by tension per unit length of the liquid N.m^{-1}, which is dimensionally same as the surface free energy. Surface tension of the liquids determines their thermophysical properties, such as boiling point. The term interfacial energy, $\boldsymbol{\gamma_{12}}$, is defined by the free energy change of the whole system per unit area increment of the interface when two materials (1 and 2) are brought into contact. Consequently, the work required to separate an interface and bring two new surfaces to an infinite separation distance in vacuum is called the *work of adhesion*, which has been firstly expressed by Dupre equation [3], [4]:

$$-\Delta \boldsymbol{E_{12}^A} = \boldsymbol{W_{12}^A} = \boldsymbol{\gamma_1 + \gamma_2 - \gamma_{12}} \qquad (\mathbf{2.1})$$

If creation of two new surfaces is the result of rupture of a single material to two parts, the work done is called *work of cohesion* as it shown below:

$$-\Delta \boldsymbol{E_{11}^C} = \boldsymbol{W_{11}^C} = \boldsymbol{2\gamma_1} \qquad (\mathbf{2.2})$$

Historically, it was Young that postulated the notion of energy balance in settling of a liquid droplet on solid surfaces (figure 2-1).

Figure 2-1: Schematic understanding of work of adhesion and cohesion

However, the vector form of the energy balance was developed by Bangham and Razouk [5] into the formula we write today as

$$\boldsymbol{\gamma_s = \gamma_{sl} + \gamma_l \, cos\theta} \qquad (\mathbf{2.3}),$$

where $\boldsymbol{\gamma_s}$and $\boldsymbol{\gamma_l}$are free energy of the solid and liquid in vacuum, respectively; and $\boldsymbol{\gamma_{sl}}$ is interfacial energy of the solid/liquid interface (figure 2-2). If the medium of the experiment is not vacuum the notation of the surface energy would change to $\boldsymbol{\gamma_{sv}}$and $\boldsymbol{\gamma_{lv}}$where $\boldsymbol{v}$ indicates the saturated vapour of the liquid as the medium of experiment.

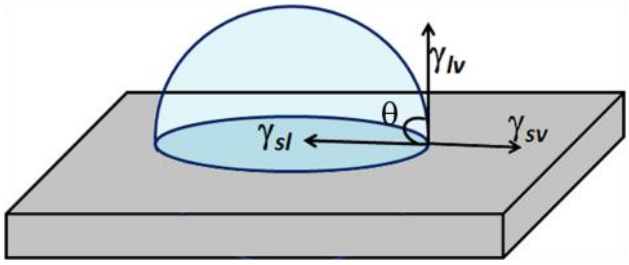

Figure 2-2: schematic understanding of three phase contact line for a liquid drop on a solid surface in vapor medium

The vertical projection of the liquid surface tension ($\boldsymbol{\gamma_{lv}\, sin\theta}$) generates the strain field on the solid below the three phase line, validating the vector form of force and energy balance. By substituting the equation 3 into equation 1 the Young-Dupre equation could be written as

$$\boldsymbol{W_{lv}^{A} = \gamma_{lv}(1 + cos\theta)} \qquad (\mathbf{2.4}).$$

Therefore, the work of adhesion between a liquid droplet and solid could be measured if contact angle and surface tension of the liquid are determined. Equations 1 to 4 are based upon the assumption of

perfect smoothness, extreme rigidity, and chemically homogeneity of the solid surface. When these conditions are met, there should be a single, unique contact angle [3], [6]. In reality, it is almost impossible to have perfect atomic smooth surfaces, which causes non-ideal contacts between materials. Interfacial events would also fail to be thermodynamically reversible as the deformation of soft solid materials might cause unfavorable energy dissipation. This is why in the case of liquid/liquid interactions the thermodynamic work of adhesion can be deemed to be reversible. In fact, reorientation of the liquid molecules into a new form does not necessitate considerable energy dissipation [6]. Finally, chemical homogeneity of the solid surface molecules ensures the equal contribution of the pair potentials in creation of a new interface, and accordingly reshaping the droplet on the solid.

Retaining the same conditions of ideal contacts, solid/solid interfaces must be constructed under perfect conditions far from any mechanism causing dissipation of energy. The macroscopic extension of Derjaguin approximation (eqn. 5) for the contact between two microscopic spherical particles could be assisted to quantify the work of adhesion between two ideally rigid (incompressible), smooth, and homogeneous spherical solids [6].

$$\boldsymbol{F = 2\pi\left(\frac{R_1 R_2}{R_1 + R_2}\right) W_{12}} \qquad (\mathbf{2.5})$$

$$\boldsymbol{F = 2\pi R \gamma_s} \qquad (\mathbf{2.6}),$$

where $\boldsymbol{R_1}$ and $\boldsymbol{R_2}$ are the radii of the solids brought to contact. Equation 6, therefore, determines the interaction between two identical solid spheres in vacuum. This equation is also valid under condition of ideal contact between ideal solids. However, omnipresent nature of elastic deformation and sometimes presence of dissipative mechanisms must be taken into account to have a realistic view to solid/solid interactions. To do so, the elastic confined continuum mechanical theories such as Johnson-Kendall-Roberts (JKR), Hertz, and Derjaguin-Muller-Toporov (DMT) will be discussed with more detail later in this chapter.

2.2 Adhesion mechanisms and importance of wetting

An “interface” is referred to the dividing line between two materials in contact. The main indicator of the interface is an abrupt and drastic change in chemical and physical properties of the materials across the line. Assuming that the surface of materials are perfectly smooth (i.e. roughness ca 0.1 nm [1], [7]), rigid, and chemically homogenous the adhesion between the materials could be solely realized through intermolecular surface forces. However, this cannot be achieved by simply bringing two solids in contact, as most often surfaces of the solid materials are rough and contaminated by different molecules or particles. Thus, to fulfill the requirement of adhesion caused only by intermolecular forces, commonly one of the mating materials is in liquid state to allow realization of an intimate contact across the interface. This compliant phase also could be deemed a polymer well above its glass transition temperature, after curing, forming a solidified conformal contact with the adjacent solid. Along with the assumption of intermolecular forces as the main origin of adhesion, adhesive interfaces could be generated by four auxiliary mechanisms which have shown schematically in figure 2-3.

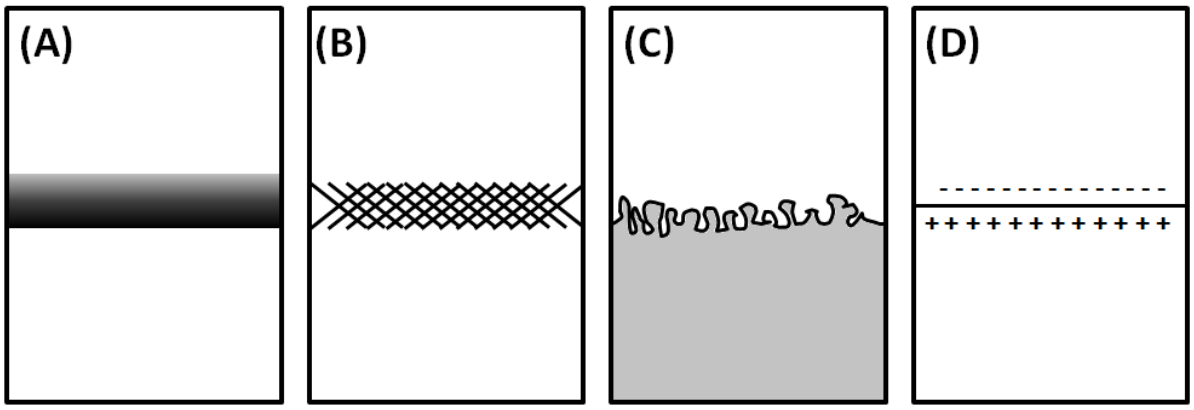

Figure 2-3: Schematic view of four auxiliary adhesion enhancement mechanisms; (A) Adsorption mechanism, (B) Diffusion mechanism, (C) Interlocking mechanism, (D) Electrostatic mechanism.

The *adsorption mechanism* or *contact adhesion* is a result of short-range intermolecular interactions between the outermost molecules of the adhesive and adherent in an intimate contact. The nature of the adsorption might be either purely physical due to the physisorption or chemical due to covalent bonds in a chemisorption process. Accordingly, if there is an intimate contact, universally present Lifshitz-van der Waals (LW) interactions, acid-base interactions, in some cases covalent bonding, and other intermolecular interactions determine the strength of the interface made by adsorption [4].

Diffusion interphase mechanism is another mechanism of generation of an adhesive interface mostly between two polymers with high degree of thermodynamic compatibility. In this case, if there is adequate contact time between two polymers with suitable mutual solubility polymer interdigitation or interdiffusion of relatively mobile chains takes place. This phenomenon leads to creation of an interphase across which the compositions and properties vary. Voyutski firstly reported that the interfacial strength of such an interphase is dependent on time, temperature, compatibility, and molecular weight of the polymers in contact [8].

Mechanical interlocking mechanism is the main reason behind adhesion enhancement of solidifying liquids in contact with rough surfaces. It is believed a larger interfacial area and consequently a greater strength of the intermolecular interactions could be expected from roughening of the surface. Additionally, solidified polymeric adhesives are capable of forming key-lock or hook-ring pairs hindering the separation or destruction of interface. Aside to these, there might be disparate dissipative mechanisms, i.e. viscoelastic or plastic deformation, and friction causing the energy loss in the process of separation.

Proposed by Derjaguin, *electrostatic mechanism* could play an important role in adhesion between two different materials. This mechanism is very similar to the concept of triboelectricity in which electrons transfer from more electropositive materials to more electronegative ones via direct tunneling. [4]. As it is apparent, proposition of these mechanisms entails perfect wetting of the liquid on the solid. However, this condition mostly could not be met as the non-ideality of the solid surfaces would cause to form imperfect contacts.

2.3 Non-ideality of the contact, where adhesion and wetting could be tailored

2.3.1 Contact between liquids and solids

Equations (1) to (4) are rigorous thermodynamic correlations with assumption of stable ideality of the contact, i.e. chemical homogeneity, rigidity, and perfect smoothness of the solid beneath. In fact, satisfaction of these conditions will lead to mechanical equilibrium, chemical equilibrium, and thermal equilibrium for the drop sitting on the solid surface. However, that is impossible in practice and imperfections could be tracked both in static and dynamic measurement of the contact angle. The

static contact angle measurement gives only the apparent contact angle which most often is not equal to the true thermodynamic contact angle. Besides, adhesion hysteresis has been observed in almost all dynamic contact angle measurement experiments, yet is the subject of great deal of investigations. However, it is acceptable now that the contact angle hysteresis is the result of non-idealities present at the interface of liquid and solid [3].

Inherent roughness or contamination roughness on the surface of the solids might entrap air pockets in cavities [9], [10]. It is believed that in static conditions, the contact interline will locate itself at edges of asperities; and small liquid masses might be completely pinned by such irregularities. If the size of the irregularities is adequately small (<< 1 μm) the interline would be able to place the advancing front to the location with lowest possible system free energy [4]. Thus, this reorientation would lead to a new thermodynamic stable state manifesting a different contact angle from that on a smooth surface. Based on the assumptions mentioned, Wenzel developed a model to predict the final equilibrium contact angle, $\boldsymbol{\theta^W}$, utilizing the intrinsic contact angle value, $\boldsymbol{\theta^e}$, in ideal smooth condition [11].

$$\boldsymbol{\cos\theta^W = r\cos\theta^e} \qquad (\mathbf{2.7})$$

In this equation $\boldsymbol{r}$ is the roughness factor which is the ratio of the real contact area to the apparent contact area. As the real area of contact is greater than that of a smooth surface, $\boldsymbol{r > 1}$. Therefore, one could tune the static contact angle of a liquid on solids with different surface energies only by adjusting the size of roughness. For high surface energy solids $\boldsymbol{\theta^e < 90^0}$. Thus, roughening of the surface will lead to Wenzel contact angles with lower than intrinsic contact angles. For low surface energy surfaces, where $\boldsymbol{\theta^e > 90^0}$, the Wenzel contact angle would take higher values than equilibrium contact angle. Wenzel approximation presumes the intimate contact between the liquid and solid, i.e. conformal or intimate contact (figure 2-4).

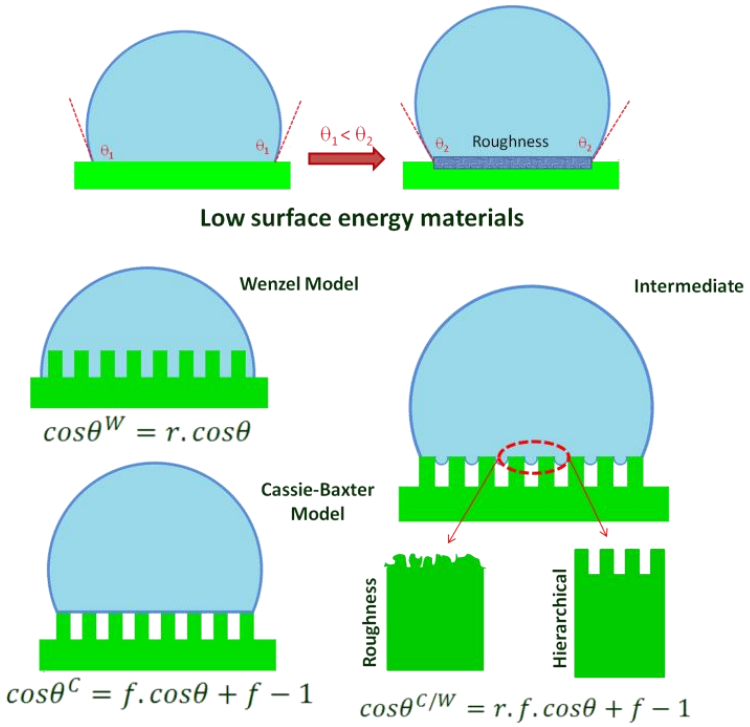

Figure 2-4: Deviation of the apparent contact area from the actual value through surface roughness, Wenzel and Cassie-Baxter models of the contact angle, and transient state of the contact angle

In addition, either inherent or time dependent induced chemical heterogeneity of the surfaces should be taken into account in some cases. Heterogeneity of the chemical composition of the solid surface might cause non-uniformity of the surface free energy. This would render reorientation of the liquid molecules and clusters to find the spot with the lowest possible free energy. Besides, this chemical heterogeneity of the surface might be a result of the different rearrangement of the solid surface molecules exposed to different media. This is mostly the case for polar solids. For instance, hydroxyls on a polymer chain are usually buried in the bulk of the solid away from the gas/solid interface. Once the solid is exposed to water for adequate time span, they rearrange themselves and the interfacial interactions would no longer be similar to what it already was [3]. Moreover, transport of the liquid molecules through the solid or gas phases in terms of the adsorption and evaporation, respectively, or solid molecules to liquid in terms of desorption could trigger the non-uniformity of the surface. Cassie and Baxter reported a similar treatment to Wenzel's for prediction of the equilibrium contact angle on chemically heterogeneous solid surfaces [9], [12].

$$\cos\theta^{CB} = f_1 \cos\theta_1^e + f_2 \cos\theta_2^e \qquad (2.8)$$

According to this equation, if a surface is split to two portions with different surface energies, each f equals to the ratio of the area of the portion with certain surface free energy to the whole surface area. Accordingly, θ_i^e would be intrinsic equilibrium contact angle corresponding to each portion. If the vapour or air in porous surfaces does not allow the liquid to penetrate, the contact mode between the liquid and the solid could be called laid or non-conformal (figure 2-4). Thus, the liquid will make contact angle of 180^o on the cavities and equation (2-8) would reduce to the following form:

$$\cos\theta^{CB} = f_1 \cos\theta_1^e - f_2 \qquad (2.9).$$

There are some complex conditions, such as chemically heterogeneous rough, and fractal rough materials. In such cases, the mode of contact of the liquid with the mating solid could not be considered either intimate or laid. Combination of Wenzel and Cassie-Baxter model has been proposed to predict the equilibrium contact angle of the liquid on such surfaces [9]:

$$\cos\theta^{W/CB} = r(f_1 \cos\theta_1^e - f_2) \qquad (2.10).$$

It is believed that the non-ideality of the contact between solid and liquid causes contact angle hysteresis. That is, measured advancing contact angle $\theta_A$is almost always larger than receding contact angle θ_R. The hysteresis in contact angle could be assumed as a manifestation of this phenomenon: "*hysteresis in adhesion energy is always present when at least one of the phases in contact is solid*" [1], [6]. In fact, thermodynamic irreversible nature of the surface alterations on the solid/liquid interface does not allow the liquid front retract on the same path it has passed in advancing. Metastable reorientation of the liquid molecules or clusters with different sizes again is the main reason behind the contact angle hysteresis caused by roughness. All other mentioned reasons for non-ideality in contact of liquid and surface in static contact angle measurement could be again listed here to justify the contact angle hysteresis.

2.3.2 Contact between two solids

It has been stated that non-ideality in contacts, where at least one side is solid, causes contact angle hysteresis. In the other word, contact angle hysteresis could be considered as of the most influencing parameter on wetting. This is also the case for the contact between two solids, where the hysteresis affects the adhesion force and energy between solids drastically. It has been shown recently that adhesion hysteresis has also remarkable effects on the friction between solids [2], [13]. Prior to discussion about the adhesion hysteresis and its effects on the adhesion and friction we should explain the most common contact theories in contact between solids.

Derjaguin approximation, recalled in equation (2-5) and (2-6), was an expression for short-range forces acting between two rigid, atomically smooth spherical solids. In practice, contact between solids is never ideal in that at least a trivial elastic deformation of the solids is always present. This was proven by Derjaguin et al. They reported that the Hertz approximation of the force between solid bodies is insufficient. According to their report, when two solid bodies are brought to contact even in zero loads slight deformation takes place [14], [15]. Based on Hertz theory of the contact, if two rigid and perfectly smooth spherical solids come into contact a black spot would form at the interface. This black spot was observed 200 years before Hertz by Newton during his experiments on contact between glass lenses. However, he could not relate the size of this black spot to the applied load. Hertz, finally, correlated the contact area to the applied force in the following fashion[1], [16–18]:

$$\boldsymbol{F = \frac{Ka^3}{R}} \qquad (\mathbf{2.11}),$$

where $\boldsymbol{F}$ is the magnitude of applied load on the spheres, $\boldsymbol{a}$ is the radius of contact area, and $\boldsymbol{R}$ is the combined radius of two spheres defined as: $\boldsymbol{R = R_1R_2/(R_1 + R_2)}$. $\boldsymbol{K}$ is reduced combined Young's modulus of two solid bodies in contact defined as:

$$\boldsymbol{\frac{1}{K} = \frac{3}{4}\left[\left(\frac{1-\nu_1^2}{E_1}\right) + \left(\frac{1-\nu_2^2}{E_2}\right)\right]} \qquad (\mathbf{2.12}).$$

Hertz did not take into account the possible effect of intermolecular interactions on the surface of two solids and assumed all of the forces are compressive. His model also assumes that loading and unloading of the solids will pass the same path showing no hysteresis. However, the most important contribution of his theory was acknowledging the fact that in reality even extreme rigid solids in contact experience deformation, which is not in agreement with the ideality of contact. As a result, he approached vertical deformation δ elastically and related it to the contact area as can be seen below:

$$\boldsymbol{\delta = \frac{a^2}{R}} \qquad (\mathbf{2.13}).$$

The Hertz approximation, however, was inadequate. Derjaguin confirmed in his experiments that even in zero loads deformation takes place to slight extent. He made a thermodynamic energy balance between the work of deformation and the work done by surface attractions. This led to development of a new interpretation of an observed non-ideality in contact, i.e. deformation. DMT theory (Derjaguin-Muller-Toporov), consequently, considers the crucial influence of intermolecular interactions in deformation of rigid bodies in contact under zero loads. Surface forces in zero loads, therefore, result in an offset in Hertz initial approximation as shown below:

$$\boldsymbol{F = \frac{Ka^3}{R} - 2\pi R W_{12}^{A}} \qquad (\mathbf{2.14}),$$

where $\boldsymbol{W_{12}^{A}}$ stands for the thermodynamic work of adhesion between two solids in vacuum under ideal conditions. Vertical deformation is related to the contact area in the same way as Hertz theory is. Short-range and ideal intermolecular interactions are finally manifested in DMT theory as a tensile stress inside the contact area. As the maximum work of separation in this theory is very similar to that predicted by Bradly's model for non-deformable spherical solids [1], [19], it was concluded that the elastic deformation does not affect the total adhesion remarkably. That is, acknowledging that there is a non-ideality in practice, but extent of its influence is trivial. Independence of the vertical deformation from thermodynamic work of adhesion also confirms this idea. The adhesion hysteresis is not considered in this theory, as well.

There appeared an insufficiency in DMT theory when Johnson, Kendall, and Robersts showed that the real contact area is practically greater than predicted by DMT. In fact, DMT does not take into account the load distribution within the contact area. Resolving this issue, they developed a modified theory which was more dependent on the adhesive forces between two solids, the so-called JKR theory[17], [20].

$$\boldsymbol{F = \frac{Ka^3}{R} - \sqrt{6\pi W_{12}^A K a^3}} \qquad (\mathbf{2.15}),$$

$$\boldsymbol{\delta = \frac{a^2}{R} - \frac{2}{3}\sqrt{\frac{6\pi W_{12}^A a}{K}}} \qquad (\mathbf{2.16}).$$

Deviation of the size of the contact area from what is predicted by DMT theory is more pronounced in soft elastomers and those materials with great attractive forces. Based on JKR theory, the vertical deformation and the work of adhesion between two solids are correlated. It shows that non-ideality in form of even elastic deformation affects the total adhesion between two solids. The reason is that elasticity facilitates the movement and this movement fosters the cracking process. Thus, if the crack runs in an interface the applied elastic energy will be spent to overcome the work of adhesion and creating new surfaces [16]. Existence of an "infinite stress" on the edge of contact area in JKR model, although impossible in reality, exactly resembles the stress singularity found in cracking experiments by Griffith [1], [17], [21].

Eventually, energy dissipation due to the adhesion hysteresis was observed in typical load-displacement curves. To elaborate, if two solid bodies are brought into contact in loading, there would be no sensible force until two bodies almost touch each other. Intermolecular attractions, then, result in a sudden jump of two surfaces in form of tensile force, so-called pull-in force. In the unloading period, the maximum separation force, i.e. pull-off force, is always greater than pull-in force. Also, whole load-displacement curves lies below the loading curve. This discrepancy in load-displacement curves manifests itself in shape of adhesion hysteresis. In fact, assumption of cracking on the contact line is a result of Brownian motion of the molecules on the edge of crack in shape of a make-and-break process of contact (figure 2-5). This could be considered as a factor impeding contact equilibrium at one particular contact diameter and resulting in thermodynamic irreversibility in contact experiments [1], [16].

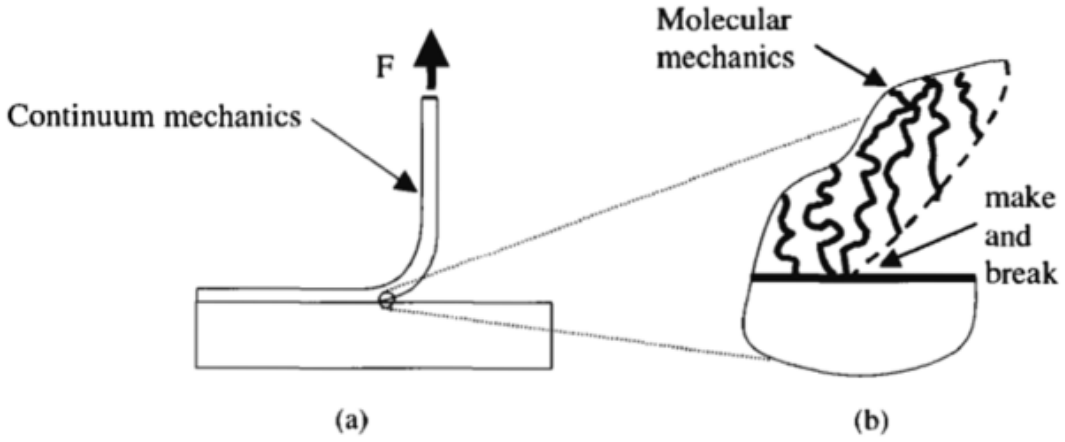

Figure 2-5: The process of make and break resulted from Brownian motion of the molecules at the crack tip[1], [16]

2.3.3 Practical adhesion and tailoring the adhesive strength

Non-ideality in contact, as it was elaborated previously, is an inevitable fact in practice. This, accordingly, causes deviation of measured adhesion, i.e. practical adhesion, from the equilibrium thermodynamic work of adhesion, i.e. ideal adhesion. To elucidate the relationship between ideal adhesion and practical adhesion a series of adhesion and peeling experiments were implemented by Gent, Andrews, and Kinloch [22–24]. They concluded that the practical adhesion in terms of mechanical work of separation includes the ideal thermodynamic work of adhesion and other dissipative mechanisms. Their conclusion could be expressed as

$$\boldsymbol{G = G_0 + \varphi} \qquad (\mathbf{2.17}),$$

where $\boldsymbol{G}$ is the energy release rate, $\boldsymbol{G_0}$ usually is presumed as thermodynamic work of adhesion, and $\boldsymbol{\varphi}$ is energy dissipation factor via various mechanisms [25]. In more complex cases, viscoelastic dissipative mechanisms are present during the separation and the relationship has shown to be multiplicative.

$$\boldsymbol{G = G_0\left(1 + \varphi(T, v)\right)} \qquad (\mathbf{2.18}).$$

In this equation, temperature dependence, $\boldsymbol{T}$, of viscoelastic dissipation has been considered. Also, energy release rate is basically defined as the energy required for decreasing the interfacial area through crack propagation process. Therefore, a factor of crack growth rate dependence, $\boldsymbol{v}$, has been considered.

Shull, however, has scrutinized the crack growth rate dependent factor with more details. He has divided the dissipative contributions to two regimes. First regime includes dissipative factors taking place in the interface or interphase, and the second regime encompasses those outside the interface. In fact, the concept of adhesion rising from thermodynamic work of adhesion and all of the auxiliary mechanisms to make an interface, recapitalized in section 2.2, are categorized in the first regime. The thermodynamic work of adhesion between two materials has been considered as the lower bound for $\boldsymbol{G_0}$ for zero rate crack growth. Accordingly, he suggests the following correlation:

$$\boldsymbol{G = W_{12}^{A}(1 + \psi(v))\big(1 + \varphi(T, v)\big)} \qquad (\mathbf{2.19}),$$

where $\boldsymbol{\psi(v)}$ is the dissipation factor particularly for the interface. The critical energy release rate could be defined as $\boldsymbol{G_0 = W_{12}^{A}(1 + \psi(v))}$ [18], [26].

In conclusion, non-ideality in contact, whether it is related to surface roughness, materials deformability, and chemical surface heterogeneity leads to practical adhesion values much greater than the thermodynamic work of adhesion. This is usually desired for technological applications. As the influence of each of these non-idealities on practical adhesion has been investigated extensively in the literature, manufacturing of special adhesives with tuned properties is not out of reach. That is, by tailoring the surface properties of the materials one could hope to manufacture smart materials with pre-designed interfacial properties. These properties are able to affect major interfacial events such as wetting, adhesion, and friction properties of the materials. Bio-inspired modification of the surface properties of materials is an emerging discipline rooted in chemistry, physics of condensed matter, and engineering. During the last decade, there were a tremendous interest and investigation in realization of smart interfaces using bio-inspired modification methods. Whether they are chemical or physical methods, they provide versatile means to control and tune the wetting, adhesion, and friction properties of the materials. The propensity of bio-inspired methods of surface modification will be discussed with more details in chapter 3.

Chapter 3
Biomimetic tailoring of adhesion, friction, and wetting

In this chapter we first discuss the mechanisms of adhesion, friction, and wetting in biological systems. Second, fabrication and synthesis techniques of artificial biomimetic materials and surfaces would be enumerated. Third, the performance of the replication of adhesive and wetting mechanisms in inspired from biological systems would be evaluated.

During billions of years of evolution, biological systems have demonstrated fascinating smart interfacial properties, i.e. adhesion, friction, and wetting, when interacting with their natural habitat. In fact, they have regulated omnipresent non-idealities of contact in nature, i.e. surface roughness, contamination, chemical heterogeneity, and non ideal mechanical properties. It is believed that functionality and smartness of biological surfaces are stemmed from intricate structure of their body outer layers, i.e. skins of animals or plants. The interaction with mating surface in nature could be divided to two categories. The first category, denoted as adhesion mechanisms, concerns with the cases where high adhesion, friction, and wetting is necessary. The second category, denoted as anti-adhesion mechanisms, includes the cases where the requirements for minimum adhesion, friction, and wetting should be met. Inspired by these attracting properties, a great deal of efforts has been devoted to understand the mechanisms associated in adhesion, friction, and wetting behavior of biological systems. Besides, a plethora of studies have been conducted to replicate such properties in artificial and synthetic surfaces and materials.

3.1 Adhesive and anti-adhesive mechanisms of biological systems

As it is mentioned in the previous section, intermolecular forces are not the only reason of adhesion in practice. In fact, they are contributing in the practical adhesion with different other factors. The factors enhancing practical adhesion are usually related to temperature and rate dependent thermophysical properties of the surfaces [4], [25], [26]. According to deformability of the materials, when two materials are brought into contact, elastic energy is stored in two bodies **(U_{el})**. During the pull-off, this stored elastic energy could dissipate in shape of crack growth and the breakage of the interface. Thus, one could expect higher adhesion if this stored energy is dissipated in the bulk of materials instead of interface, or is reduced to lower extend.

Persson expresses two criteria of strong adhesion to fulfill this phenomenon [27]. The first mechanism is “long dissipative bonds”. That is, interface between two adherents should involve “long dissipative bonds” in order to enhance the bulk dissipation of stored elastic energy by elongation of interfacial bonds in pull-off. Stored elastic energy dissipation in bulk of the materials could also take place via other mechanisms, such as viscoelasticity, plastic deformation, friction, and so forth. The second criterion lies on maximization of real area of contact. According to energy balance during an interfacial failure, $\boldsymbol{U_{el}}$ is the driving force of the separation besides the external tension. As energy required for creating unit area of an interface is $-\boldsymbol{W_{12}^{A}}$, if the real contact area is maximized the contribution of $\boldsymbol{U_{el}}$ would be decreased. These two are strategies for tackling the problems that roughness causes in adhesion of materials. It is believed that the surface roughness decreases the adhesion between two solid bodies up to the point that macroscopic solids usually do not adhere to each other [28]. The real contact area would be intensified if one of the adherents is soft solid or liquid. Soft solids, furthermore, are more prone to experience dissipation of energy as it is explained in previous chapter. Having liquid at the interface also intensifies the likelihood of construction of capillary bridges, enhancing the total adhesion between mating surfaces (figure 3-1) [27], [29].

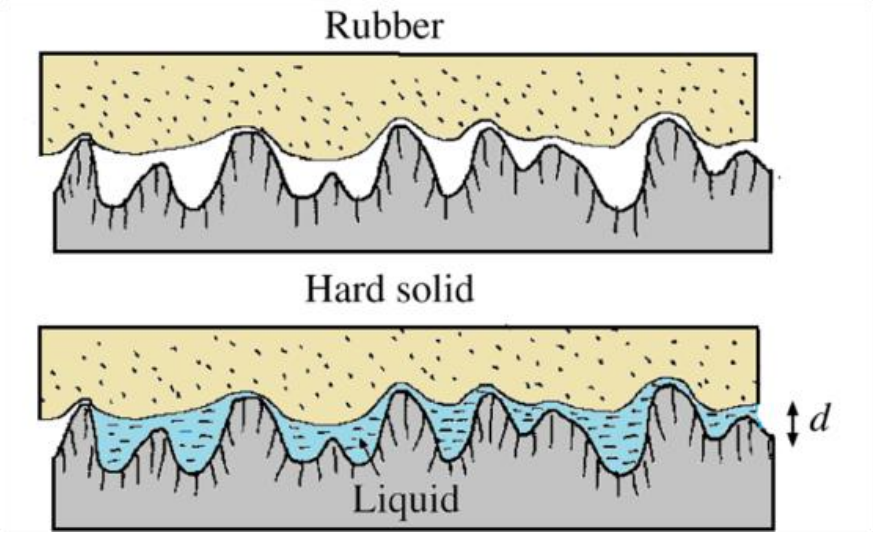

Figure 3-1: Reduction of the real contact area through surface roughness and enhancement of the real contact area by introduction of liquids in the interface [27].

3.1.1 Anti-adhesive mechanisms in biological systems

On the contrary to adhesion properties of some biological systems, some others benefit from super-hydrophobic and anti-adhesive properties, the properties that introduced the concept of self-cleaning in biological systems. This, most often, could be attained by minimization of the contact area and use of repellent chemicals on the surfaces. In fact, animals use these strategies to keep their organs clean and dry. This might be utilized for several purposes such as facilitating their locomotion. For instance, the skin of fast-swimming sharks is covered by riblet structures aligned in the direction of flow (figure 3-2-B). It is expected that presence of mucus on these structures results in localization of super-hydrophobic spot on shark skin. Therefore, localized application of hydrophobic materials will alter the flow field around the riblets in some way beneficial to the goals of increased drag reduction [30]. As another case in point, butterfly wings are privileged of anisotropic wetting behaviour (figure 3-2-C). In fact, directional micro and nanostructures on their wings act as a water repellent organ. This property also has influence on motion of butterflies when the orientation of structures on wing is in direction or opposite of air flow[31]. Super-hydrophobic surfaces could also be found in plants. The most well-known example of plants benefiting from this property is lotus. Lotus leaf is usually covered with randomly distributed convex nano-asperities (figure 3-2-D). Based on the Cassie-Baxter model of wetting, if the surface energy of the surface is low, roughness would result in increase in contact angle. This is the case for the leaves of a group of plants including lotus which are covered with a low surface energy waxy chemical. As a result, water can be rolled up and move on the surfaces with this topography and chemistry. The same mechanism is being exploited in water striders legs to minimize the interaction with and they move on water (figure 3-2-A).

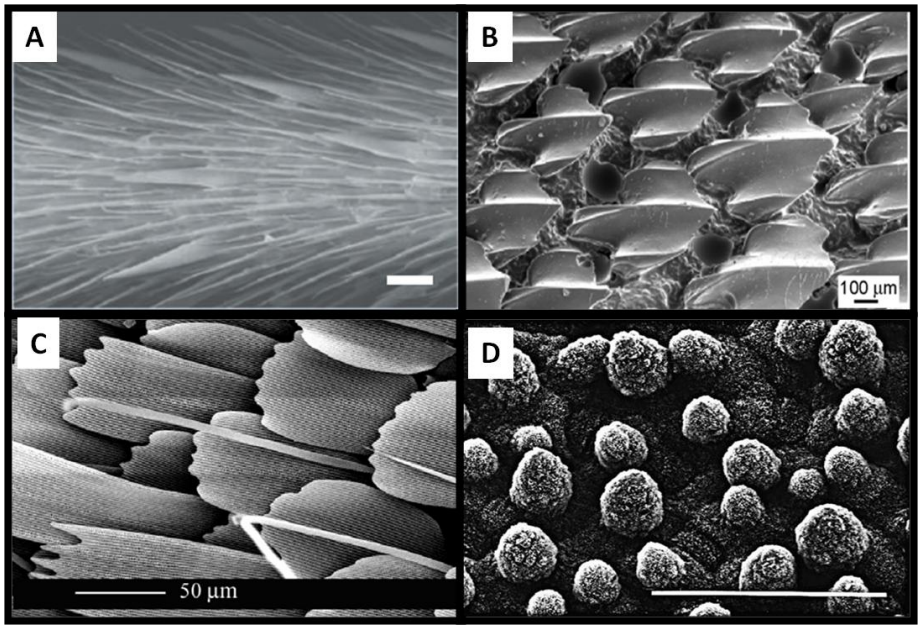

Figure 3-2: SEM images of (A) water strider leg[32], (B) shark skin[30], (C) butterfly wing[33], and (D) lotus leaf [34].

Super-hydrophobic nature of lotus leaf and anisotropic wetting behavior of butterfly wing has intrigued researchers to attempt to fabricate synthetic surfaces with similar properties. It has been reported that the hydrophobicity and self-cleaning characteristics of materials could encompass a wide range of applications in industrial, agricultural, domestic and military fields, such as snow proof, water proof, fog proof, pollution guarding, anti-oxidation, aerobat, submarine, radar, etc [31]. Static and dynamic contact angle measurements usually are used to study wetting behaviour of such synthetic structures. Water roll up angle is also has been introduced as an index of water repelling of a surface, mostly being used in anisotropic wetting experiments. In fact, water roll up angle is the angle in which water drop on a superhydrophobic surface starts rolling up (figure 3-3).

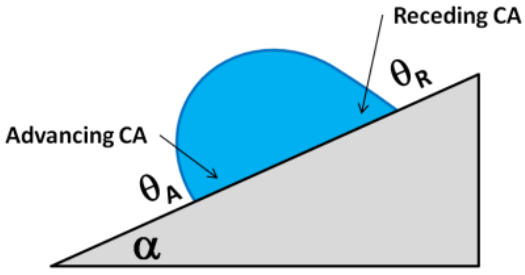

Figure 3-3: Contact angle hysteresis resulted by tilting of the substrate and movement of the drop, in case of superhydrophobic surfaces the critical angle is water roll up angle

3.1.2 Adhesion mechanisms in biological systems

Adhesion to mating surfaces is favorable for most of the insects, lizards, and marine animals as it renders their locomotion on natural surfaces with various physiochemical and topographical properties. It is impossible to have an ideal contact free from inherent roughness of natural surfaces, contaminated adherent surfaces, contaminated adhesion medium like flooded and wet conditions, and chemical heterogeneous surfaces. However, biological systems are capable of adhering to natural surfaces in a tailored fashion. It is postulated that nature uses a combination of two strategies to tackle this problem which are smooth and hairy toe pads (figure 3-4).

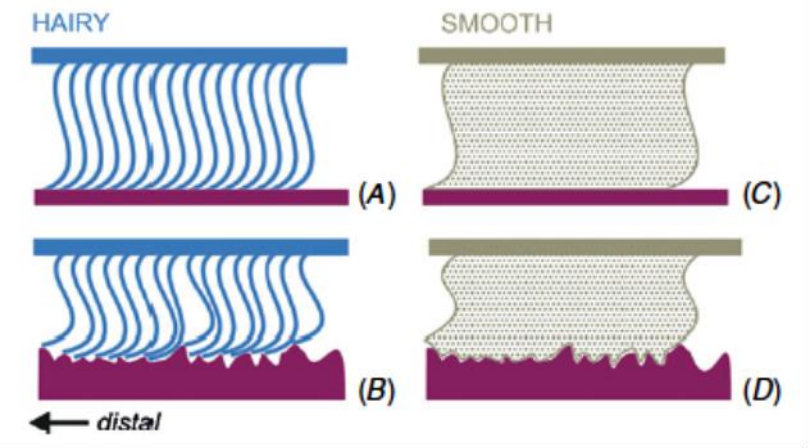

Figure 3-4: Strategies of contact area enhancement in biological systems, (A) and (B) refers to constructive role of hairy toe pads in making contacts with enhanced area, and (C) and (D) shows soft smooth deformable pads adapting to the surface roughness[29].

Some animals using smooth toe pads inject wetting liquids in the contact area in order to enhance the adhesion [27], [29], [35]. Tree frog and grasshoppers are the main examples of this category. The structure of tree frog toe pad has been shown in figure 3-5. Hexagonal arrays epithelial cells separated by large grooves increase the bending elasticity of the toe pads. The grooves also are filled with watery mucus facilitating the large contact area and capillary bridges with rough surfaces. In grasshoppers the smooth toe pads bear tiny filaments oriented at some angel to the surface. This structure facilitates replication of the surface roughness in contact [27], [29]. Generally, functional principles of smooth pads such as adaptability, viscoelasticity, and pressure sensitivity are the basic principles being used in commercial pressure sensitive adhesives (PSAs).

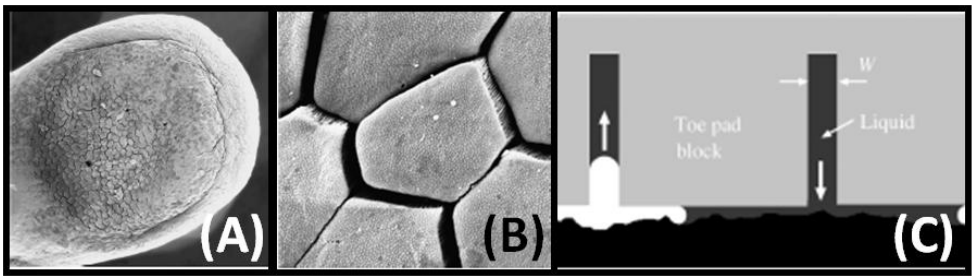

Figure 3-5: SEM image of toe of a three frog (A and B), and capillarity assisted mechanism of adhesion utilized by tree frogs[27].

Toe pads and feet of insects and lizards mainly are made of keratin-like materials which are elastically stiff. Thus, roughness adaptability is hindered. Hairy structure of these animals' locomotion organs, therefore, facilitates achievement of higher area of contact with rough surfaces. The tip of filaments also has embroidered with cup-like or spatula-like plates increasing the real contact area and friction to the surface. Size and number density of the hairs and terminal plates are proved to be proportional to the weight of the animal. For smaller animals the density of hairs and terminal plates is lower. In this case, the hairs are usually wet by glandular liquids and capillary bridges via wet adhesion help the animals to attach and move on different surfaces. For heavier animals like lizards and geckos, the hairy structure of the toe pads is much more intricate and contains several levels of hierarchy. Figure 3-6 indicates the hairy toe structure of beetle, fly, spider, and gecko feet.

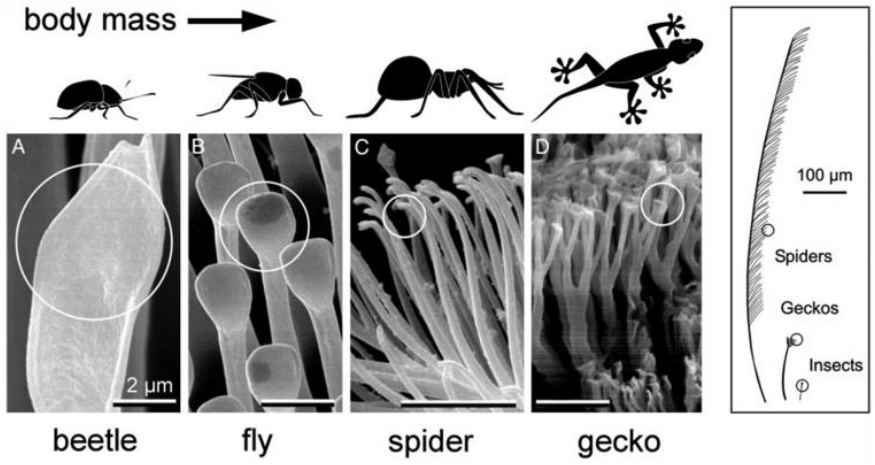

Figure 3-6: Scaling of the terminal toe hairs in different animals and its inverse proportionality to the animal body weight [36].

As gecko possesses the most effective and sophisticated system, a myriad of efforts has been conducted by researchers to understand the mechanism behind its adhesion and locomotion. Gecko also has grabbed the attention of researchers as a perfect prototype for replication; as a result, most of the synthetic bio-inspired adhesives are fabricated based on gecko toe structure. Therefore, in this chapter, we aim to recapitalize the most important trials in understanding of the adhesion mechanism and fabrication of gecko-inspired adhesives during the past decade.

3.2 Gecko adhesive system

3.2.1 Scaling

There are more than 1000 species of geckos all around the world. Among them, Tokay gecko or Gekko gecko has been mostly investigated due to its availability and size. In fact, Tokay gecko is the second largest species attaining lengths around 0.3 to 0.4 meters for males, and 0.2 to 0.3 meters for females with weights up to 300g. Outstanding ability of geckos in attachment and walking on almost any kind of surfaces with different orientations has been attributed to their β-keratinous skin morphology especially the complex hierarchy of their toes pads (figure 3-7). Intricate structure of gecko toe pad begins at the first level with tens of lamellar scansors with 1 to 2 mm in length. Lamellar scansors are branched to thousands of uni-direction oriented and uniformly distributed arrays of curvy stalks known as setae (14000 setae/mm^2). Their size typically is in range about 100 µm in length and 5µm to 10 µm in diameter. Every single seta is branched to 100-1000 spatulae which are terminated to thin triangular projections. Spatulae connected to the apex of these triangular tips, commonly have 0.2 to 0.5 µm height, and 0.2 µm diameter; their tip thickness and width are about 0.01 µm and 0.2 to 0.3 µm, respectively (figure 3-8). Two front toes of Tokay gecko can tolerate 20 N force (the required force to pull a climbing gecko down from an 85^0 inclined vertical surface). Considering the 14000 setae/mm^2, every single seta could generate 6.2 µN force and 0.09 µN/mm^2 shear stress on average. All 6.5 millions setae of an average 50g gecko can generate theoretically 1300 N (133 kg) shear force, enough to hold two humans. Also, gecko can run on almost every surface with speeds up to 1 m/s implying that any attachment-detachment cycle can take place in tens of milliseconds. Assuming the maximum theoretical adhesion force generated in attachment of a gecko, it seems that a huge force is required for detachment process. As a 0.5 N force is required to hold a 50 g gecko, only 0.04% of gecko setae are necessary to hold its whole body against the gravity, which means it benefits from a huge safety margin [37–42].

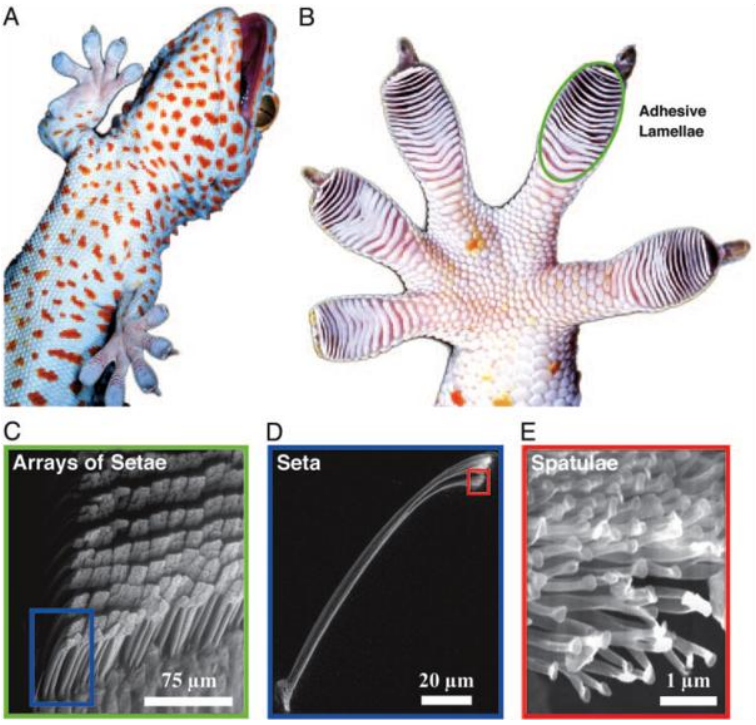

Figure 3-7: SEM image of the hierarchical structure of the Gecko gecko toe pad[43].

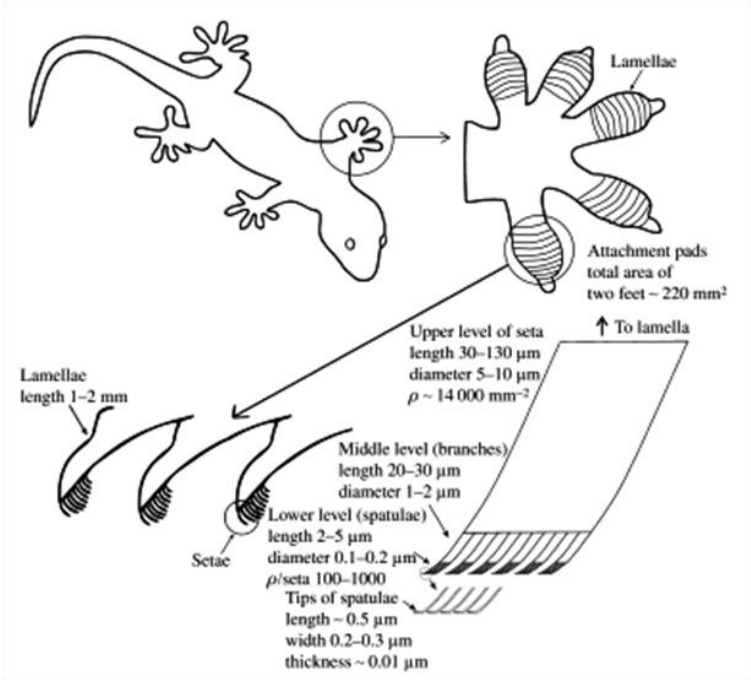

Figure 3-8: Schematic view of the gecko toe pad scaling and hierarchy[40]

3.2.2 Properties of gecko adhesive system

Autumn has enumerated seven main properties of gecko adhesive system in [39]. He noted that the gecko adhesive system possesses both adhesive and anti-adhesive properties which have been observed in biological systems. By scrutinizing the chemistry of the gecko toe skin and also the geometry of the contact on different surfaces, it has been proved that gecko adhesive system is inherently anti-adhesive! To elaborate, Autumn and Hansen estimated the fraction of setal arrays in contact with mating surface when setal array is unloaded. Using Baxter approximation of contact angle on rough surfaces, they concluded that gecko setae array is superhydrophobic in nature. Besides, as it is explained in section 2, non-idealities of contact may remarkably influence of the adhesion. Inherent roughness of both substrates and setal array of gecko foot, in fact, impedes the effective contact in vertical direction under zero loads[37], [41], [43]. Similarly to lotus leaves, they postulated that gecko adhesive benefit from a self cleaning system. Grooming of adhesive organs also has not been observed in gecko as they effectively utilize their adhesive system during the shedding cycles. 93° contact angle of water droplet on eye spectacle scales of tokay gecko showed inherent low surface energy of gecko skin. Eventually, 160° contact angle on gecko steal array buttressed superhydrophobic and self-cleaning nature of gecko setal arrays [43]. Together with mentioned evidence, these reports encompass anti-adhesive properties of gecko adhesive system which are 1) anti-adhesive in default, 2) anti self-adhesive, and 3) self-cleaning.

Considering anti-adhesive nature of gecko adhesive system, the impressive adhesion strength could be attributed to remaining four properties. In fact, geckos utilize these properties to overcome non-idealities of the contact and make the best adhesion possible with the mating surface. As it is mentioned, van der Waals forces are known as the most influential interactions rendering the observed adhesion strength in geckos. The short range and geometry dependent nature of the van der Waals forces, therefore, necessitates minimum distance with the mating surface. It has been shown by Autumn and Hansen that 6% of contact of setal array under zero preloads could be increased to 46% if the setal array is pushed toward the substrate and dragged[44].

In 2006, a series of experiments on locomotion of gecko has been performed. The main parameter studied was the influence of combinatorial loading of setal array. That is, combination of small vertical loading on setal array was followed by 5-μm proximal shear resulted in 100 adhesion enhancement comparing to the values were obtained in experiments without these conditions[45]. The

ratio of the preload to adhesion (coefficient of adhesion μ') also was shown to be in range of 8 to 16. The low detachment force of gecko adhesive toe pads was also investigated in that study. It is proved that attachment and detachment of setal array from mating surface is anisotropic and there is a critical angle of orientation, i.e. 30°. That is, if the setal shaft is faced to the substrate with angles lower than 30°, frictional adhesion dominates. Detachment, then, takes place for the orientation of setal arrays in shaft angles of more than 30°. Thus, remaining four properties of gecko adhesives could be listed as 4) material independent adhesion, 5) directional adhesion, 6 and 7) strong attachment with small preloads and easy detachment.

Interestingly, all of the mentioned mechanisms are utilized by geckos to overcome the problem of non-ideal contacts. Physical, topographical, and chemical heterogeneity of the natural surfaces, indeed, could be overcome through seven properties of gecko adhesives. Chemical heterogeneity of the surface could be compensated by smart alteration of surface chemistry. Roughness and physical heterogeneities could also be compensated by anisotropic and directional attachment mechanism. Influence of multi-level hierarchy of the toe structure and modification of the stiffness of the toe in different levels has also been studied and would be elaborated later in this chapter.

3.2.3 Mechanisms of adhesion of gecko

Despite the fact that setal structure of geckos has been well described by many scientists over a century, their attachment mechanism was a subject of great disputes. Haase was the first scientist introduced the gecko adhesion system both as preload-dependent and directional; moreover, he was the first one postulated that molecular interactions are the major forces responsible for adhesion of geckos to different surfaces[39], [46]. During this century, seven major categories of attraction mechanisms were proposed as the responsible potentials for gecko adhesion. Secretion of liquids in toe pads, presence of suction cups, purely friction assisted mechanism, micro-interlocking, electrostatic interactions, van der Waals interactions, and capillary forces were subjected to scrutiny for this reason. However, van der Waals and capillary forces acquired most scientific justifications, while other ones were discarded through various experiments.

In brief, the proposed mechanism of attachment by means of sticky secretion was ruled out for absence of any glandular tissues in the gecko adhesive pads[39]. Next, the challenging issue of

attribution of attachment by miniature suction cups on gecko toe pads was disproved in two sets of experiments by Dellit [47] and Autumn [38]. The adhesion tests in vacuum conducted by Dellit suggested that the suction is not involved in the gecko adhesion system; moreover, 9 atm adhesive stress measured by Autumn and coworkers contradicted this theory. Even though electrostatic attractions have been proved to be effective in enhancement of gecko adhesion [48], its major potential was rejected after X-ray bombardment when geckos still could attach to metal in ionized air [47]. Furthermore, strong attachment of geckos to inverted, polished and smooth surfaces (e.g. SiO_2 MEMS semiconductor and polished glass) debilitated the possibility of domination of friction and micro-interlocking mechanisms in gecko adhesion. Finally, among all potential mechanisms, van der Waals and capillary grabbed approbation of scientists [39].

Adhesion tests on hydrophilic surfaces seemed to be incapable of distinguishing between the importance of capillary and van der Waals forces in gecko adhesion. Hiller [49–51]conducted a groundbreaking experiment changing the face of surface and adhesion science [6], [39]. By correlating shear force with respect to water contact angle on surface, he suggested that the adhesion depends on the surface free energy. Afterwards, he reported his observations of incapability of geckos to stick to poorly polarisable superhydrophobic polytetraflouroethylene (PTFE, Teflon) compounds. As a result, capillary effect, as an inseparable effect of hydrophilic surfaces, might have a grave effect on strength of gecko adhesion [52]. However, he had not considered the effect of surface polarizability on van der Waals forces. The efforts to differentiate between these two forces as the major attraction potential continued until some discoveries by Autumn and his colleagues. They showed that the setae arrays of geckos are extremely hydrophobic (water contact angles ~ 160.9^0)[44]. They, also, conducted a series of adhesion and friction tests between single seta array and various polarisable surfaces having different degrees of polarity (hydrophilicity/hydrophobicity). They used hydrophobic GaAs and Si MEMS semiconductors and hydrophilic SiO_2 as their testing surface. Interestingly, they observed trivial difference between adhesion of seta arrays to both hydrophilic and hydrophobic surfaces. Comparing Hiller's result with their new findings, they conclude that polarizability was the main difference in Teflon experiment conducted by Hiller and their experiments using hydrophobic semiconductors. On the ground that van der Waals force totally depends on the polarizability of the surfaces, they showed sufficiency of van der Waals forces for gecko adhesion [38].

Although attempts corroborating the sufficiency of van der Waals force in adhesion of gecko to different surfaces were compelling, trials to address the contribution of capillary forces continued. Huber and coworkers conducted AFM force measurement of single spatulae on substrates with different degree of hydrophilicity and hydrophobicity. They also repeated their experiments in different humidities. They concluded that the humidity influences gecko adhesion on the spatular level and the extent of influence is related to the level of humidity[53]. Their report was buttressed by Sun and coworkers' report on substantial influence of humidity and hydrophobicity of the substrate on single spatula [54].

In fact, humidity could have two effects on adhesion: 1) humidity modifies the contact geometry (as described in section 2), and 2) it decreases the van der Waals forces. Autumn states that these two factors balance each other and the final result is an increase of adhesion in higher levels of humidity. He claims that the results by Sun et al. could be justified better in the framework of van der Waals forces instead of capillary[39]. The effect of humidity on adhesion could also be attributed to alteration of chemical compounds on the surface of adhesive. Pesika and coworkers carried out several adhesion and friction experiments on an isolated array of setae. They implemented the experiments in different humidity levels. They found a change in the hydrophilic– hydrophilic balance of the surface of the setal array when exposed to water in different periods of time. This leads to a conformational change in the surface proteins and alteration of surface properties toward being less hydrophobic [55].

3.3 Synthetic gecko-like adhesive systems

Generally there are some guidelines to enhance the practical adhesion. Intuitively, maximization of contact area and stored elastic energy dissipation are the main tasks to be met. In more details, according to equation 2-19, there are three parameters could be tailored to obtain maximum possible practical adhesion. Firstly, adherent and adhesive must be chemically well compatible. Also, the contact between adherent and adhesive must be maximized. This could be manifested through high thermodynamic work of adhesion and good wetting. Secondly, processes leading to energy dissipation could enhance practical adhesion. The most important example is to utilize the elasticity and level of deformation of the adherent and adhesives. This parameter dependents on temperature and velocity of the testing. Thus, the last parameter is the testing procedure. These are the parameters being considered in manufacturing of commercial adhesives and coatings, such as PSAs.

The aim of fabrication of biological adhesives is to mimic the main properties of their adhesive system, which has shown to be stemmed from their intricate structure. Recalling the structure and properties of the gecko toe pad and gecko adhesive system, one could realize the main features to be met in fabrication of synthetic dry adhesives. Figure 3-9 summarizes the features that biological adhesives usually possess and how they could contribute into adhesion enhancement and smartness[29].

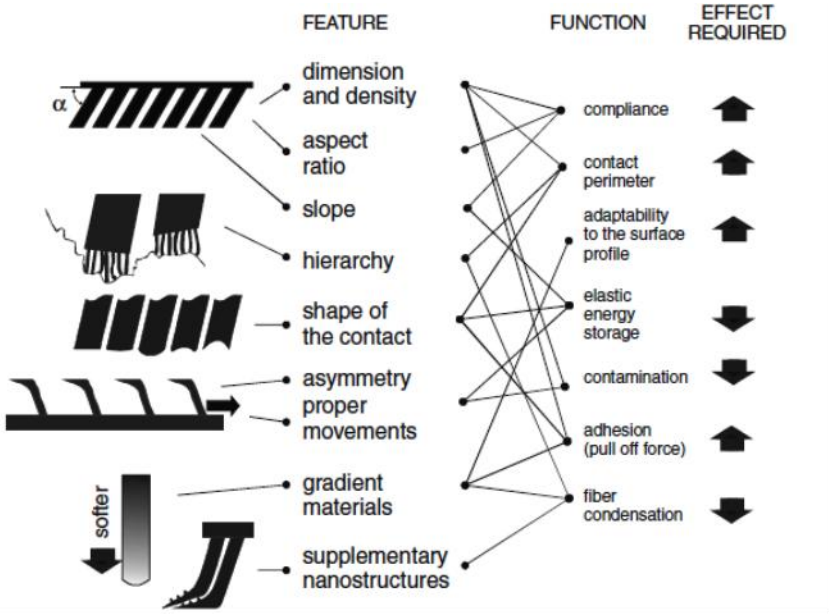

Figure 3-9: Crucial features of a biologically adhesive system[29]

A dry gecko-inspired adhesive should possess high aspect ratio (AR) fibrillar structure, i.e. lower diameter and higher length. To achieve the smartness and anisotropicness, the fibrils should be slanted. To maximize the contact area with the mating surface in a certain preload, the fibrils' tips must be embroidered with spatular structures. And finally, to maximize roughness adaptation and deformability, it should be hierarchical[56]. Attaining these characteristics was actually the obstacle scientists faced with and overcome during the past decade.

Complex structure of biological systems necessitated employment of different micro and nanofabrication techniques to replicate their main characteristics. Therefore, both top-down and bottom-up techniques have been employed during the last decade in order to replicate the gecko toe

pad structure. The main questions to be addressed in fabrication process were: Which materials should be used? How the fibrils structure and arrangement could be controlled? How could fibril tips be made and tailored? And how could hierarchical structures be achieved?

Various organic and inorganic materials have been used in synthesis of artificial bio-inspired adhesives. However, polymers were the most common materials exploited for this purpose. Carbon nanotube (CNT) was the only organic material used for fabrication of bio-mimetic structures. Both low and high AR fibrils have been made in both random distributed and well-defined arrangement. Fabrication of slanted fibrils and different fibril tip shapes were also achieved. Finally, all of these characteristics were replicated in addition to hierarchy. Although the problems of fabrication seems to be resolved, there are many shortcomings in fabricated structures, impeding realization of commercial and effective gecko-inspired dry adhesive.

3.3.1 Fabrication and performance

In terms of techniques of fabrication, except a few reports on bottom-up and MEMS-based fabrication techniques, all other reports use molding and lithography based methods. Thus we have divided the methods of fabrication into two categories. The first category concerns with the reports and techniques in which micro-pillars are fabricated using a bottom-up procedure. The second category addresses the reports in which micro-pillars are fabricated using a top-down technique. Except a few reports, the main task in all of the reports is to fabricate the master mold for replication of micro and nanopillars. There are a few reports on direct fabrication of pillars tip structures from master molds.

3.3.1.1 Bottom-up methods of fabrication

There are a few reports on bottom-up fabrication of fibrillar structures as gecko-like adhesives. For instance, deposition of carbon nanotubes has been utilized as a method to grow high AR nanopillars. Zhao et al. manufactured a vertically aligned multi-wall carbon nanotube (MWCNT) structures mimicking gecko toe pads in spatula level (figure 3-10-D). They measured the thermodynamic work of adhesion of their structure and concluded that van der Waals force is the main mechanism of adhesion to glass substrates[57]. Although they attained shear and normal stresses up to 10 N/cm^2, the large preload in testing of the fabricated patches could be counted as of the shortcomings of this work. In 2007, Ge and coworkers fabricated multi-scale flexible CNT based dry adhesives (figures 3-11-B and C). They fabricated micro scale MWCNT patches in the first level, mimicking the seta level

in gecko toe pad. Addition of second level of grown CNTs in nanoscale they replicated the hierarchical structure of gecko toe pads to spatula level. This increased the shear forces up to values 4 times higher than shear force of a real gecko toe pad, i.e. 36 N/cm^2[58]. Qu and coworkers reported 100 N/cm^2 shear force obtained by fabrication of vertically aligned CNT (figure 3-10-A). However the normal force retained values comparable to that of gecko feet (about 10 N/cm^2). They attributed the high shear force of their structure to increase the contact line between CNT array and substrate. This attained by deposition of a second layer of CNT on top of the first level structure. Indeed, increase in the length of CNT resulted in increment of shear induced contact line and adhesion[59]. Low contact area obtained by CNT based adhesives necessitates higher preloads to induce shear and increment of side wall contacts. Thus, these adhesives could not be used in the applications where the strong normal force is required with small preloads.

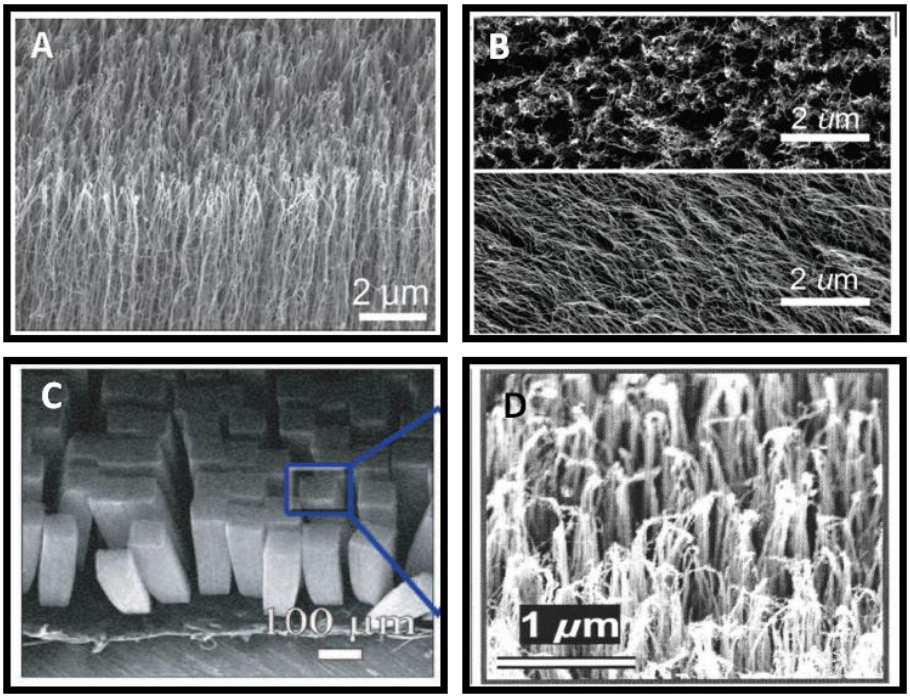

Figure 3-10: CNT based synthetic structures, (A) from[59], (B) from[60], (C) from[58], and (D) from [57]

In 2005 a combination of MEMS top-down and bottom-up method of fabrication was reported by Northen et al.. Organic nanorods were deposited on arrays of flexible silicondioxide platforms. The SiO2 platforms were supported by single high aspect ratio silicon pillars which were fabricated via

MEMS fabrication technique. They attained a significant increase in adhesion over solid organorod covered substrates[61], [62]. A fully reversible adhesive based upon this method was fabricated in 2008. The reversibility was tested in a magnetic field inducing sequential change in orientation of organorods and accordingly contact area of the adhesive (figure 3-11)[63]. Small fabricated area, costly procedure of fabrication, and random arrangement of nanofibrils obtained could be listed as of the issues for bottom-up fabrication methods**.**

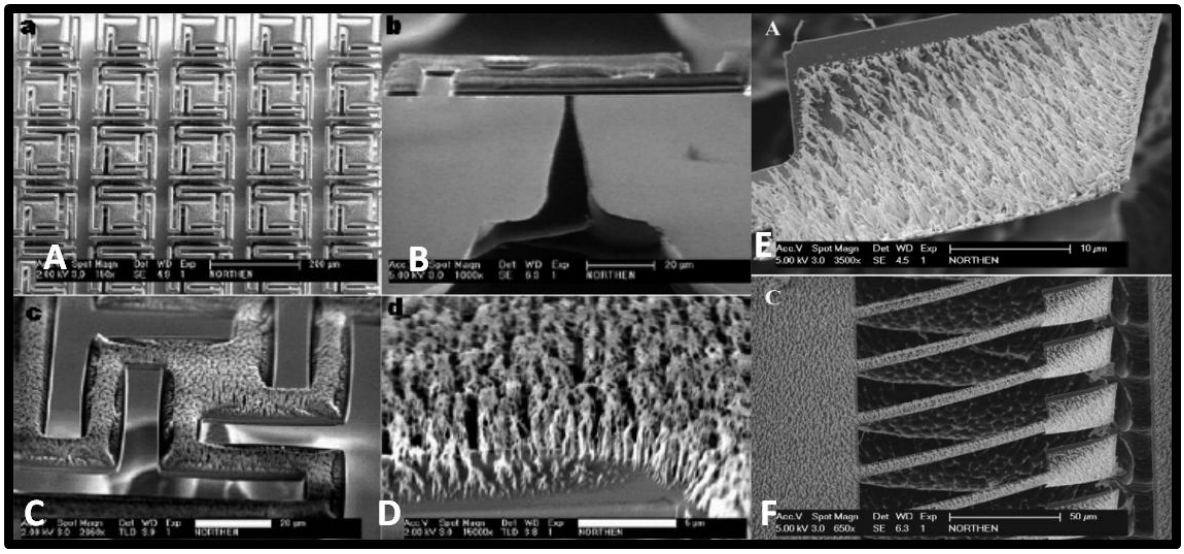

Figure 3-11: MEMS based synthetic gecko-inspired adhesives, A-D from[61], [62], E and F from[63]

3.3.1.2 Top-down methods of fabrication

Geim and coworkers were the first group to report a well-defined submicrometer pillars array mimicking gecko adhesive system. Pillars were directly fabricated on polyimide thin films via e-beam lithography technique (figure 3-12). They attained 3 N/cm^2 normal adhesion, values less than corresponding value in an actual gecko toe pad. They concluded that the adhesive strength is proportional to the adhesive area. The fabricated structure failed in repetitive adhesion testing. Buckling and condensation of pillars were concluded as the main reason behind this failure[64].

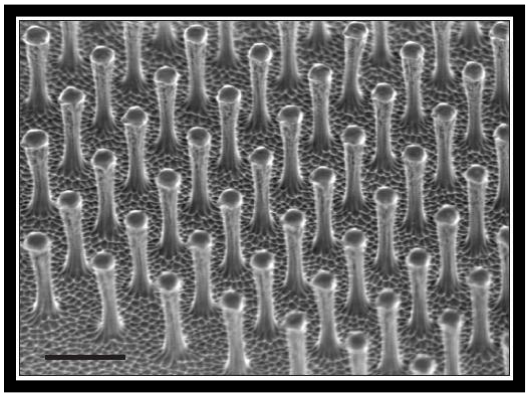

Figure 3-12: Polyimide micropillars fabricated via e-beam lithography[64]

Casting techniques were the main methods to fabricate polymeric micropillars during the past decade. These methods require combination of conventional lithography and etching processes for fabrication of master molds. Fabrication of low defect samples with higher areas is possible through these methods. The cost of the operation is also more reasonable comparing to bottom-up methods of fabrication. The first attempt for the fabrication of miniature surface protrusions using casting technique was reported by Sitti and his coworkers. They used AFM tip to create nano-holes on commercial wax as the master mold for replication. They also used alumina and polycarbonate commercial membranes as the master mold. Then they replicated the positive pattern on silicon rubber and polyester. The fabricated samples did not possess the main characteristics of biological adhesives. But, preliminary micro/nano-hair prototypes showed adhesion close to the predicted values for natural specimens[65]. Fabrication using membranes as molds was reported rigid polymers such as polypropylene or polyethylene. The high friction coefficient of and self-cleaning properties these structures were the most important achievements. Although, rigidity and low surface energy of these polymers used in this method eased fabrication of high AR fibrils, no well-defined structures were achieved [66–70].

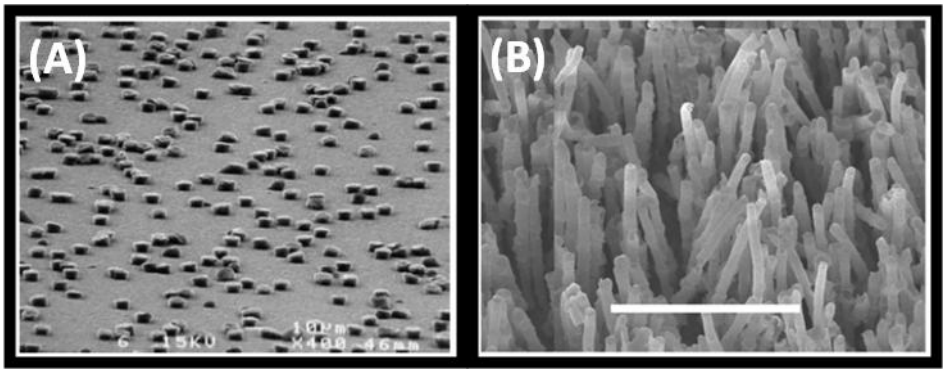

Figure 3-13: Nanopillars casted from AFM pierced waxy master-mold from[65] (A), polyethylene and propylene micropillars fabricated from membrane casting[66–70] (B).

Combination of different micro and nanofabrication techniques, such as lithography, RIE, and DRIE was employed to create well-defined structures as master molds. In 2004, well-defined PDMS patterns were fabricated by molding of the liquid PDMS into silicon master molds. The master molds were fabricated using DRIE [71], [72] (figure 3-14-A). DRIE method for fabrication of micro-holes on silicon based substrates was repeated in some other papers [73–76]. However, low etch rate of RIE and expensive and time consuming process of DRIE led researchers toward easier methods with comparable or even better efficiency. The alternative method was to use a Novolac epoxy based negative photoresist, so-called SU-8, as a structural layer in fabrication of master molds. Rigidity, low surface energy, high quality optical performance in lithography, and high chemical resistance of this material made it as the first choice of fabrication for simple fibrillar or more complex structures. Properties mentioned above, also, facilitated fabrication of high AR features and fibrils, in some cases up to 100 [77]. Arrays of both microholes and micropillars have been fabricated. Microholes are mostly used as the master mold for replication of polymer structures [78–83] (figure 3-14-B). However, rigidity of SU-8 micropillars has also been utilized for fabrication of soft elastomeric microholes. In two different reports, replicated PDMS microholes were used as a flexible master mold for fabrication of second polymer replica, i.e. PU or epoxy)[84], [85] (figure 3-14-C and D).

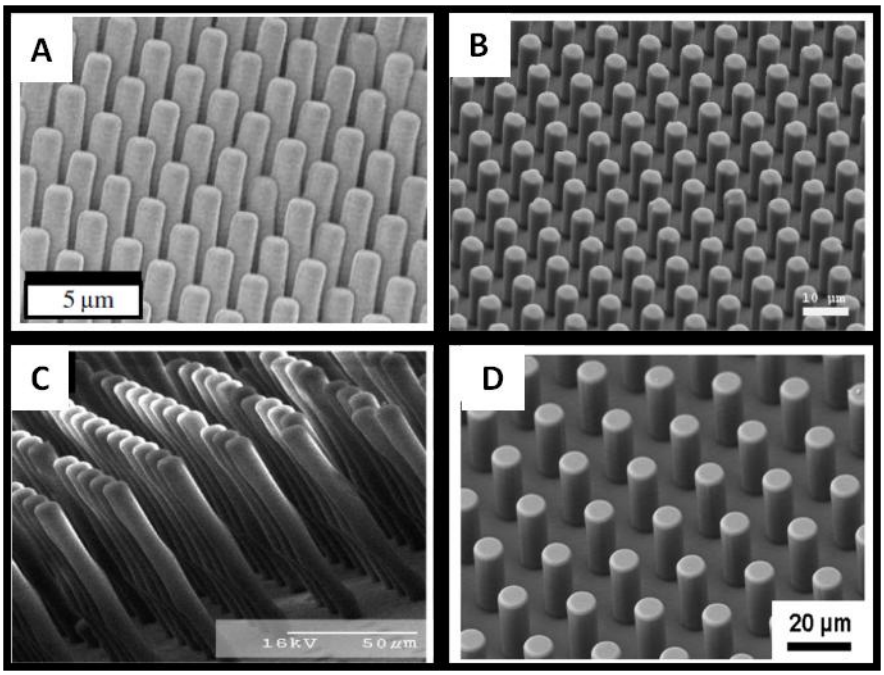

Figure 3-14: PDMS micropillars fabricated through soft lithography of DRIE prepared master-molds from (A) [72], PDMS pillars from SU-8 master-mold from[78] (B), SU-8 micropillars from [84] (C), and epoxy micropillars from SU-8 master mold[85].

In another work, Shahsavan et al. directly used rigid SU-8 micropillars to enhance conformal adhesion to soft elastomers[82]. Even though fabrication of high AR microholes and micropillars was viable by SU-8, there are some shortcomings. Extreme stiffness of the SU-8 micropillars does not allow elastic deformation and consequently elastic energy dissipation. This causes debilitation of adhesion in spatular contact with the mating surfaces [82]. Since soft polymers such as PU and PDMS are used commonly as the replicas, achievement of high AR pillars is impeded. That is, condensation and collapse of soft pillars would take place beyond a critical height[71], [72]. Also, peeling off the replicated polymer would be cumbersome by increase in AR of the structures [82]. Accordingly, alternative materials were suggested to be used in molding based fabrication methods. For instance, Suh and his coworkers proposed a novel capillarity-driven rigiflex lithography aided method of fabrication [86]. They combined this method with stretching of the formed pillars in temperatures higher than glass transition temperature. They used PMMA and PS instead of soft polymers to prevent collapse and condensation of the nanopillars. The fabrication was performed in the feature sizes lower than 100 nm. However, their procedure required e-beam lithography of silicon

positive master mold in the first place, followed by casting of PUA as the flexible negative master mold. On the contrary all other active groups, they placed their master mold up-side-down on the spun solidified polymer. Then they heated the polymer to temperatures above the glass transition temperature and used vacuum to assist capillary rise in the PUA cavities[87], [88].

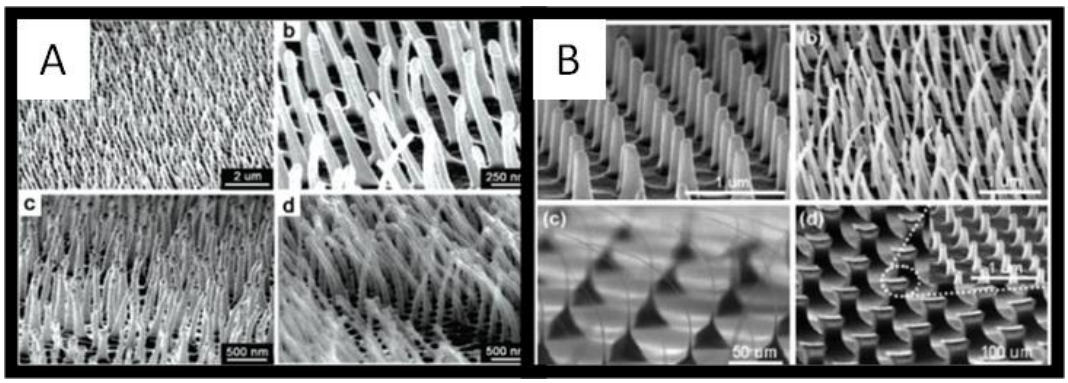

Figure 3-15: Structures fabricated through capillary assisted soft lithography, (A) from[86], and (B) from [87], [88]

3.3.1.3 Geometry variation of fibrillar structures

High adhesion strength and smartness of the surface could not be achieved only by fabrication of simple straight pillars. Although very high aspect ratio pillars might enhance adhesion or shear, they lack expected functionality of gecko toe pads. Such a structure inherently suffers from low contact area with mating surface. Also, straight pillars do not indicate anisotropicness in adhesion, which is the main reason of smartness. Another issue for simple straight pillars is roughness adaptability and higher level of deformability, which only could be achieved through a hierarchical structure. Owing to these facts, several reports have been focused on fabrication of micropillars possessing these properties.

Kim et al. fabricated polyurethane micropillars with spatulae tips via DRIE method followed by soft lithography technique. The spatular tip shapes were fabricated using isotropic etching followed by DRIE. Their structure demonstrated macroscale adhesion pressures up to 18 N/cm^2 for a preload pressure of 12 N/cm^2[73], [89], [90] (figure 3-16-A). The similar technique was implemented by other groups[91–93] (figures 3-16-B-D).

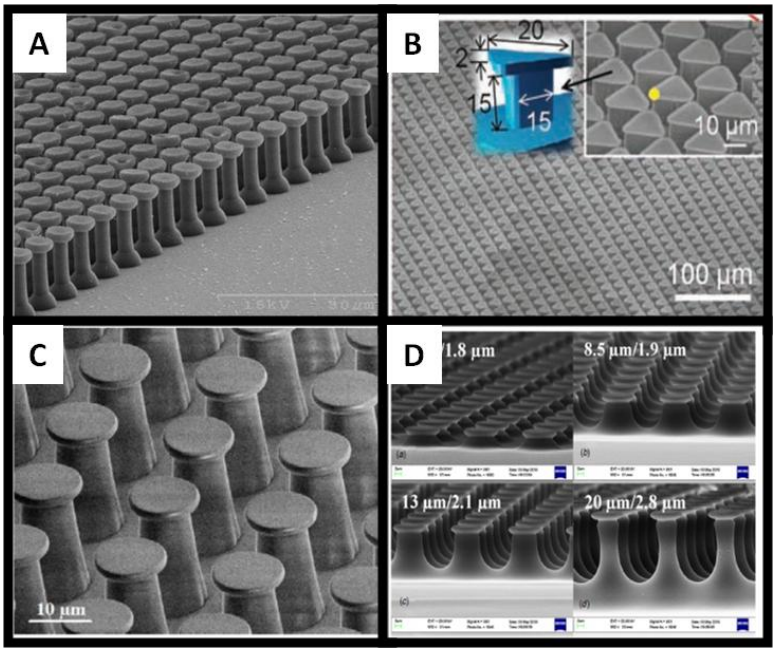

Figure 3-16: Mushroom shape terminated PDMS micropillars, (A) from[73], (B) from[74], (C and D) from [91-93]

del Compo and coworkers introduced a novel method of fibre tip fabrication in 2007. The method is based on consecutive inking and stamping using elastomeric precursors with various viscosities and cross-linking kinetics (figure 3-17). Different tip shapes, such as symmetric and asymmetric spatular, spherical, concave, and hollow tubes were fabricated through this method[94]. Within these structures, asymmetric spatular structure and symmetric spatular structure (mushroom-shaped) enhanced the adhesion remarkably. These structures resemble the gecko spatular structure. Also, JKR pull-off force of the concave structure increased to higher levels comparing in higher preloads. This was attributed to the micro-suction effect in the contact interface. Comprehensive study on the effect of tip shape and pillars geometry has been conducted in their following papers[83], [95].

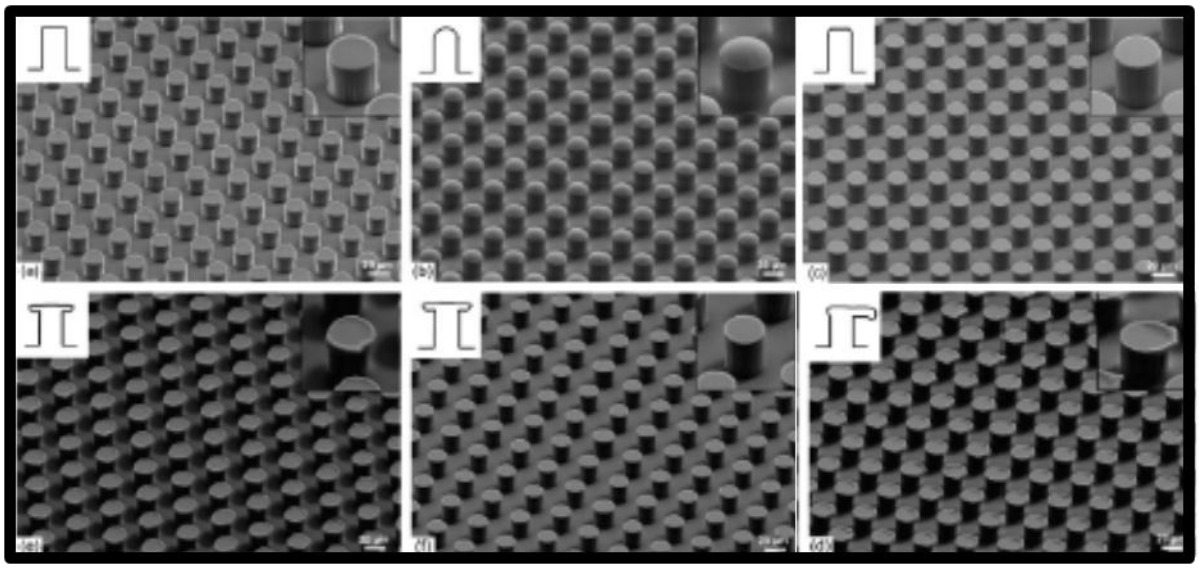

Figure 3-17: PDMS micropillars with different tip shapes fabricated through inking-printing method[94]

In 2007, Sitti's group used tilted UV-lithography of SU-8 to fabricate slanted micropillars. Using Snell's law, they calculated the 45º angle of UV exposure to obtain 25º slanted SU-8 micropillars[84], [96]. As the tips of the fibres were not embroidered with spatular or mushroom-shaped structures, adhesion did not enhance. Following this study, they coupled their method to del Compo and Arzt's technique to fabricate slanted spherical and spatular tip shaped micropillars. As a result, they obtained 23-fold adhesion enhancement and 4.6 times friction increment on spatular tip shaped micropillars comparing to the values obtained on flat samples (figure 3-18-A and B)[97].

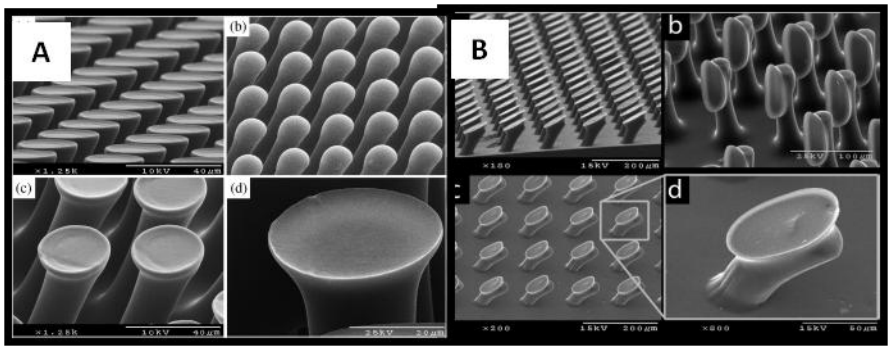

Figure 3-18: Anisotropic mushroom shape terminated pillars, (A) from [97] and (B) from [96]

Greiner and coworkers tried to fabricate double level hierarchical micropillars. They fabricated master mold out of SU-8 through a two-step lithography technique. PDMS micropillars with two levels of hierarchy, then, were fabricated through soft molding technique. The resulted structures substantially decreased the adhesion. They attributed this decline to decrease in contact area with the indenter tip(figure 3-19-A)[98]. Jeong et al. combined their micro capillary assisted lithography technique with slanted etching and isotropic etching. As a result they obtained hierarchical structures with straight pillars in base and slanted mushroom-shaped nanopillars on top. To attain slanted nano-holes, they used Faraday cage to guide the plasma in RIE. The hierarchical nanoscale patterns maintained their adhesive force even on a rough surface (roughness < 20μm) because of an increase in the contact area by the enhanced height of hierarchy (figure 3-19-B)[99]. Finally, Murphy and coworkers fabricated two and three level hierarchical micropillars with mushroom shaped tips and slanted geometry. They utilized the inking and stamping technique for fabrication of tip structures in the first level. For the smallest feature, they used isotropic etching of silicon to fabricate mushroom shaped tips. Using stamping they let the liquid polymer on the tip of larger pillars penetrate to the smaller pores. To safely remove the smallest mushroom shaped structures, whole master mold was etched away. They obtained remarkable adhesion enhancement through this method. However, 400 μm base pillar diameter was far greater than the scales that gecko setal arrays possess (figure 3-19-C) [100]. Another simple method of fabrication of hierarchical structures was introduced by Zhang et al based on capillary assisted soft lithography of SU-8. In fact, heating of SU-8 to temperatures higher than glass transition temperature allowed capillary rise of flat SU-8 thin films in holes with different scales[101]. However, they did not study interfacial properties of this structure.

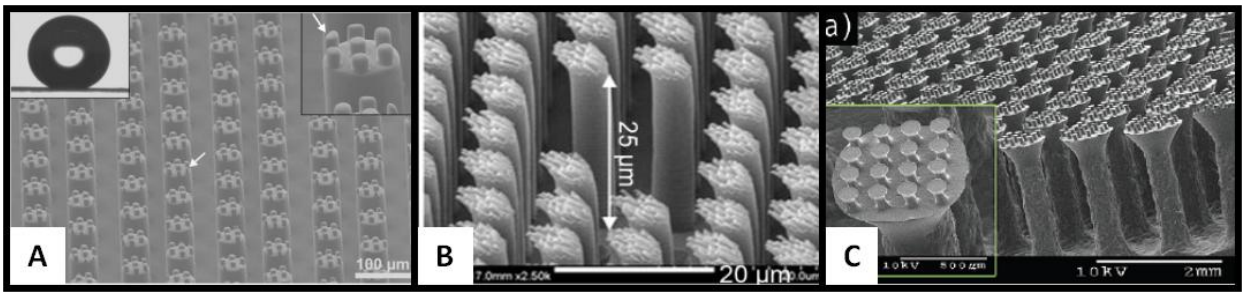

Figure 3-19: Hierarchical micropillars, (A) from [98], (B) from[99], and (C) from[100]

Chapter 4
Dry adhesion properties of biomimetic patterned surfaces

4.1 Introduction

Strength and toughness of an adhesive are studied both in making contact and separation. Intuitively, an adhesive must have an intimate contact with the adherent to maximize the possibility of the intermolecular interactions. The uniformity of the stress in making contact also is important as a stable contact is more difficult to break than an unstable. On the other hand, the process of decohesion should be delayed together with energy dissipation to realize the conditions of a good adhesive. Generally, adhesive property of a fibrillar surface is result of a competition between two parameters: adhesion attenuation due to reduction of contact area and adhesion enhancement due to increase of energy dissipation. Several mechanisms have been developed addressing adhesive properties of fibrillar materials from mentioned scopes of view. There exist mechanisms with contact mechanics approach, where the contact area and uniformity of the stress in contact are the major issues. There also exist fracture mechanical mechanisms referring the potential role of fibrillar structures in maximization of the energy dissipation during detachment cycles.

Surface splitting theory is one of the most renowned contact mechanical mechanisms. Using the basic principles of contact mechanics, this mechanism quantitatively explicates the effective role of splitting up a contact into finer sub-contacts in overall adhesion enhancement. This theory uses the proportionality of the adhesion force to linear dimension of the contact in JKR theory ($\boldsymbol{F_{pull-off} = \frac{3}{2}\pi R\gamma}$). It suggests that splitting of a contact to n sub-surfaces (setae structure in insects and animals) would increase the length over which adhesive force is defined to $\boldsymbol{R/\sqrt{n}}$. Thus, the total adhesion force would increase to $\boldsymbol{F'_{pull-off} = (R/n).F_{pull-off}}$. Consequently, it was used to justify the reason why the density of the setae structure on the locomotive organs of the animals is inversely proportional to their body weight[36], [52], [102].

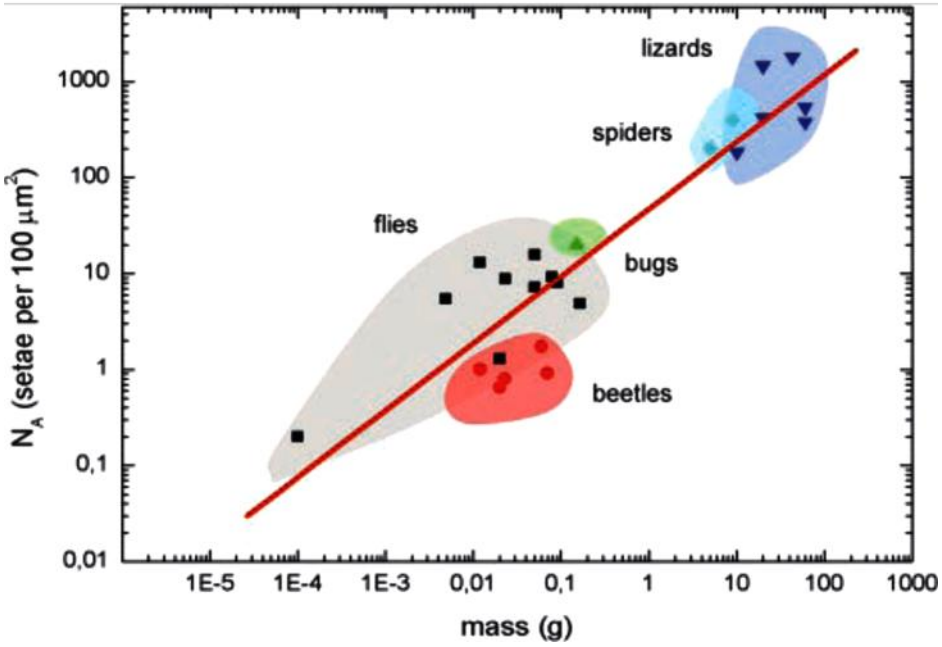

Figure 4-1: Dependence of the terminal element density of the attachment pads on the body mass in animals possessing hairy-pad [36]

According to Federle [35], this theory is not practically adequate as it inherently assumes that the pull-off stress is uniformly distributed over all of sub-contacts and all bonds break simultaneously. This does not take place in reality specially when the peeling is the main mechanism of detachment and all of the stress is concentrated on the peel front to propagate the crack. In fact surface splitting pull-off force might be overestimating as Hui has shown that equal load sharing could happen for only a small number of fibrils nearby the peel front[72].

Enhancement of compliance of the material is another mechanism discussed about adhesion properties of fibrillar structures. Based on this theory, fibrillar structures enhance the compliance of the surface and make it more adaptable to rough surfaces. Besides, deleterious effect of surface roughness in dwindling contact area could be compensated by deformation of the fibres in different directions[27], [29], [103]. Hui and coworkers have theoretically shown that the work of adhesion linearly increases with the compliance when the compliance is large compared with the roughness-height standard deviation [104]. As the extension of this theory, hierarchical structure of the animal toe pads has been modeled as a spring foundation composed of several parallel springs in a level

connected in series to other levels. This arrangement has been shown to reduce the spring stiffness effectively leading to higher surface adaptability [40], [105–107]. In addition to healing the imperfections in contact, more compliant fibrillar structures could be deemed as an elastic energy dissipation modulator. That is, strength and toughness of a fibrillar adhesive has been proved to be greater than that of a smooth adhesive in decohesion. As a result adhesion enhancement could be expected through maximization of the contact area. [71], [108], [109].

Other mechanisms include fracture mechanics models. In this category, processes of crack initiation and propagation in detachment of a fibrillar surface are compared with such events on smooth surfaces. The amount of energy dissipation through crack propagation instabilities is deemed to be higher in fibrillar surfaces. This model is based upon Griffith criterion of crack propagation. A crack will propagate through the bulk of a material when the elastic energy release rate is at least equal to energy the required to create two new surfaces. This happens once the crack length exceeds a critical length introduced by Griffith [21]. This criterion has been used to interpret the detachment mechanism taking place in a fibrillar surface. When the scale of the material is comparable to or smaller than the critical crack length described by Griffith, the adhesive strength increases and may come close to the maximum theoretical strength of the interface[108]. It is believed that a material with comparable size to the critical crack length can act as a crack trapper.

Jagota et al. have explained this process in a 2D modeling peeling process. In case of a smooth adhesive tape being peeled off, the energy dissipation would be equal to interfacial release rate per unit area of the adhesive. This, actually, fulfills the assumptions of Kendall peeling model in which stretching of the backing material is hindered by its elasticity and energy dissipation is localized to assist movement of the peel front [110]. However, the stored elastic energy in fibrils of a fibrillar surface is not released back to the bulk of material and is being lost. This is postulated as the spatial path for energy transfer is obstructed by inter-fibrillar space. As a result the energy transfer would choose the further distance in the bulk of the backing material requiring more energy dissipation[108].

Later on, Glassmaker et al. experimentally validated the crack trapping phenomenon in thin film terminated micropillar structures. According to their observation, the crack front is intermittently trapped and released unstably when facing a fibril in its pathway. This term is renowned to contact

line pinning in which the contact front is pinned between two surface protrusions. To elaborate, crack propagation is stable when the rate of energy release rate is negative ($\frac{dG}{dl} < 0$) and it is unstable when this rate is positive ($\frac{dG}{dl} > 0$), where *G* is the elastic strain energy released locally from the material adjacent to the crack tip and *l* is the crack length (figure 4-2)[111]. If we use contact radius instead of crack length, the sign of the derivative would be reverse as assumed in [112], [113]. The stable crack propagation does not require further external energy to develop the crack, whilst unstable crack propagation requires aid of external stress to move the crack front. The periodic nature of the fibrillar structures result in a periodic process of energy storage and dissipation which is analogous to the phenomenon of lattice trapping of a crack which has the consequence of enhanced work of fracture and irreversibility [111]. The same mechanism has been utilized by Crosby and his coworkers studying the potential role of pancakes, holes, and chemical patterns in tuning of the adhesion [112], [114], [115].

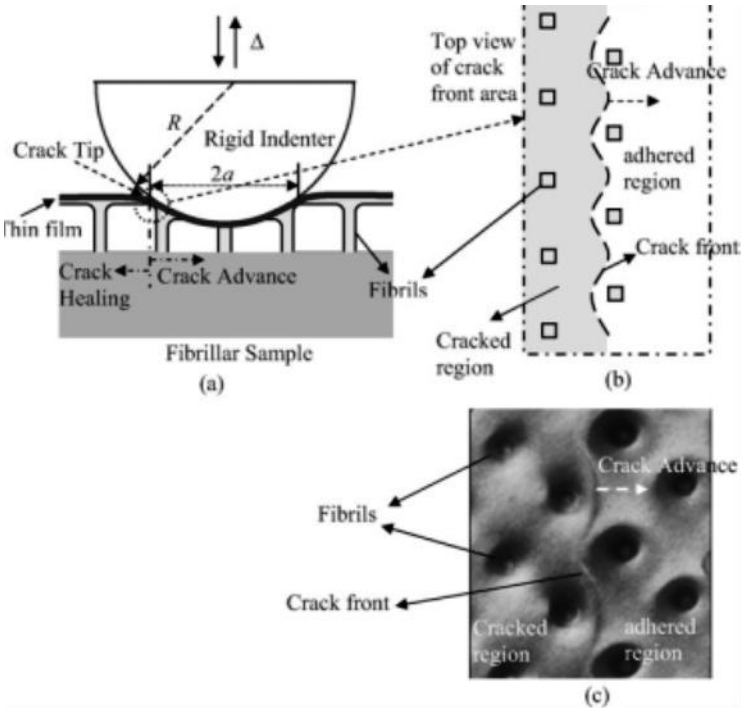

Figure 4-2: Crack bulging and instabilities during an indentation test reported by **[111]**

For the special case of the thin film terminated fibrillar structures, the required energy for propagation of the crack trapped between fibrillar could not be achieved from the thin film topped on pillars. This

fact causes extra energy dissipation due to deformation of the thin film and accordingly more pronounced adhesion enhancement.

4.2 Experimental

Master-molds consisted of arrays of micro-holes made on silicon wafer were fabricated through DRIE technique in Western Nanofabrication Facility, ON, Canada. The holes were arranged in a hexagonal lattice of circles with 50μm in diameter, having a center-to-center spacing of 115μm and 150μm in depth. Fabrication of micropillars was carried out via conventional soft-lithography technique using PDMS as the final replica. To do this, PDMS elastomer kits (Sylgard® 184, Dow Corning) were used to prepare a 10:1 weight ratio mixture solution of resin and curing agent. A certain amount of solution was poured on the silicon master-molds to maintain the thickness of the elastomer films constant. The PDMS coated master-molds were kept at 120°C for 1 hr to be cured. Once cured, the PDMS films containing the micropillars were peeled manually from the master-molds. To decrease the effect of timing on the mechanical properties, fabricated samples were kept at least one week in desiccator prior to testing. To avoid any defect to the pillars during the peeling, all of the master-molds were coated with Self Assembled Monolayers (SAM) of heptadecafluoro- 1,1,2,2, tetrahydrodecyltrichlorosilane (Gelest Inc. MA, USA) through the method described in [116]. The final thickness of cured PDMS films was controlled to be 1000 ± 100μm. The structure of fabricated micropillars was characterized by optical microscope and scanning electron microscope.

Dipping method developed in [111] was used to fabricate thin film terminated pillars. For this purpose, a thin layer of PDMS was spun on a low surface energy microscope glass slide. The reduction of the surface free energy was achieved by coating a SAM of heptadecafluoro- 1,1,2,2, tetrahydrodecyltrichlorosilane on glass as described earlier. The thickness of the thin film was controlled through adjustment of spinning time and speed. 3gr of liquid PDMS mixture was dispensed on the microscope slide and spun 30s with specific speed. Figure 4-3 illustrates the PDMS spin curve obtained through mentioned protocol. Thickness of the thin films was measured using optical interferometer microscopy.

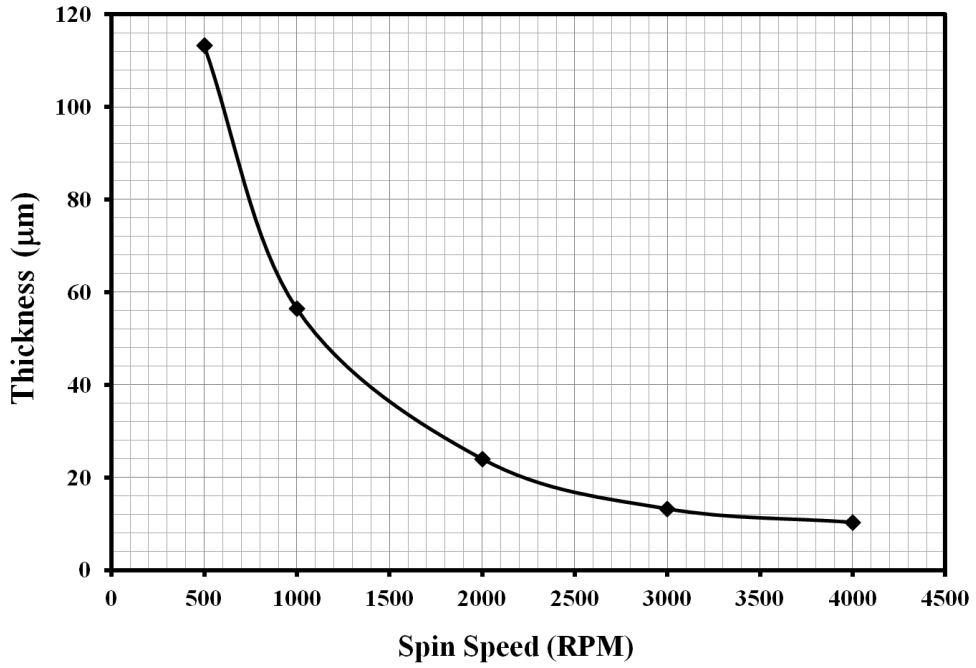

Figure 4-3: Variation thickness of the PDMS thin film via variation of spin speed

Afterwards, fabricated micropillar arrays were placed up-side-down on the thin PDMS layer. A small load, usually ca. 7gr, was applied on the pillars to ensure realization of the contact between pillars tips and thin film. The whole system was placed in oven for 1hr at 120°C and the cured sample was peeled off gently. To investigate the effect of viscoelasticity of the terminal thin film, the ratio of the resin to curing agent was increased from 10:1 to 25:1. All of the procedures to make a thin film terminated micropillar array were repeated and conditions were maintained constant for repeatability of the data. The schematic procedure of the fabrication has been shown in figure 4-4.

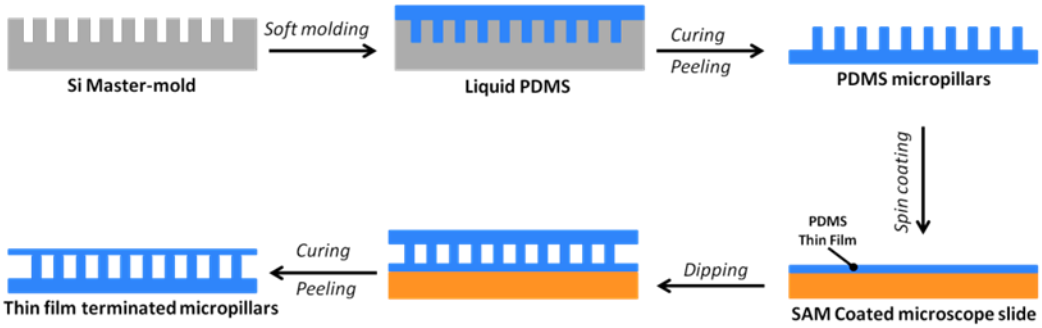

Figure 4-4: Process of soft-molding followed by dipping for fabrication of thin film terminated pillars

A series of indentation tests on micropillars was performed by a custom made indentation set-up using a 6mm diameter hemispherical fused silica UV grade (Ispoptics Co., NY, USA). The indentation set-up was equipped with an inverted optical microscope. The indentation tip was washed with ethanol and treated with UV-Ozone for two hours before running experiments. Indentation was carried out in displacement controlled mode with velocity of 1μm/s and different preloads. The pull-off force and vertical displacement were recorded during the tests to determine the adhesive properties of the samples.

4.3 Results

Figure 4-5 shows the structure of fabricated micropillars without and with terminal thin film. Two different thicknesses were chosen to study the effect of thickness of the terminal film on the overall adhesion strength. Figure 4-5-A indicates the micropillars before covering with thin film. Figure 4-5-B is the structure of micropillars terminated by a thin film of thickness 25μm. The spin speed for this sample was 1800 RPM. Figure 4-5-C indicates the same structure but with thin film thickness of less than 10μm. The spin speed for this sample was 4000 RPM. The surface defect for simple pillars array and also thin film terminated structures could be inspected visually and was approximated less than 5%.

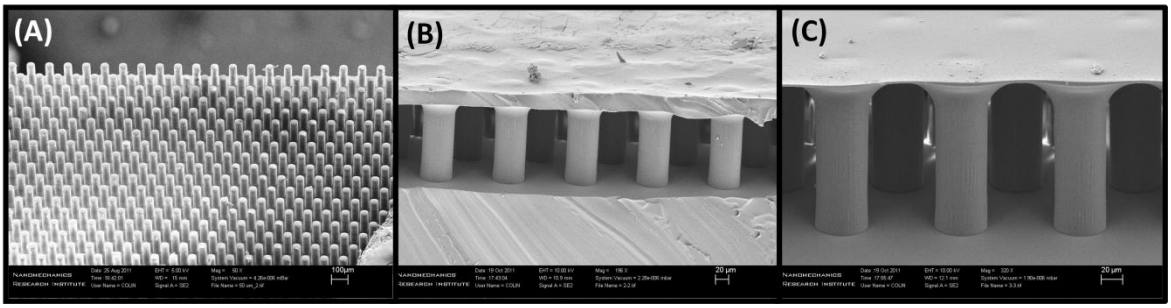

Figure 4-5: Micropillars with 50μm diameter and 150μm height (A), micropillars topped with thin film 25μm in thickness (B), and micropillars topped with thin film 10μm in thickness (C)

Typical force vs. displacement curves for indentation tests with 25mN preload on the prepared samples are depicted in figure 4-6. As it is expected, patterning of the polymer with simple

micropillars dramatically decreased the pull-off force. However, both adhesion hysteresis and pull-off force are increased substantially by introduction of the thin film on the top of the pillars.

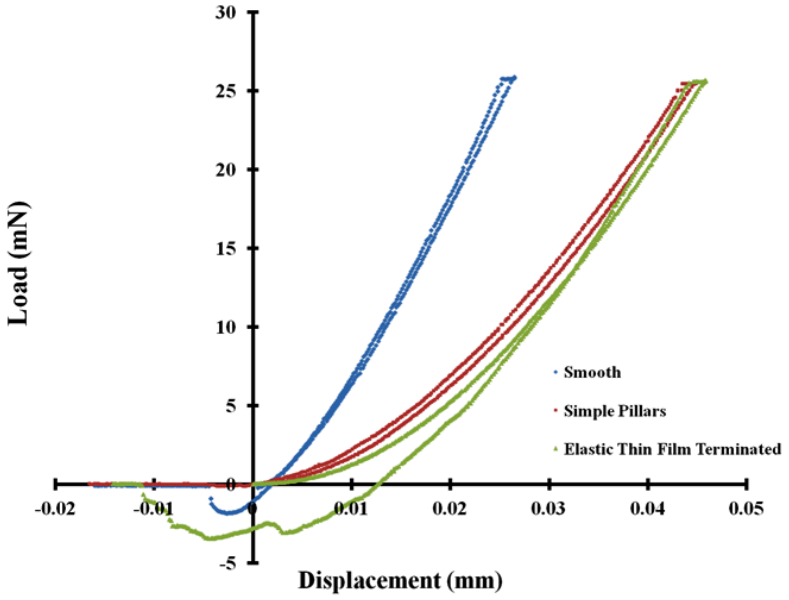

Figure 4-6: Typical load vs. displacement curve for indentation tests on different fabricated samples

Pull-off force for the smooth control sample, simple pillar structures, and pillars covered with terminal thickness of 10μm could be accumulatively compared in figure 4-7.

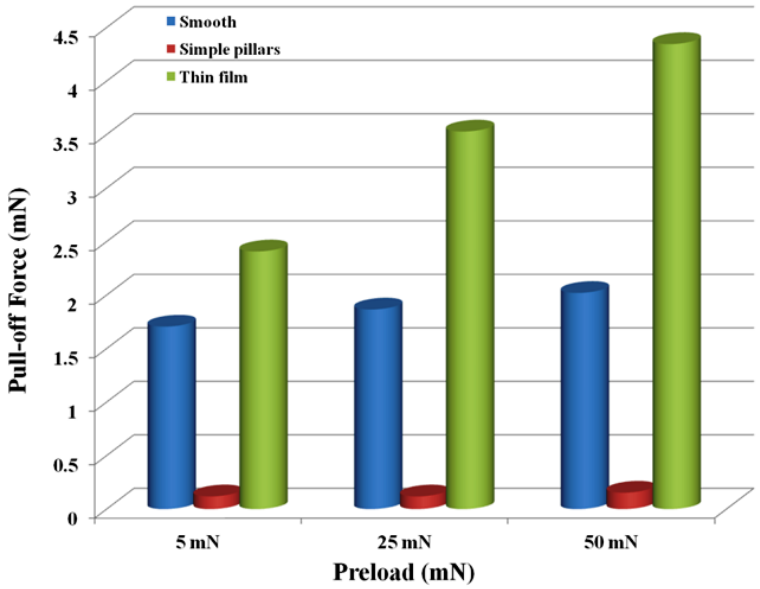

Figure 4-7: Comparison of the pull-off forces for the smooth control sample (left bar), simple micropillars (middle bar), and 10μm thin film terminated pillars (right bar) for different preloads

To study the effect of terminal film thickness on the adhesion, micropillars were topped with a thicker thin film. The thickness of this film was around 25μm. Pull-off forces for the samples with thinner terminal thin film are apparently greater than those of pillars covered with thicker films (figure 4-8). The film thickness has a key role in propensity of the thin film deformation and elastic energy dissipation. In fact, thinner the film, more elastic energy dissipation could be achieved [111], [117], [118].

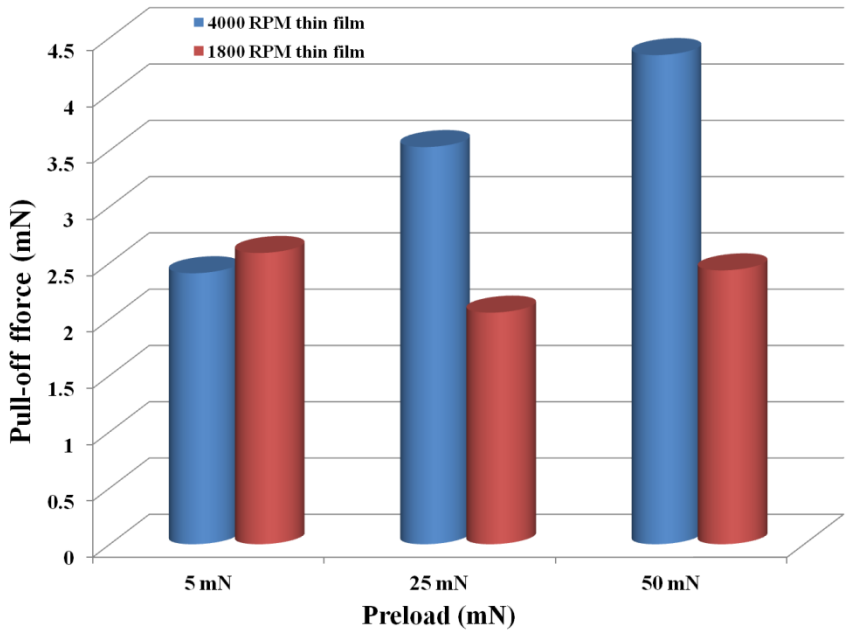

Figure 4-8: Effect of thickness of the terminal film on the pull-off force, thinner film (left bar), thicker film (right bar)

To study the effect of viscoelasticity of the terminal film we chose the lower thickness to repeat the experiments but with 25:1 resin to curing agent ratio this time. As expected, introduction of a viscoelastic thin film increased both pull-off force and adhesion hysteresis drastically (figure 4-9).

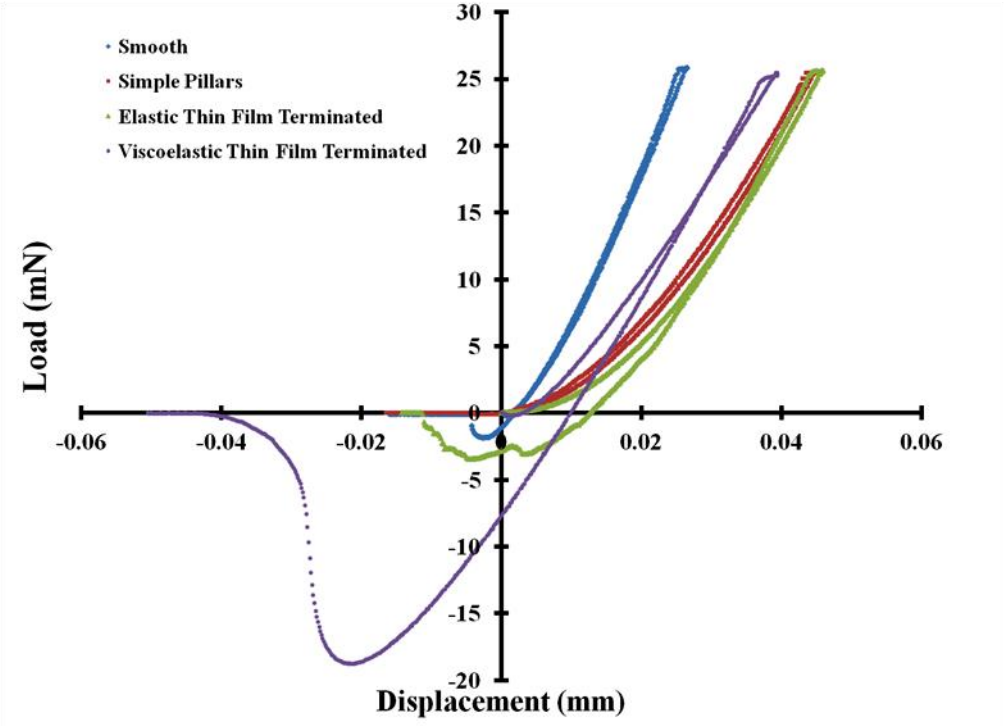

Figure 4-9: Typical indentation curves for four different fabricated samples

Through all of the methods tested in this study, viscoelastic thin film terminated pillars had the greatest adhesion and simple micropillar structures had the lowest adhesion (figure 4-10).

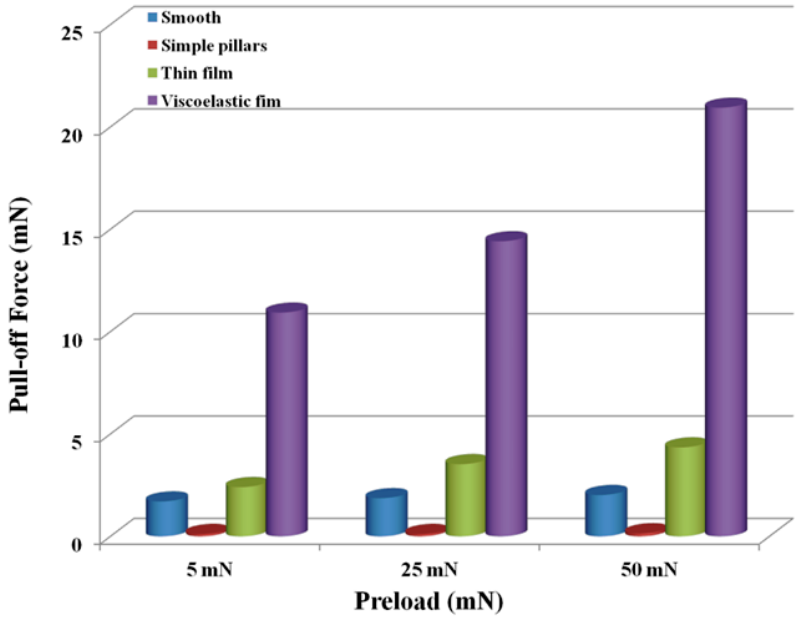

Figure 4-10: Comparison of the pull-off force for the smooth control sample (last left bar), simple micropillars (second left), 10μm thin film terminated pillars (right bar), and viscoelastic 10μm thin film terminated pillars (last right bar) for different preloads

4.4 Discussion

Propensity of the biomimetic patterns to fine tune the adhesive properties of the materials has been well addressed in the literature. It could be concluded that final adhesive properties of a material embroidered with such structures is the result of a competition. In one hand, patterning of the surface causes drastic reduction of the real contact area. On the other hand, there are other mechanisms such as crack arrest in surface and subsurface of the material, surface splitting, and compliance enhancement which increase the adhesion strength and toughness. In fact, competition is between reduction of the contact area and all energy dissipative mechanisms present in such a structure.

Thin film terminated micropillars have been introduced as a promising mean to increase the dry adhesion properties of polymers[111], [117], [118]. This method eliminates the detrimental effect of contact area reduction on adhesion of the material, while increases the deformability and compliance of the material near the surface. The main reason behind adhesion enhancement is periodical nature of energy gain and dissipation as crack propagation instabilities taking place between pillars. During the process of crack trapping the terminal thin film is the only alternative for the energy transfer. Thus,

excessive elastic energy dissipation could occur in the surface. As the crack trapping mechanism only takes place on the subsurface level of the material, the dissipation of the energy in mushroom shaped pillars is higher. The crack propagation instabilities on the surface level assists further dissipation of energy in mushroom shaped structures. In addition to these mechanisms, introduction of the viscoelastic thin film on top of the pillars remarkably enhances the dissipation of the energy in shape of viscoelastic losses. In fact, in addition to crack trapping in sub-surface, elastic energy dissipation in pillars and thin film, viscoelastic energy losses help to increase the adhesion. This could be considered as a combination of adhesion mechanism in dry fibrillar adhesives and one could be seen in pressure sensitive adhesives (PSAs).

4.5 Conclusion

A viscoelastic thin film terminated structure was fabricated through soft lithography followed by dipping method. In addition to the adhesion enhancement mechanisms associated with a thin film terminated structure, the viscoelastic energy dissipation of our structure has intensified the pull-off about 10 folds comparing to the smooth surface. Based on the report by Jagota and his coworkers, it is anticipated that the increment of the inter-fibrillar space would increase the adhesion of the purely elastic structure up to 9 folds. We believe that this manuscript is the first reporting such combination and results in the literature.

Chapter 5
Dry friction properties of biomimetic patterned surfaces

5.1 Introduction

Amonton's law of friction deems the linear proportionality of the friction force to the normal load in shear($\boldsymbol{F_t = \mu F_n}$)[119–123]. $\boldsymbol{\mu}$ is the coefficient of friction which equals to $\boldsymbol{tan\theta}$for simple static friction [119], [124], [125]. However, Bowden and Tabor noticed the existence of friction forces even in zero normal loads. They originally attributed this to the inherent presence of intermolecular and adhesive forces. They proposed the proportionality of the friction force to molecular real area of contact for extremely small loads and introduced the term of interfacial friction($\boldsymbol{F_t = S_c A}$). $\boldsymbol{S_c}$is the shear stress between two surfaces. The dependence of $\boldsymbol{A}$ to the normal load was well described by JKR model for adhesive contacts and Hertz model for non-adhesive contacts [119]. Later on, Homola, Israealchvili, and coworkers performed a subtle series of experiments on friction of two molecularly smooth mica surfaces by Surface Force Apparatus (SFA). They introduced a generalization of Amonton's law with the following form: $\boldsymbol{F_t = S_c A + \mu F_n}$. This model emphasizes on the effect of the range of normal load on the friction force. That is, for the boundary friction of rough surfaces with wear, it is anticipated that friction force follows the Amonton's law for the loads larger than the adhesion force between mating surfaces. On the other hand, if the friction is dominated by interfacial interactions, which most likely happens in case of the small normal loads, the Bowden and Tabor theory of friction could describe the system well. Accordingly, during the interfacial friction, the load interestingly would not be linearly proportional to the normal load. In Hertzian contact, instead, linear relationship would be between $\boldsymbol{F_t}$ and $\boldsymbol{F_n^{2/3}}$ or more generally, for the JKR contact, the friction would follow the contact area dependence on the applied load in JKR theory.

There are a large number of reports studying the effect of random roughness on friction, and biomimetic surface micro/nano-patterning on adhesion. Nonetheless, the proclivity of well-defined miniaturized patterns to modify the friction properties of the surfaces experiencing shear force is far less studied. In these studies, the validity of the basic principles of friction theories for two smooth surfaces in contact have been examined or modified for the patterned surfaces in contact. The effect of pattern geometry such as pillars size and spacing, pillars tip shape, and anisotropic friction in terms of pillars tilting angle has been studied under different applied normal force and friction

velocities[60], [66], [68], [81], [96], [118], [125–139]. Simultaneous measurement of contact area through different methods has been accomplished in some other works[60], [68], [125], [127–129], [133]. These all have been studied in the framework of the fundamental friction laws, such as Coulomb's and Amonton's laws, and Tabor and Bowden model of friction.

It is expected that the patterning of materials surfaces with bio-mimetic structures, such as micropillars or fibrils, would decrease the friction due to decrease of real contact area. For instance, Varenberg and Gorb have studied the influence of surface patterning of the compliant PolyVinylSiloxane on friction. They observed a remarkable reduction in both coefficient of friction and pull-off force in shear even though the pillars were mushroom terminated. As a result, they proposed that fibrillar microstructure could generate a binary on/off state in friction with surprisingly stabilized and minimized elastomer friction[128]. This result was supporting the report by Yoon et al., in which the effect of aspect ratio of PMMA nano-pillars on friction had been studied in various applied normal forces during the sliding [126]. They reported an overall decrease in friction coefficient of the patterned surfaces comparing to the smooth films. However, they observed increment of the friction with increasing the aspect ratio of the pillars which was attributed to the improvement in real area of contact. Hence, this trend intensified when the AR or the normal force exceeds the values in which the pillars experience bending leading to increase of contact area through pillars side-wall contact. This also could be buttressed by almost proportionality of real contact area to normal force for elastic contact of smooth and rough surfaces[121], [124]. In a similar study, but on the PDMS micro patterns, He et al. remarked that the overall reduction of real contact area is a consequence of surface patterning. The parameter changed in their study was center to center spacing of the pillars, which could be considered as an index for surface coverage by micropatterns. The aspect ratio of the samples could barely reach to 0.1. Although they did not measure the contact area in shear, they speculated theoretically that the nature of the friction for their system is interfacial friction. They tried to determine the contribution of adhesive interactions and mechanical deformation based on JKR model of contact in both micro and macro scales. They found that the sensitivity of the friction to the contact area is more pronounced for contact between macroscale probe and microstructured surfaces[130]. Wu-Bavouzet, indeed, counts this report as one of the studies in which the normal applied load is greater than the adhesive force between mating surfaces. This elucidates that the contact follows the non-adhesive limit of JKR model or nearly Hertz model[125]. As a key parameter, the effect of contact mode in most of the studies was not taken into account. In

continuation of the work by Verneuil and coworkers[140], Wu-Bavouzet et al. investigated the effect of contact mode on the friction of the micro-patterned PDMS surfaces[125]. Keeping the AR of the micro-pillars lower than 1.5, they scrutinized the friction behaviour in different normal loads and velocities with simultaneously measurement of the real area of contact. They varied the aspect ratio of the pillars systematically and used a critical length factor that under certain preload the contact mode shifts from laid or non-conformal contact to transient and finally conformal or intimate contact. Considering the Bowden and Tabors model of friction ($\boldsymbol{F_t = S_c A}$), they have postulated that the real area of contact is linearly proportional to the ratios of intimate and laid contact, i.e. $\boldsymbol{F_t = S_c(\mu A_{intimate} + \beta A_{laid})}$. In a rather more complex study, Shen et al. implemented a series of friction testing on the film terminated PDMS mirco-pillars. The center to center spacing between the pillars was the parameter changed during the experiments. The dramatic increase in static coefficient of friction was reported as a result of introduction of thin film on top of the pillars. The dynamic coefficient of the friction reported to be similar to the original value of the smooth surface. In fact, they have preserved the real area of contact by fabrication of a thin film on the top of the pillars; thus, the dynamic coefficient of the friction gas been proved unchanged. However, increment of spacing between pillars has dramatically enhanced the static coefficient of friction, which is attributed to propensity of the micro-patterns in crack arresting and crack propagation instabilities during the initial separation. Therefore, they maintain the real area of contact using the film terminated structures and the reduced stressed volume could be assumed as the main causes for this observation[118].

In this manuscript we aim to investigate the effect of surface patterning on the friction of the polymeric surfaces. The key parameters varied in our study are AR of the micropillars and preload during the shear. All of the three AR chosen for the pillars, 1.5, 3, and 4.5, are higher than ones studied in similar works[125–127], [130], [140]. The range of preloads during the shearing was selected from 1 mN to 75 mN. The experiments were coupled with imaging at the start of the shearing with CCD imaging system. By this, the initial condition of the micropillars before sliding and contact mode during the sliding was speculated. Finally, the obtained results were examined in the framework of the conventional theories of friction to elucidate the potential role of high AR micropillars in tailoring the frictional properties of the polymeric surfaces.

5.2 Experimental

Master-molds consisted of arrays of micro-holes made on silicon wafer were fabricated through DRIE technique in Western Nanofabrication Facility, ON, Canada. The holes were arranged to be in a hexagonal lattice of circles with 15 μm in diameter, having a center-to-center spacing of 30 μm and varied depths ranging from 22.5 μm to 68 μm. Fabrication of micropillars was carried out via conventional soft-lithography technique using PDMS as the final replica. To do this, PDMS elastomer kits (Sylgard® 184, Dow Corning) were used to prepare a 10:1 weight ratio mixture solution of resin and curing agent. A certain amount of solution was poured on the silicon master-molds to maintain the thickness of the elastomer films constant. The PDMS coated master-molds were kept at 120°C for 1 hr to be cured. Once cured, the PDMS films containing the micropillars wee peeled manually from the master-molds. To decrease the effect of timing on the mechanical properties, fabricated samples were kept at least one week in desiccator prior to testing. To avoid any defect to the pillars during the peeling, all of the master-molds were coated with Self Assembled Monolayers of heptadecafluoro- 1,1,2,2, tetrahydrodecyltrichlorosilane (Gelest Inc. MA, USA) through the method described in [116]. In this way, the final thickness of cured PDMS films was controlled to be 1000 ± 100μm. The structure of fabricated micropillars was characterized by optical microscope and scanning electron microscope.

A series of indentation tests on micropillars was performed via a custom made indentation set-up using a 6mm diameter hemispherical fused silica UV grade (Ispoptics Co., NY, USA). The indentation tip was washed with ethanol and treated with UV-Ozone for two hours before running experiments. The indentation set-up was equipped with an inverted optical microscope. The behaviour of the micropillars under different preloads was monitored and studied prior to the friction testing. Simple friction tests were performed by a Nano/Micro Tribometer (CETR-UMT-2, Bruker, CA, USA) using the same indentation tip (figure 5-1). Two different load cells were used to detect low and high forces. The nominal working range for the more delicate load cell (FVL) was from 1 to 100mN with the resolution of 10μN. Loads higher than 100mN were detected by another load cell (DFM-1) with working range of 100mN to 10N with the resolution of 0.5mN. Normal loading was carried out at a constant displacement rate of 1μm/s in vertical direction, with preloads ranging from 1mN to 75mN. Once the desirable preload reached, the sliding of the sample beneath the glass probe started and the lateral force was measured by the load cell. The sliding velocity was kept constant at 10μm/s for all experiments with 2mm stroke in one direction. Local coefficient of friction for each

data point was measured automatically according to Amonton's law of friction. The experiments have been carried out at least four times on different spots on the samples.

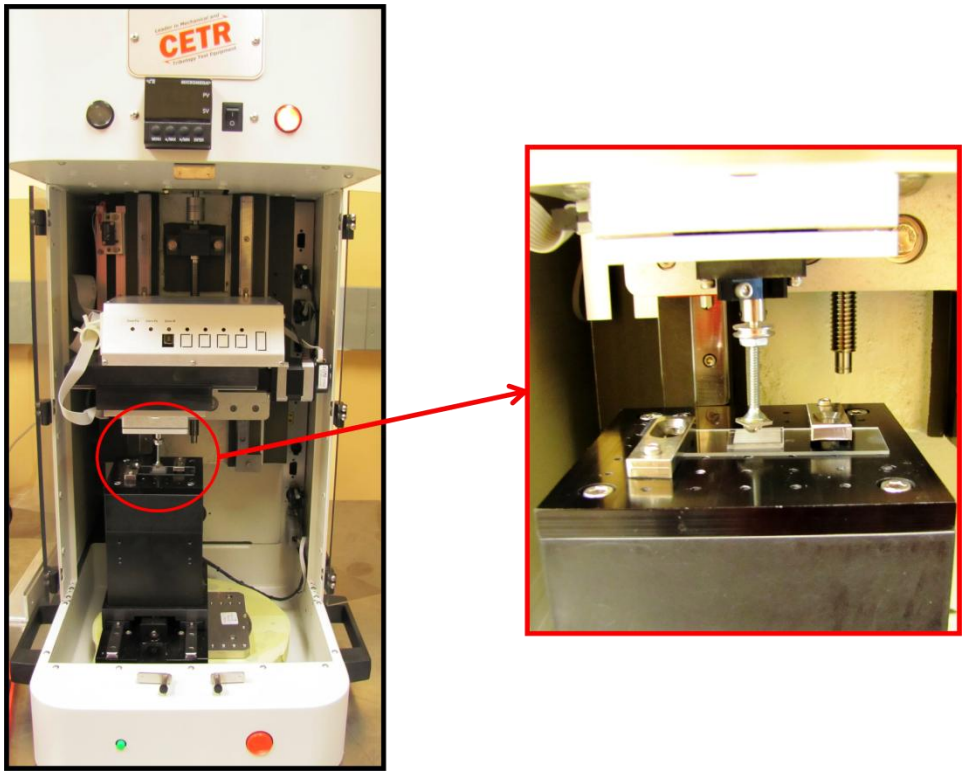

Figure 5-1: CETR universal material tester and close shot on the friction set-up

5.3 Results

Prior studies on adhesion of the biomimetic microstructured polymers revealed the determining role of AR in final response of the adhesives [64], [71], [72], [109], [115], [141]. Effect of AR on the friction also has been studied as a key parameter in several reports [126]. Nonetheless, the value and range of variation of AR were quite small comparing to the values and range of variation in this study. Figure 5-2 shows the structure of micropillars fabricated via soft molding method. The AR of the pillars varies systematically from 1.5 to 4.5 with an essentially constant center to center spacing of 30 μm and the diameter of 15μm. Equation below was used to determine the maximum height possible for PDMS pillars with the designed diameter in order to avoid condensation of the pillars[72].

$$\left(\frac{\pi^4 E^* r}{2^{11}\gamma_s}\right)^{1/12}\left(\frac{12Er^3S^2}{\gamma_s}\right)^{1/4} \geq h \qquad (5.1),$$

where $S$is the center-to-center spacing between pillars, $E^*$is the reduced Young's modulus of both indenter and sample, and E is the Young's modulus of the material. Accordingly, straight pillars were fabricated without any condensation.

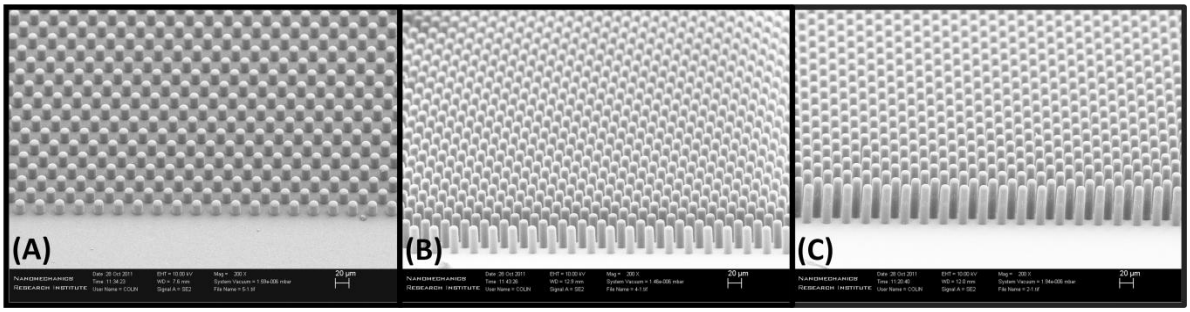

Figure 5-2: Micropillar arrays with different aspect ratios: (A) AR 1.5, (B)AR 3, and (C)AR 4.5

Prior to the friction testing, the pillars were undergone different normal loads in a series of indentation tests. The indentation tests were coupled with bottom view imaging of the contact area. Corresponding images from the geometry of contact and structure of the pillars under normal compression was captured and shown in figure 5-3-A-F.

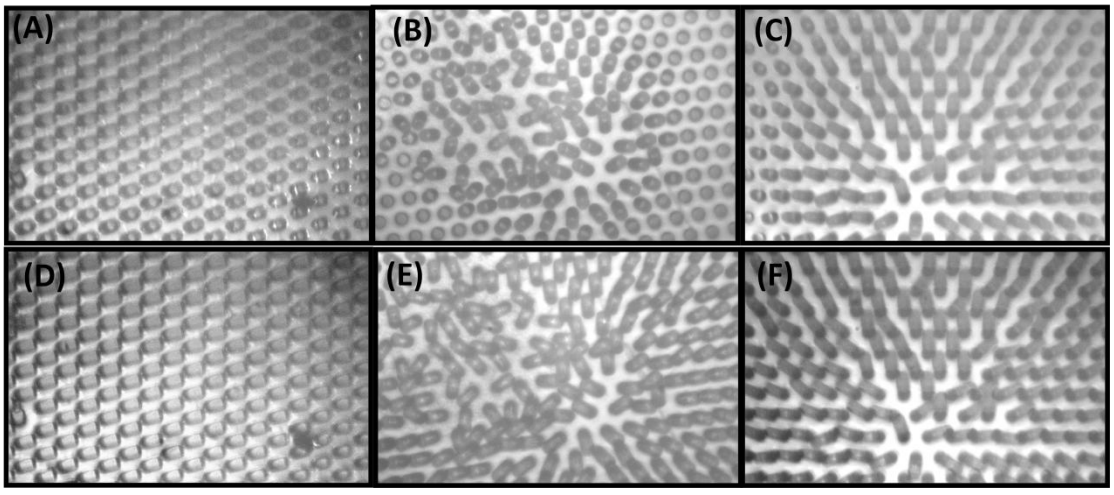

Figure 5-3: Beginning local buckling for pillars of AR 1.5(A), 3(B), and 4.5(C), Complete buckling in the monitored contact area for pillars of AR 1.5(D), 3(E), and 4.5(F)

Figures 5-4-A and B depict typical load vs. time graphs for a simple unidirectional friction test for micropillars with three ARs and compare them with the friction of a control smooth surface. Figure 5-4-A is for the tests with the lowest preload, i.e. 1mN, and Figure 5-4-B belongs to friction under highest preload, i.e. 75mN. Apparently, micro-patterning of the polymer has dramatically decreased the friction force and accordingly friction coefficient. The variation of friction force against change in AR is notable mostly between AR 1.5 and AR 4.5.

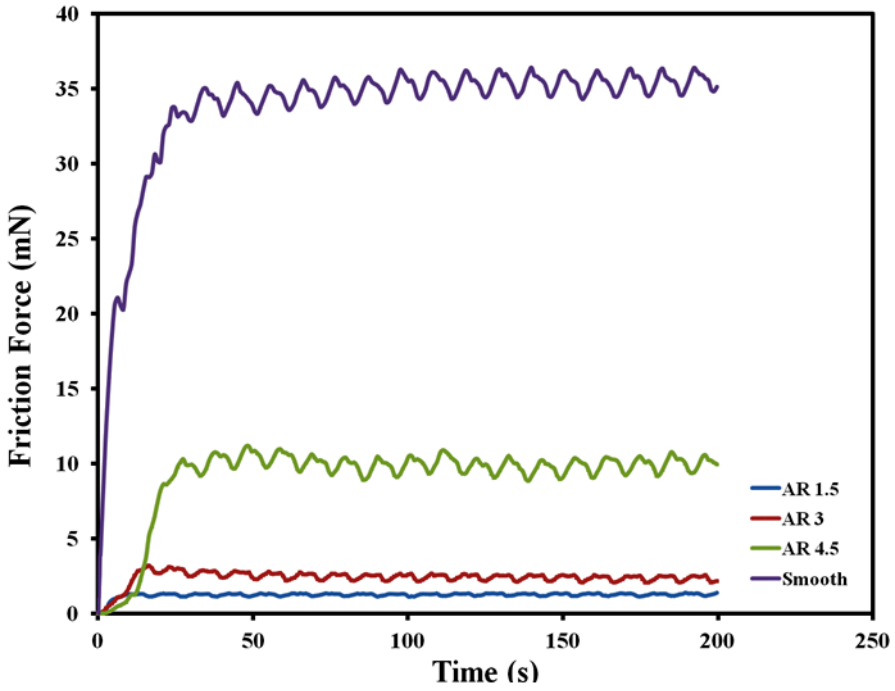

Figure 5-4-A: Load vs Displacement curve for friction test on pillars with different ARs under preload of 1mN

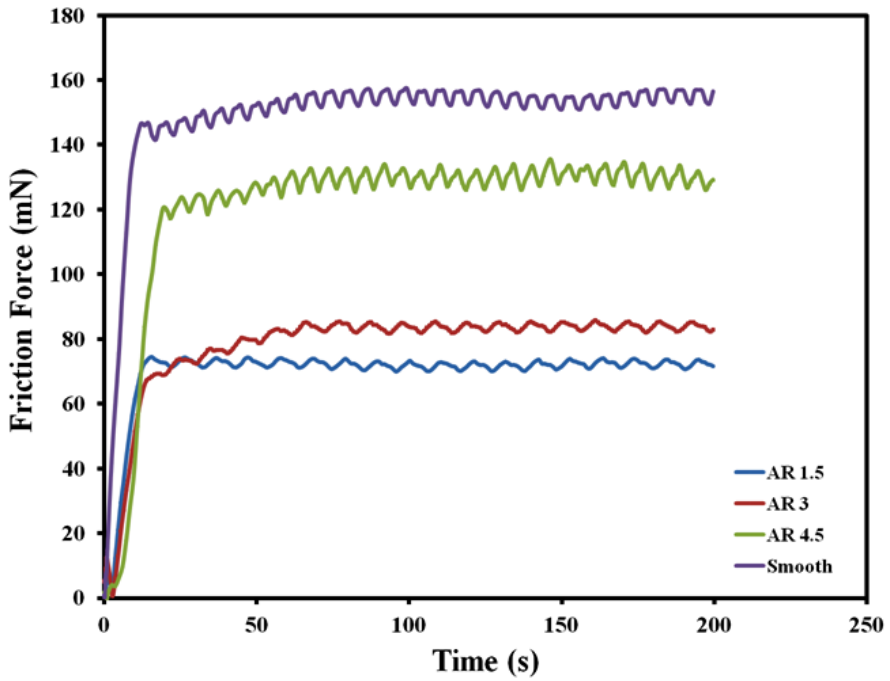

Figure 5-4-B: Load vs Displacement curve for friction test on pillars with different ARs under preload of 75mN

Dynamic coefficient of friction (COF) for the samples was calculated via two methods. In the first method, COF of each point was calculated and averaged over the steady friction force range. Figure 5-4 illustrates the variation of COF for different preloads. Alteration of the COF is leveled-off for preloads higher than 12.5mN. The values of the COF for samples with AR of 1.5 and 3 converged in preloads higher than 25mN.

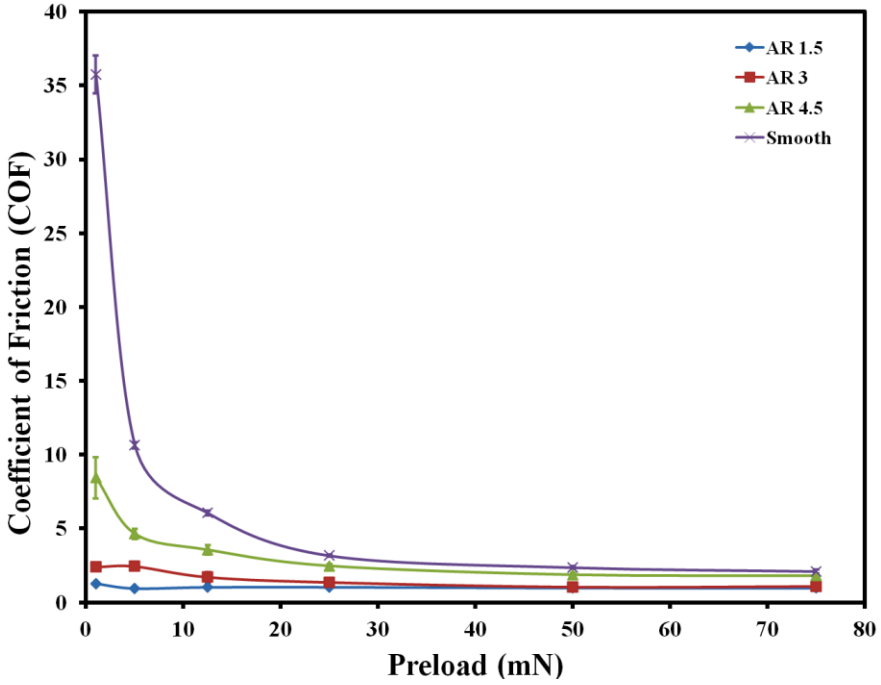

Figure 5-5: Variation of COF against change of preload for different samples

In order to calculate the COF based on Amonton's law of friction, a plot of friction force vs. preload was depicted in figure 5-5. The average of friction force for each data point over the range of steady friction was measured and used for this purpose. However, calculation of COF through this method neglects the potential effect of inherent adhesive forces acting between two sliding materials [126].

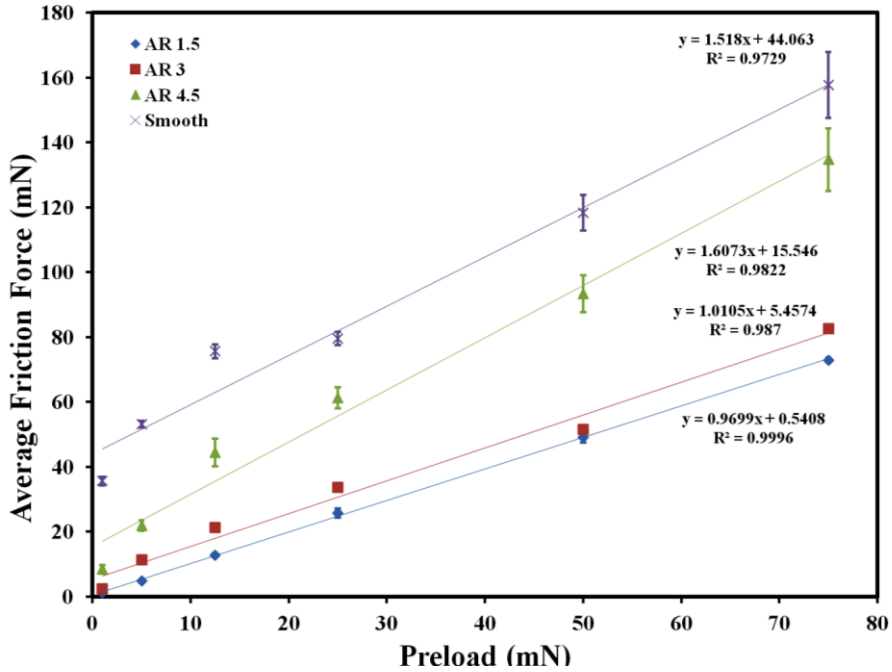

Figure 5-6: Fitting the friction data to the Amonton's friction law

5.4 Discussion

There exist several parameters affecting the friction of a system composed of two sliding materials. Some of the parameters are concerned with only one of the materials in contact, whilst some others are related to their interaction and interface. Roughness geometry and size, deformability and materials characteristic at the surface, and surface energy of the materials are the parameters in the first category. Ratio of the roughness size of two materials, amount of applied normal load during the sliding, sliding velocity, and adhesion or interfacial strength are the parameters for the whole system. To study the type of friction and effectively analyze the data obtained from a friction test, one should scrutinize all of the mentioned factors. Generalized form of Amonton's law of friction somehow encompasses all of these parameters:

$$F_t = S_c A + \mu F_n \qquad (5.2)$$

He's work is similar to our work, but the indentation tip, although comparable in size, is made up of steel which is less adhesive to PDMS. The AR of the pillars is 0.1 in that work, far less than what we have studied here[130]. The geometry and size of the patterns and the sliding speed is quite different

in Okamoto's report [127]. Kramer's work seems very close to our study, but they have confined their system to very low AR pillars to avoid bending and deformation of the microstructures [135]. Wu-Bavouzet et al. and Verneuil and coworkers have studied friction and adhesion of PDMS/PDMS systems. Also, the range of force and AR they have studied are far less than the values we have reported in this manuscript.

5.4.1 Overall decrease of friction: Effect of contact area reduction

Except Kramer's study, all other related works reported decrease in friction force as a result of decrease in real contact area. In fact, they assumed that the type of friction is interfacial friction based on [119], [120]. Karamer and coworkers observed an increase in friction and attributed it to the surface splitting theory developed by Arzt in 2003 [36], but in shear mode. The shear test in that work is implemented by microscope slides realizing a uniformly distributed force on the micropatterns. The normal force is set to zero; thus, the shear tests mostly resemble a 0^{o} peeling test.

Figure 5-4-A and B show a decrease of friction by introducing the patterns on the PDMS. Moreover, the linearity of the friction force to the normal preload could be seen in figure 5-6. Although this might be interpreted as common friction behaviour with wear following Amonton's law of friction, no conclusive statement could be made at this point. As a matter of fact, previous studies have postulated that the shear tests on PDMS smooth and micropatterned surfaces in a wide range of applied normal loads is interfacial friction[125], [127], [130], [135], [140], [142]. On the ground that there is no access to the simultaneously bottom view imaging we assumed the friction is interfacial with no wear. The SEM images after each set of friction tests also confirmed no remarkable plastic deformation or wear on the samples experiencing the forces up to 75mN.

Bottom view imaging was carried out prior to the friction testing to investigate the geometry and properties of the interface under certain preloads. As is can be seen in figure 5-2, there exists a contrast between the micropatterns and the surrounding area. This has been referred to presence of thin layer of air entrapped between surface protrusions and backing material. This results in a special mode of contact in which the indenter tip and the substrate have not made an intimate contact. In fact, the indenter tip has laid on top of the micropillars or is moving somewhere lower than the top but suspended [125], [140]. We used the formula developed by Verneuil et al. [140] as a theoretical evidence for the type of contact in our experiments. A critical height for the surface microstructures

has been introduced in which the mode of contact shifts from laid or suspended to intimate. This formula has been developed for zero applied normal loads by making a balance between interface deformation energy cost and adhesive energy cost. To elaborate, if the height of the structures is less than measured critical height, the adhesive force would be strong enough to deform interface in order to create a conformal contact which causes disappearance of patterns. In the following equation $\boldsymbol{h_c}$ is the critical height for transition of the mode of contact, $\boldsymbol{W}$ is the work of adhesion for the smooth surface against indentation tip, $\boldsymbol{r}$ is the radius of the micropillars.

$$\boldsymbol{h_c \sim \sqrt{\frac{W}{E^*} r}} \qquad (\mathbf{5.3})$$

By substituting the corresponding values for our system into the above equation, i.e. $\boldsymbol{W = 44\ \frac{mN}{m}}$, $\boldsymbol{E^* = 1.1 MPa}$ and $\boldsymbol{r = 7.5 \mu m}$ we obtain $\boldsymbol{h_c \sim 540\ nm}$ which is far less than the heights we have studied. Another point could be used to prove the idea of suspension of contact in our study is absence of notable static friction as it is shown in [125]. Accordingly, we could conclude that the contact is laid and real contact area has been decreased, which is the main reason of the reduction of friction force.

As we were not able to determine the contact area during the sliding, we plotted $\boldsymbol{F_t}$ vs. $\boldsymbol{F_n^{2/3}}$ to determine that our study follows which model of contact. According to the figure 5-6, linearity of the friction force to Hertzian preload indicates that the contact between glass tip and PDMS samples are in non-adhesive regime of the JKR model. Wu-Bavouzet also pointed out that if the applied normal load is greater than the adhesive force the friction would follow non-adhesive regime of the JKR model. Our study lies in this category. The deviation of the friction on smooth sample from linear fitting in figure 5-6 is more pronounced and could be related to higher contribution of adhesive forces.

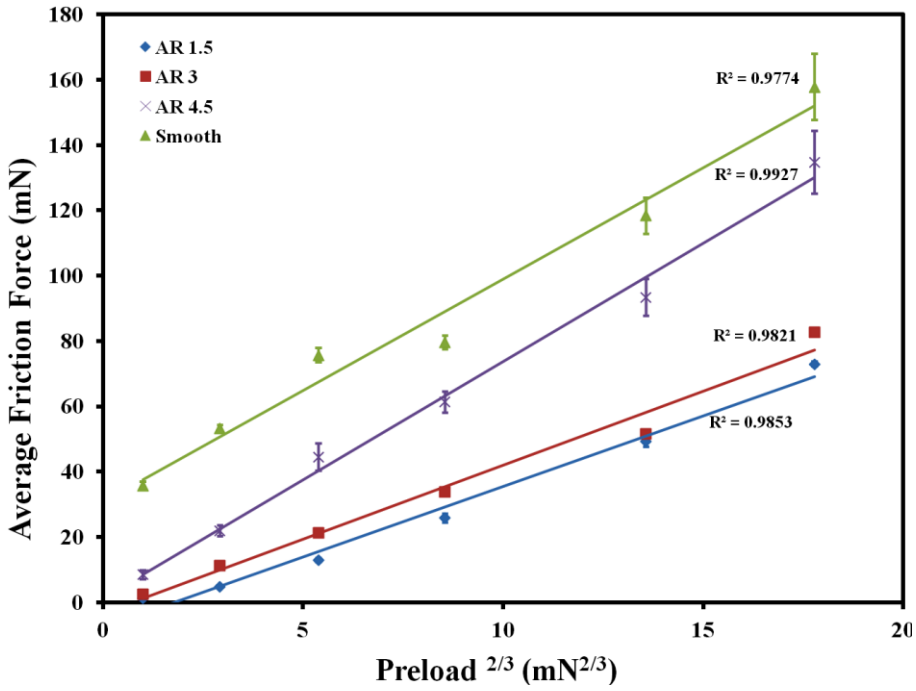

Figure 5-7: Fitting the average friction force to the Hertzian preload

5.4.2 Increase of friction with increase of AR: Effect of surface compliance

In a similar study, He and his coworkers have theoretically calculated the ratio of the adhesive term to the elastic term based on the JKR model of static contact[130]. It is shown that increase in applied normal load would result in a decrease in the contribution of adhesive forces in a JKR contact model. This fact attenuates the adhesive forces competing with energy costs by deformation of the pillars both in compression and bending modes. This trend continues until an approximately Hertzian model of contact is achieved. Based on the Hertz theory we have:

$$a^3 = \frac{RF}{K} \qquad (5.4)$$

Hence, it is expected to have an increase in contact radius for a certain preload if the stiffness of the surface decreases. It is believed that introduction of the micropatterns on the surface decreases the combined or reduced Young's modulus and this intensifies with increase of AR [104].This supports the idea of the increase of the contact area and consequently friction due to increment of AR. This is in agreement with the results in [125], [126]. However, further investigation is going on to prove this idea for our system.

As the type of contact is laid and pillars diameter and spacing have been maintained constant, the only remaining mechanism of enhancement of real contact area could be attributed to contact with pillars side-wall. This localized increase in contact area could be achieved by bending of single pillars. Figures 5-2 indicate the advent of bucking of the pillars for three different aspect ratios. Figure A-C show the advent of partial collapse of the pillars and D-F indicates the full collapse of the pillars in the monitored area of contact. Collapse begins in forces about 8mN for AR 4.5 pillars, 27mN for AR 3 pillars, and 80 mN for the AR 1.5 pillars. This indicates that the energy required for bending of the shorter pillars is much greater than that of the high AR pillars. Critical buckling load for the lowest AR pillars was higher than the maximum applied normal load in sliding, i.e. higher than 75mN. Quantitative elucidation of the contribution of each energetic, i.e. adhesive, bending, compression, and stretching energies, could be implemented by subtle calculation of material characteristic and mechanical properties which is out of the scope of this manuscript.

5.5 Conclusion

Micropillar arrays with different ARs ranging from 1.5 to 4.5 were successfully fabricated through DRIE and soft-lithography techniques. The friction tests on the fabricated samples with different preloads showed no wear or plastic deformation on the samples. The mechanism of the friction could be considered interfacial friction as described by Homola in [119]. Thus, introduction of the micropatterns causes decrease in real contact area and accordingly friction force and coefficient of friction. Friction force is proportional to $\boldsymbol{F_n^{2/3}}$, indicating a Hertzian fashion of contact or non-adhesive JKR contact. Micropillar arrays with higher ARs possess greater friction force values. Increment of real contact area through side-wall contact could be resulted from bending and elastic deformation of the high AR pillars. It appears that high AR ratio pillars could be considered as a versatile tool for tuning of the friction especially in the normal loads below the saturation. In fact, based on the application and range of load the AR of the pillars could be used to adjust the friction force to a wide range of values.

Chapter 6
Conformal adhesion enhancement of biomimetic microstructured surfaces

6.1 Introduction

The amazing aptitude of some insects and lizards, such as geckos, to stick readily and rapidly to almost any surface (whether it is hydrophilic or hydrophobic, rough or smooth, dry or wet) has attracted extensive research interests on the development and application of biomimetic structures. Recent studies have attributed the adhesive ability of geckos to the material properties of their foot pads – sophisticated structural morphology and elasticity coupled with such intermolecular forces as the universal van der Waals forces. The gecko adhesive pads contain arrays of β-keratin lamellae. Each lamella consists of thousands of micron-sized stalks which are terminated by millions of spatular pads having nanoscale dimensions. These millions of spatular pads allow for a large "real" contact area to form so that the gecko foot pads can adhere to almost any surface via the weak but universal van der Waals force [38], [54], [103], [143–145]. More recently, the rapid switching between gecko foot attachment and detachment has been investigated by taking into account the geometry of the fibrillar structure, the coupling effects between adhesion and friction, and the macroscopic action of the gecko toes [146–153]. The physical and biological studies of the gecko adhesive system have suggested that micro and nanoscale patterned or fibrillar structures at an interface may be good candidates to tune adhesion [109], [115], [154–156].

The tuning of the adhesion properties at an interface through the general design principle learned from the biological adhesive systems has been investigated by a number of researchers. Ghatak, Chaung and their coworkers studied the adhesion between an incision-patterned PDMS elastomer layer and a flexible plate. They suggested that multiple crack arrest and initiation on such patterned substrates result in extra dissipation of the elastic energy [155], [156]. Crosby and coworkers have conducted a series of JKR-type adhesion experiments and showed that adhesion between glass and PDMS substrates patterned with low aspect ratio cylindrical posts (50-250μm in diameter) could be altered from 20 to 400% of the adhesion strength for non-patterned interfaces [115]. Lamblet and Poulard and their coworkers have utilized the micro-patterning (1.5 -8μm in diameter) to enhance the weak adhesion between PDMS and acrylic adhesive tapes. They demonstrated through peeling

experiments that the coupling roles of deformability and aspect ratio of microscopic patterns in enhancing adhesion and showed the elastic deformation of the patterns can lead to a noticeable extra adhesion increase [109]. These studies and many others [27], [39], [42], [56], [157], [158] on the design, fabrication and testing of biomimetic adhesives have focused mainly on spatular surface contacts. It has been generally accepted that the micro-structured surfaces are more deformable having larger fracture zones than non-structured ones; and, the separation of discrete microscale contacts can dissipate a large amount of extra elastic energy so as to enhance their adhesion.
In contrast to the studies of the non-conformal spatular contact adhesion of micro-structured surfaces, there are only a few studies of the conformal adhesion of the micro and nano-structured surfaces. The conformal adhesion is far less explored and understood. Several recent studies of the use of biomimetic micro/nanoscale structures for medical applications have revealed the importance of the conformal adhesion, where a strong adhesive bond as well as compliance and conformability to tissue surfaces are required [81], [136], [159–161]. Lee and coworkers demonstrated a possible method to enhance the adhesion between a micro-structured surface and a soft biological tissue using polydimethylsiloxane (PDMS) as a surrogate for biological tissue. Micro-patterning of the surface of a silicon wafer enhanced the peeling strength of laminated PDMS without any chemical treatment. As the aspect-ratio of the surface structures increased, the adhesion strength increased and leveled off at an aspect-ratio of 3 [159]. Mahdavi and coworkers reported a study of gecko-inspired tissue adhesives for enhancing tissue adhesion. In that study, the adhesion was optimized by varying dimensions of the nanoscale pillars, including the ratio of tip diameter to pitch and the ratio of tip diameter to base diameter [160]. The tissue adhesion enhancement was suggested to be associated with the enhanced conformal contact between the tissue and patterned adhesive elastomer film. More recently, Vajpayee et al. reported an interesting study of the adhesion selectivity using rippled surfaces in which complementary surfaces showed enhanced adhesion with increasing rippled amplitude [162].

In this manuscript, we report an experimental study of conformal adhesion of a polymer film on the biomimetic micron-sized surface structures. We hypothesize that the local adhesion and friction events of pulling micro-pillars out of the embedded polymer film would significantly enhance the global adhesion strength at the interface. For testing this idea, we changed the interfacial contact from a planar contact to three-dimensional “composite” structures by laminating a piece of liquid PDMS-coated tape on top of micro-pillar arrays. Curing of these PDMS/SU-8 laminates at elevated

temperature established micron-zipped structures through conformal contact. A series of peeling experiment coupled with optical interference imaging were performed to investigate the adhesion enhancement as a function of the height of the micro-pillars and the associated delamination mechanisms. To our knowledge, this is one of the first few systematic studies of the conformal adhesion of biomimetic micron-structured surfaces. The local friction-based adhesion enhancement mechanism may have profound implications for the effective assembly of similar or dissimilar material components at ever-smaller scales.

6.2 Experimental

Arrays of micro-pillars made of photoresist polymer SU-8 (SU-8-25, Microchem Co. Newton, MA, USA) in a hexagonal pattern were fabricated using the photolithography technique in the cleanroom environment. The SU-8 pillars are 10 μm in diameter, having a center-to-center spacing of 25 μm and varied heights ranging from 5 μm to 60 μm. Rectangular areas of micro- pillar arrays (3.5 cm in width and 7 cm in length) of SU-8 were fabricated on silicon wafers. The quality of the micro-patterned surfaces was examined by both an optical microscope and scanning electron microscope. The samples with defects less than 5% of the surface area were used in this study. PDMS elastomer kits (Sylgard® 184, Dow Corning) were used to prepare PDMS tapes by dip-coating PDMS on paper strips. Paper strips (ReproPlusBrite Cascades Inc. Quebec, Canada) (1 cm wide, 70μm thick, and 21.5 cm long) were coated with a thin layer of a 10:1 weight ratio mixture solution of PDMS resin and curing agent. Once the paper strips were saturated with PDMS solution, a glass roller was used to remove extra PDMS solution and escape trapped air bubbles. To form conformal contacts between the elastomer and the micro-structured surfaces, paper strips saturated with uncured liquid PDMS resin were gently placed over the surfaces; no external pressure was applied. As expected, the liquid PDMS wetted both smooth and patterned SU-8 surfaces and filled the spaces between the micro-pillars immediately when the PDMS tape came in contact with the surface. Once cured, the conformal contacts were established at the interface. In this way, the final thickness of cured PDMS tapes was controlled to be 600 ± 50μm. The tensile modulus of the PDMS tape was about 1000 times larger than that of pure PDMS elastomers.

Surface free energy of the cured PDMS and SU-8-coated silicon wafer were characterized using sessile contact angle measurements according to Wu's method [163]. Contact angles of six liquids: 1,3-Butanediol, diiodomethane, dimethylsulfoxide, formamide, glycerol (Sigma - Aldrich), and

deionised distilled water were measured using a custom-made apparatus in which at least 5 images of the liquid droplets about 5 μL deposited on the surfaces were analyzed to extract the contact angle at the three-phase contacting line. The critical interfacial energy release rate of PDMS on SU-8 was measured by indenting a 6 mm diameter smooth PDMS hemispherical probe on a 50 μm-thick layer of SU-8 coated on silicon wafer. Same PDMS elastomer kits were used to prepare the PDMS probe as that used in PDMS tapes. SU-8 thin film was prepared following the same procedure as the micro-structured samples. The indentation was carried out by an Instron-like materials tester (Texture Technologies Corp. MA, USA) at a constant displacement rate of 10μm/s, with a preload of 50 mN and a holding period of 10 min between loading and unloading processes. Using the JKR theory, the effective adhesion energy $\boldsymbol{W_{eff}}$was estimated from the pull-off force $\boldsymbol{F_{pull-off}}$ as $\boldsymbol{W_{eff} = -F_{pull-off}/1.5\pi R}$, where R is the radius of the hemispherical probe [20].

180^0 peeling tests were performed to evaluate the adhesion strength of PDMS/SU-8 laminates using the same materials tester from Texture Technologies Corp. All the experiments were carried out in ambient conditions at room temperature. The PDMS/SU-8 laminates were attached to a rigid aluminum plate, which was then clamped in the lower cross-head of the tensile tester. The free end of the PDMS tape was then bent and clamped into the upper cross-head. To eliminate the edge effects, the paper/PDMS strips were carefully trimmed prior to the peeling experiments. The PDMS tapes were peeled from the smooth towards patterned regions of the substrates at velocities ranging from 10 to 1200 μm/s. The bending curvature of PDMS tape in the peeling front was recorded and analyzed in terms of the plastic deformation of the PDMS tape. The surfaces of peeled PDMS tapes and substrate surfaces were examined using an optical profilometer (Wyko 1100, Veeco Instruments Inc. NY, USA) to determine the failure mechanisms.

6.3 Results

Prior studies of the biomimetic mirco/nano structured surfaces had revealed that the aspect ratio of the surface features plays an important role in their adhesion behaviours [64], [71], [72], [109], [115], [141]. Thus, we varied the aspect ratio of the surface features and investigated its effect on the conformal adhesion strength. The height of micro-pillars in a hexagonal pattern was systematically changed with an essentially constant center-to-center spacing. Figure 6-1 shows typical SEM images of the surfaces patterned with micro-pillars. All pillars are smooth and have a uniform height for each sample. There were no lateral contacts between the pillars.

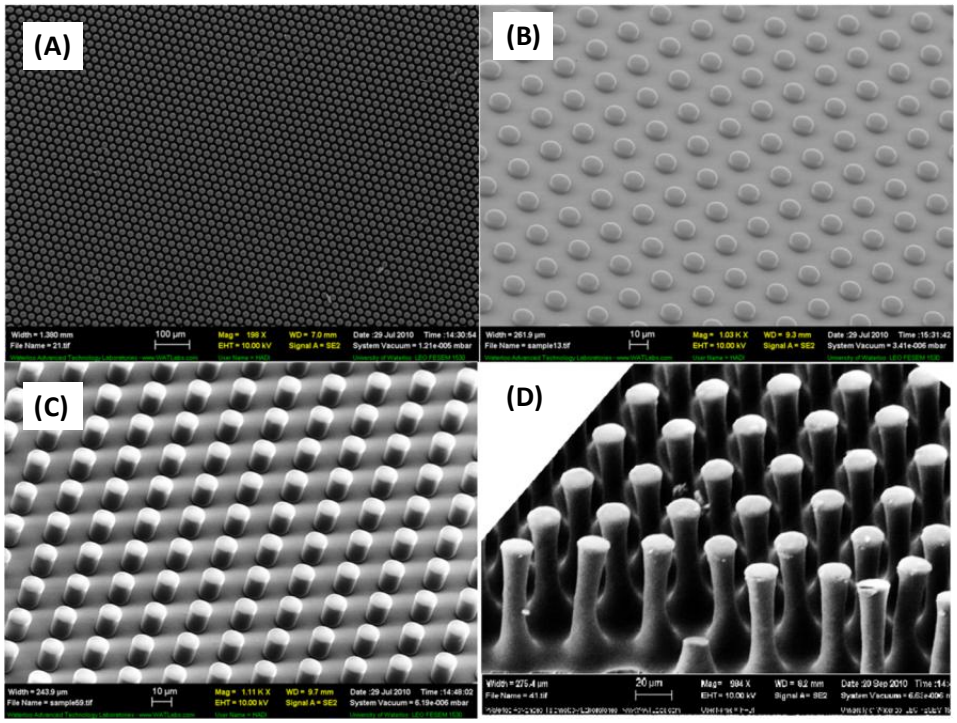

Figure 6-1: Typical SEM micrographs of fabricated micro-pillars. (A) aspect-ratio of 0.5 at a low magnification, (B) aspect-ratio of 0.5 at a high magnification, (C) aspect-ratio of 1.5, and (D) aspect-ratio of 5.6.

Table 6-1 enumerates the geometrical parameters of arrays of micro-pillars of eight different aspect-ratios (AR). The apparent area of the micro-pillar arrays in conformal contact with the PDMS tape was $\boldsymbol{A_0 = 3500\ mm^2}$. The actual surface area or total available area A_a for conformal contacts was calculated from the hexagonal pattern and the geometries of the micro-pillars by the equation (6-1). The ratio of the actual surface area to the apparent surface area, determined by equation (6-2), was used to quantify the enlargement of surface area due to the micro-patterning.

$$\boldsymbol{A_a = A_0\left(\frac{4\pi r h}{\sqrt{3}i^2} + 1\right)} \qquad (\mathbf{6.1})$$

$$\boldsymbol{\varphi_a = {A_a}/{A_0}} \qquad (\mathbf{6.2})$$

where *h*, *r*, and *i* denote the pillars' height, radius, and center-to-center spacing, respectively. Another geometrical factor that could be of interest is the spacing volume ($\boldsymbol{V_s}$) between the micro-pillars, which equals the volume of the negative patterns (i.e. the voids) left on the peeled PDMS tape. $\boldsymbol{V_s}$ was calculated by the equation (6-3). The volume fraction φ_V of the voids to the total volume of the non-patterned films with the same thickness was determined by equation (6-4), where the total volume $\boldsymbol{V_t}$ is approximately 210 mm^3 for a strip of 600 μm in thickness, 1 cm width, and 3.5 cm length.

$$\boldsymbol{V_s = hA_0\left(1 - \frac{2\pi}{\sqrt{3}}\left(\frac{r}{i}\right)^2\right)} \qquad (\mathbf{6.3})$$

$$\boldsymbol{\varphi_V = {V_s}/{V_t}} \qquad (\mathbf{6.4})$$

Table 6-1: Geometrical parameters of the SU-8 surfaces patterned with micro-pillars

Sample	Diameter, d (μm)	Height, h (μm)	Aspect-ratio, AR (=h/d)	Total surface area $A_a(mm^2)$	Spacing volume, $V_s(mm^3)$	φ_a $(=A_a/A_0)$	φ_V $(=V_s/V_0)$
0	0	0	0	3500	0	1	0
1	8	4	0.5	4150	14	1.19	0.07
2	8	6	0.8	4475	21	1.28	0.10
3	10	12	1.1	5886	41	1.68	0.19
4	11	14	1.2	6515	46	1.86	0.22
5	13	20	1.5	8779	69	2.51	0.33
6	10	22	2.2	8068	78	2.31	0.37
7	12	29	2.4	10566	100	3.02	0.47
8	11	35	3.2	11373	121	3.25	0.58
9	11	61	5.6	17180	211	4.91	1.00

To form conformal contacts between the elastomer and the micro-structured surfaces, liquid PDMS resin was brought into contact with the surfaces and then cured as described in the Experimental. Figure 6-2 illustrates the conformal contact and geometry of 180º peeling. The smooth surfaces were split into many discrete micro-regions, forming a "composite" interfacial region or an interphase whose thickness increases with the height of micro-pillars.

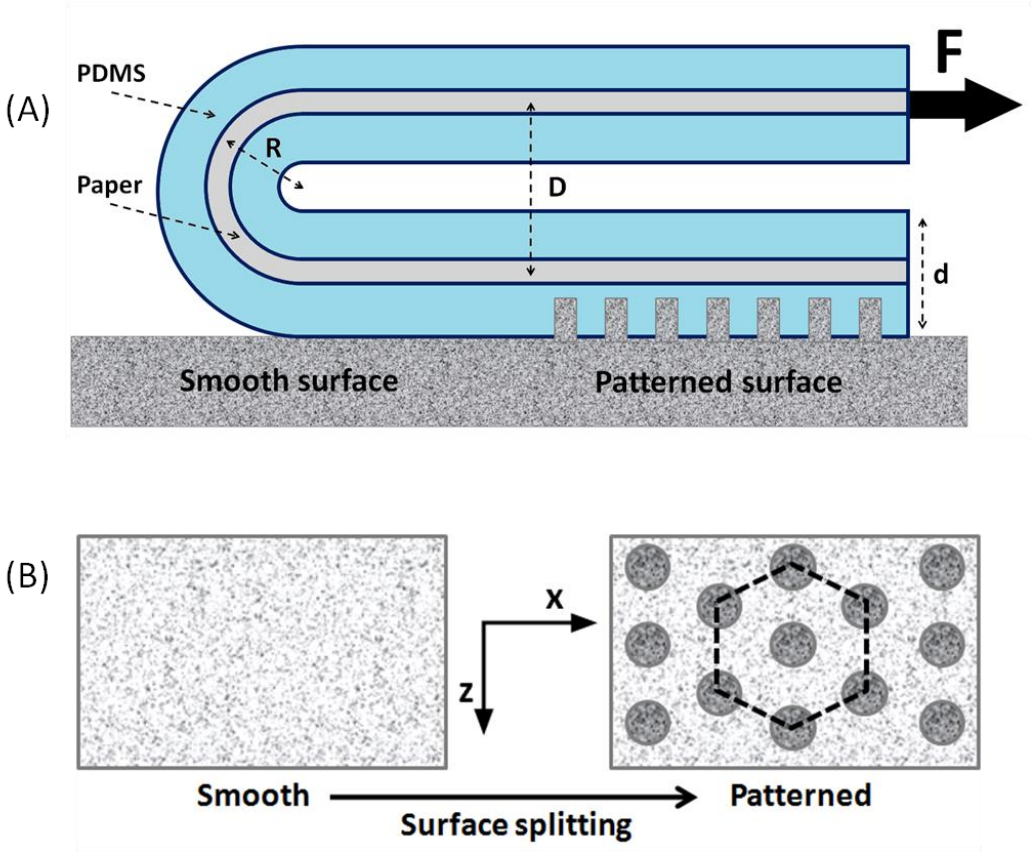

Figure 6-2: Schematic illustration of the conformal adhesion on smooth and micro-patterned surfaces and the geometry of 180° peeling. (A) side view of the peeling geometry, (B) top view of the conformal contact on smooth (left panel) and micro-patterned surfaces (right panel).

The thermodynamic work of adhesion between PDMS and SU-8 were evaluated using the Dupré equation [4],

$$\boldsymbol{W_0 = \gamma_1 + \gamma_2 - \gamma_{12}} \qquad (\boldsymbol{6.5})$$

where $\boldsymbol{\gamma_1}$, $\boldsymbol{\gamma_2}$ and $\boldsymbol{\gamma_{12}}$ are the free surface energy of the SU-8 and the PDMS and the interfacial energy between them, respectively. The numerical values of these free energy terms were determined experimentally by the sessile contact angle measurements of six liquids according to the Wu's method [163]. $\boldsymbol{\gamma_1}$ =18 mJ/m^2, $\boldsymbol{\gamma_2}$ = 33 mJ/m^2, and $\boldsymbol{\gamma_{12}}$ = 4 mJ/m^2. Accordingly, the work of adhesion was calculated from equation (6-5) $\boldsymbol{W_0}$ = 47 mJ/m^2. We further characterized the adhesion

of PDMS on smooth SU-8 surface in terms of interfacial energy release rate or effective adhesion energy by indenting a hemispherical PDMS probe on the SU-8 –coated silicon wafer. Figure 6-3 shows the indentation geometry and the force-displacement curve at the displacement velocity of 10μm/s. The effective adhesion energy $\boldsymbol{W_{eff}}$was estimated from the pull-off force $\boldsymbol{F_{pull-off}}$ as $\boldsymbol{W_{eff} = -F_{pull-off}/1.5\pi R}$. It was found to be 490 mJ/m^2, which is about ten times larger the thermodynamic work of adhesion, perhaps because of the polymer chain diffusion or other dissipation mechanisms at the contacting surface [125], [164]. The equivalent force of W_{eff} is 4.9mN/cm, which is above the force resolution (1mN) of the load cell of the peeling tester. This value was used as a conservative estimation of the critical interfacial energy release rate between the PDMS elastomer and smooth SU-8 surfaces because the peeling force from smooth SU-8 surfaces were lower than the force resolution of the peeling instrument as described below.

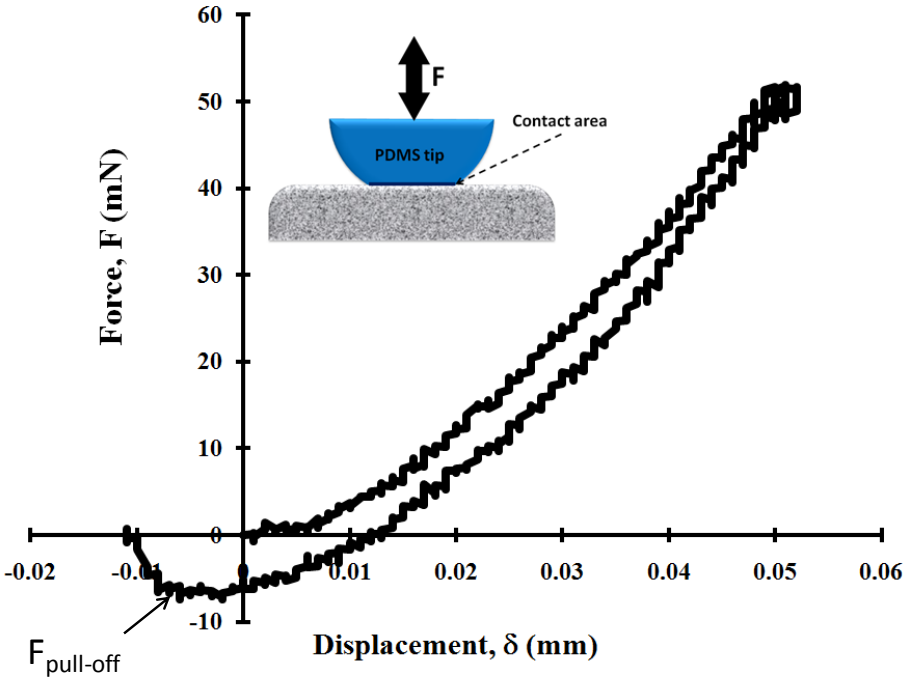

Figure 6-3: Force vs displacement curve of indenting a hemi-spherical PDMS tip on the smooth SU-8 surface.

The strengths of conformal adhesion on the surfaces patterned with micro-pillars were evaluated by 180º peeling tests. The tests started from the smooth region toward the micro-patterned region. Figure 6-4-A shows typical force-displacement curves of peeling PDMS tapes from surfaces patterned with micro-pillars of 22 μm high or an aspect ratio of 2.2 at peeling velocities ranging from 10μm/s to 1200μm/s. The peeling force on the smooth region was hardly to determine because they

reached the limit of the resolution of the force sensor of the peeling tester. When the peeling fronts met the patterned areas, the peeling forces increased rapidly to a high steady-state force plateau. The peeling forces fluctuate in the steady-state region, indicating a significant peeling stick-slip phenomenon. We used the average peeling forces and their standard deviations in the steady-state regions to quantify each peeling curve on the micro-patterned surfaces. Figure 6-4-B plots the average peeling force as a function of peeling velocity. The peeling velocity had no significant effect on the peeling forces. This observation suggested that there were no significant viscoelastic components in the PDMS/SU-8 laminates.

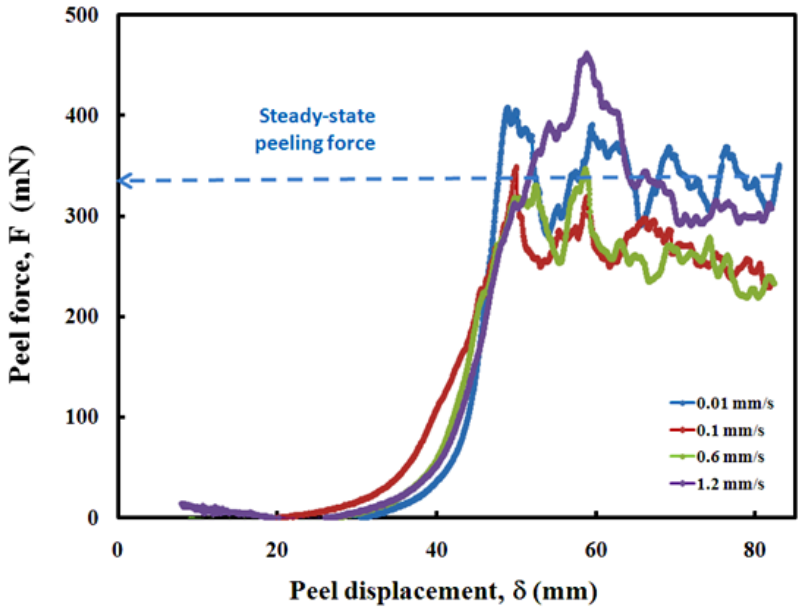

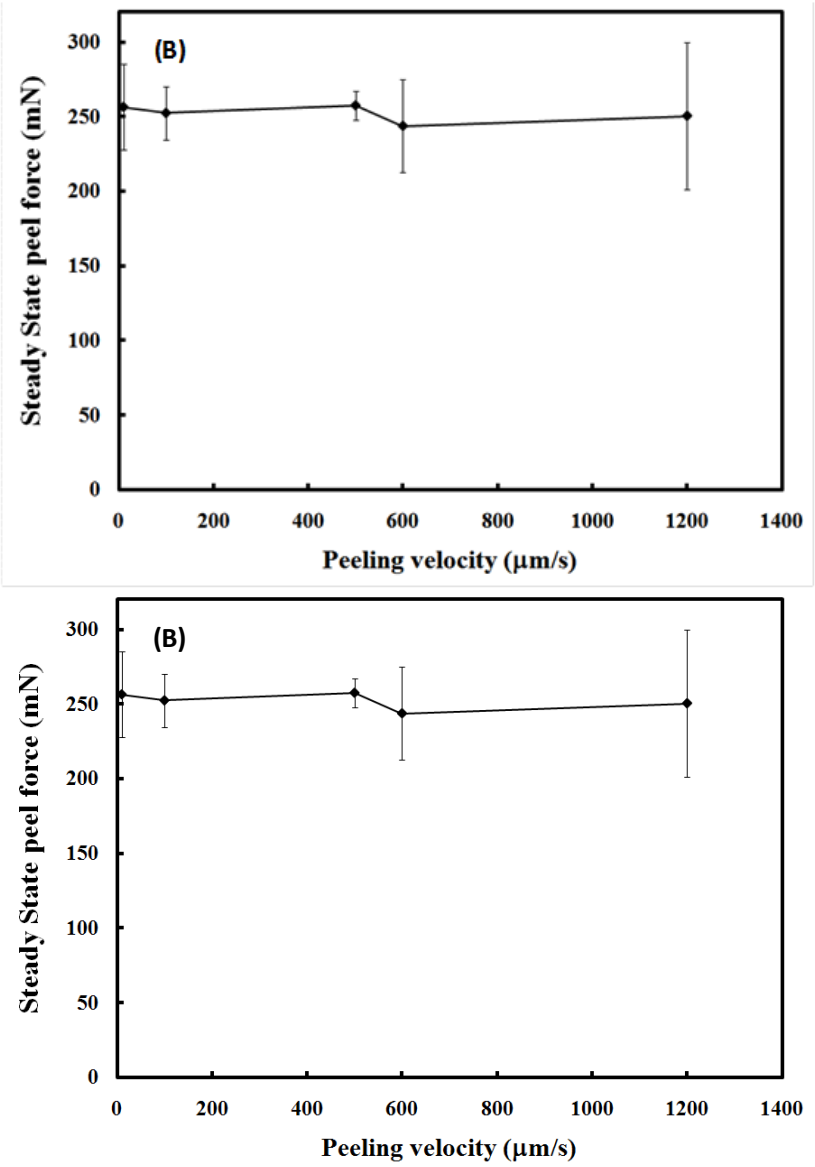

Figure 6-4: (A) Typical peel force vs peel displacement curves of surfaces patterned with micro-pillars of 22 µm in height at varied peeling velocities, (B) Plot of the steady-state peel force on the micro-pattered surfaces as a function of peeling velocity.

Figure 6-5 shows the force vs displacement curves of peeling PDMS tapes from smooth surfaces toward surfaces patterned with micro-pillars of varied heights or aspect-ratios at a constant velocity of 500 µm/s. We noticed that both the force plateau and the magnitude of force fluctuation increased with the aspect ratios. To make the analysis further, we use the average value of steady-state peeling

forces over the patterned regions to determinate the interfacial energy release rate for each sample ($\boldsymbol{G_c}$) according to Kendall's equation [20], [110].

$$\left(\frac{\boldsymbol{F}}{\boldsymbol{w}}\right)^2 \frac{\mathbf{1}}{\mathbf{2}\boldsymbol{tE}} + \left(\frac{\boldsymbol{F}}{\boldsymbol{w}}\right)(\mathbf{1} - \cos\boldsymbol{\theta}) - \boldsymbol{G_c} = \mathbf{0} \qquad (\mathbf{6.6})$$

where $\boldsymbol{F}$ is the peeling force; $\boldsymbol{t}$, $\boldsymbol{w}$, and $\boldsymbol{E}$ are the thickness, width and stretching modulus of the PDSM tape, respectively; $\boldsymbol{\theta}$ is the peeling angle. Although PDMS elastomer is stretchable, the PDMS-coated paper is not because of the high tensile modulus of the embedded paper strip. Thus, the first term, i.e. the elastic energy stored during the stretching of the peeling strip, is negligible. For 180° peeling tests, the interfacial energy release rate can be estimated from the reduced Kendall equation

$$\boldsymbol{G_c} = \mathbf{2}\left(\frac{\boldsymbol{F}}{\boldsymbol{w}}\right) \qquad (\mathbf{6.7})$$

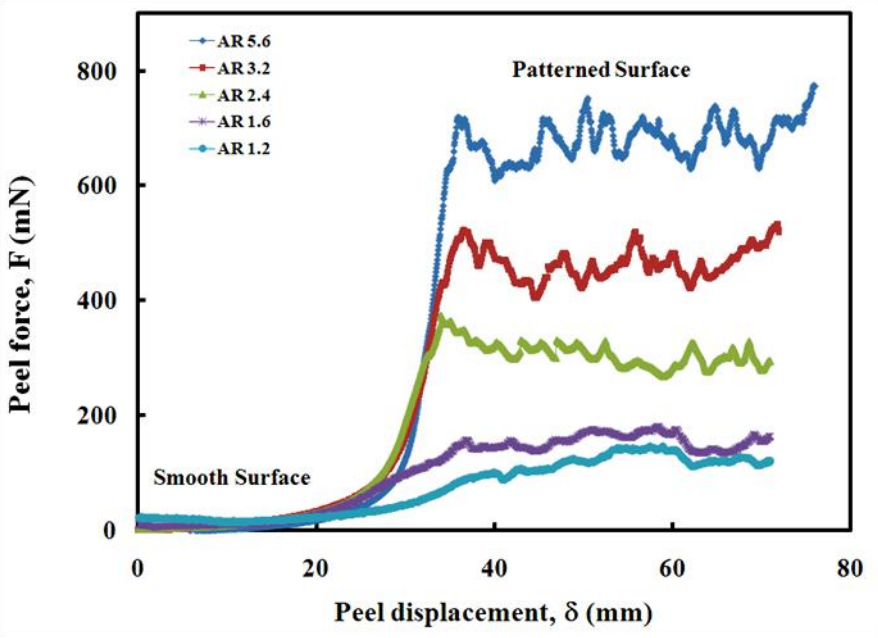

Figure 6-5: Typical peel force vs displacement curves from surfaces patterned with micro-pillars of varied aspect-ratios as the peeling velocity of 500 μm/s.

Figure 6-6-A shows the calculated critical interfacial energy release rate $\boldsymbol{G_c}$, as a function of the height of micro-pillars, $\boldsymbol{h}$. All of the experiments were carried out at least 4 times. It is remarkable that the $\boldsymbol{G_c}$ increased from almost zero on the smooth surface up to 270 J/m^2 on micro-patterned surfaces of $\boldsymbol{h = 61\mu m}$. The $\boldsymbol{G_c}$ vs $\boldsymbol{h}$ curve is non-linear and approximately follows a parabolic fitting curve. Figure 6-6-B shows the standard deviation of the local force fluctuations in the steady-state region as a function of the micro-pillar height. The standard deviation increases with the height of micro-pillars.

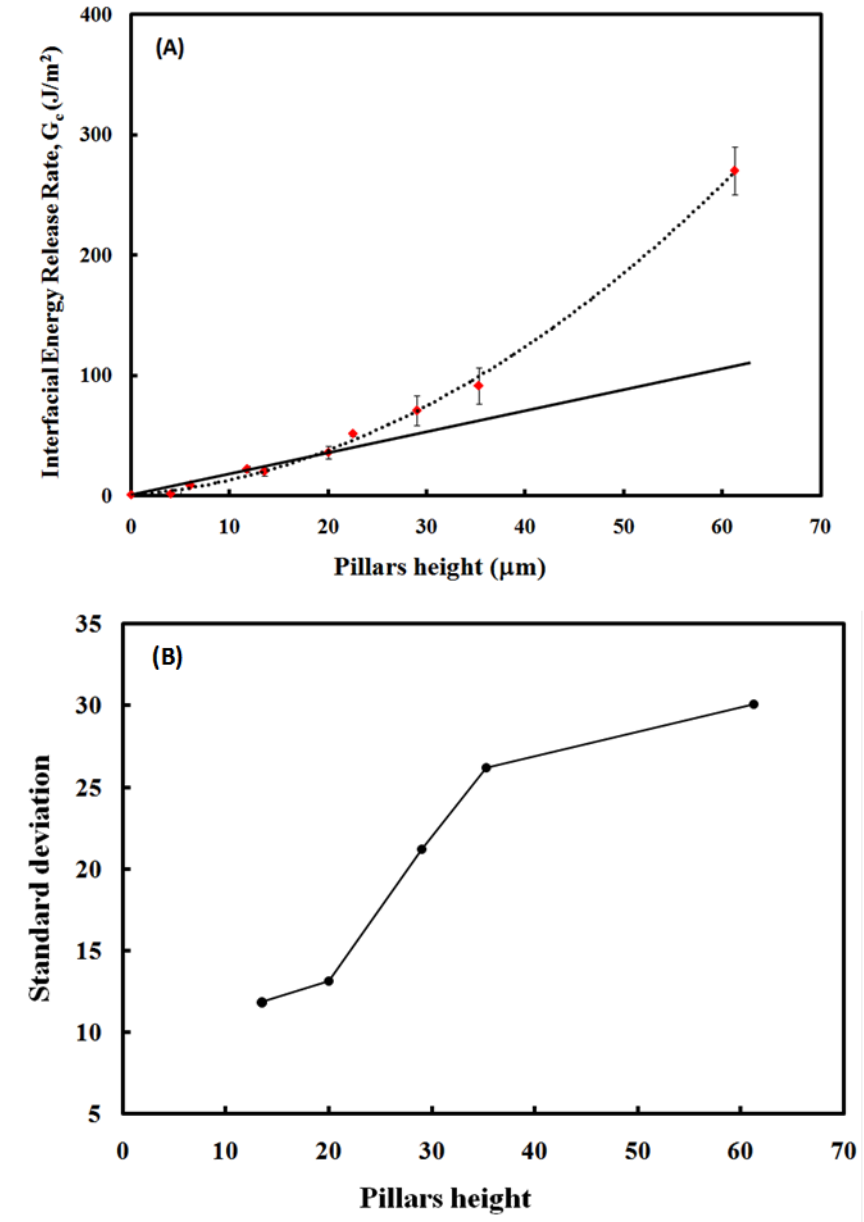

Figure 6-6: (A) Interfacial energy release rates G_c of peeling from surfaces patterned with micro-pillars of different heights. The dotted line is a parabolic curve fitting best to the data. The solid line is an initial linear fitting line, (B) The standard deviations of the fluctuated forces of the peeling curves in Figure 5 on the micro-patterned surfaces as a function of the height of micro-pillars.

In addition to the peeling force, we noted that the bending curvature of PDMS tape at the peeling front increased dramatically when the peeling front met the micro-patterned regions. According to the Gent's theory [165], the plastic contribution to the measured peeling force $\boldsymbol{F_y}$ is related to the radius of the bending curvature *R*, the film thickness *d*, and the yield stress $\boldsymbol{\sigma_y}$ and yield strain $\boldsymbol{e_y}$ of the material at peeling zone:

$$\boldsymbol{F_y = \frac{1}{4}(\sigma_y e_y d)\left[\left(\frac{d}{2Re_y}\right) + \left(\frac{2Re_y}{d}\right) - 2\right]} \qquad (\mathbf{6.8})$$

At small values of the radius of the bending curvature $\boldsymbol{R}$, the first term in the brackets in eq. (6-8) becomes dominant and the equation simplifies to $\boldsymbol{F_y \approx (\sigma_y d^2)/8R}$. Figure 6-7-A-D shows that the radius of curvature decreases as the height of micro-pillars increases. Hence, the plastic contribution to the measured peeling force increased with the height of micro-pillars. Furthermore, there was only a slight residual deformation for the flat sample (Figure 6-7-E) while significant residual curvature of the peeled strips observed for high aspect-ratio micro-pillars (6-7-F-H).

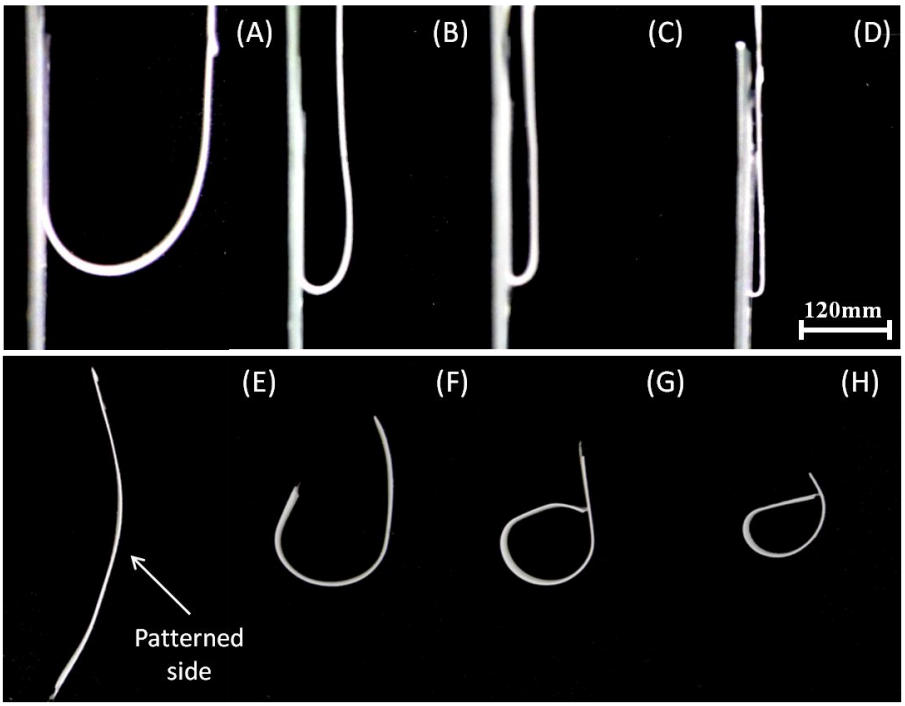

Figure 6-7: Optical images of the bent PDMS tape (the top panels) in peeling and corresponding residual deformation of the peeled tape (the bottom panels) from the smooth surfaces (A and E), and surfaces patterned with micro-pillars with heights of (B and F) 23 μm, (C and G) 35 μm, and (D and H) 61 μm.

The failure mechanism of conformal adhesion was investigated by examining the micro-patterned surfaces and micro-holes left on the PDMS tape using an optical interference imaging system. Figure 6-8 shows the optical images and profiles of the surfaces patterned with micro-pillars (h=12 μm) in the top panels and the negative patterns transferred to PDMS ("micro-hole") in the bottom panels. The micro-pillars were intact after peeling and there was no PDMS residue in the spaces between micro-pillars. This observation indicated an interfacial failure. That is, the micro-pillars had been completely pulled out from the PDMS. For the low aspect-ratios (AR<3.2), the micro-holes have the same dimensions as the micro-pillars as shown in the X- and Y-profiles of the micro-pillars and micro-holes, verifying that the conformal contacts were indeed established. However, for the high aspect-ratio pillars with AR = 3.2 as shown in Figure 6-9, shear lips were observed on the edge of PDMS micro-holes along the peeling direction. These shear lips did not recover or relax with time. Thus, the shear lips may be permanent wears caused by pulling micro-pillars out of the PDMS matrix.

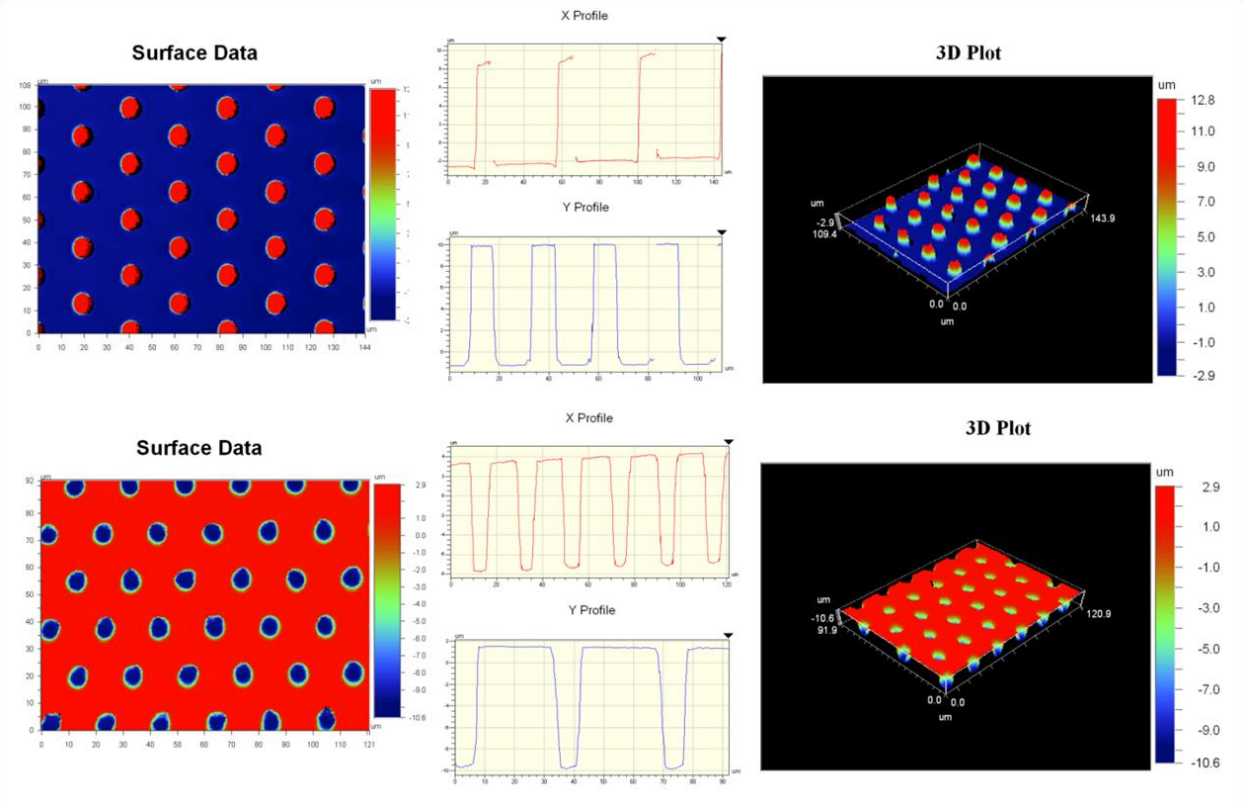

Figure 6-8: Typical optical interferometry measurements of surfaces patterned with micro-pillars of 12 μm in height (top panels) and the micro-holes transferred to the PDMS tape (bottom panels): 2-D images in the left column, X- and Y- profiles in the middle column, and 3-D images in the right column.

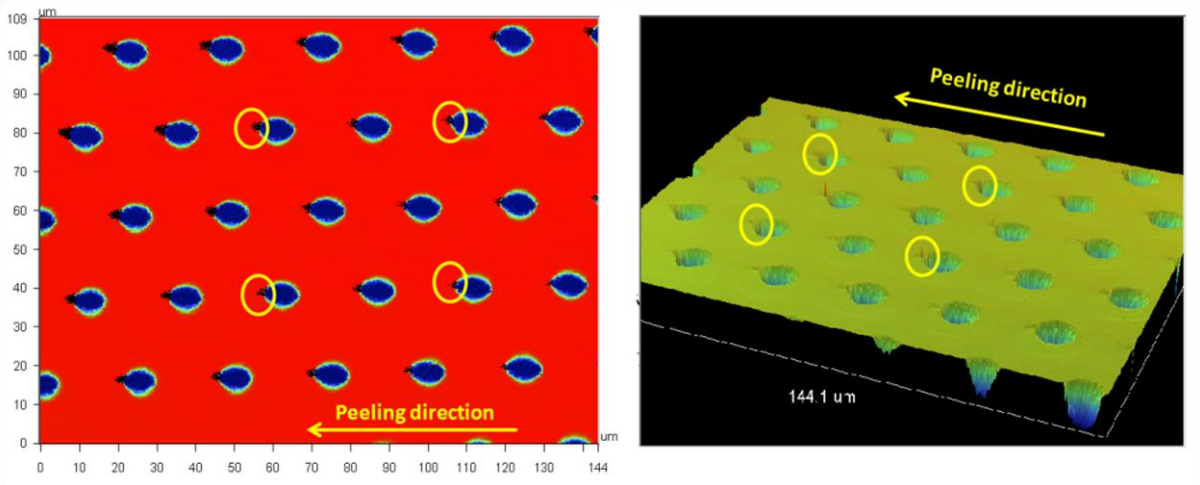

Figure 6-9: Optical interferometry 2-D (left panel) and 3-D (right-panel) images of the micro-holes on the PDMS tape peeled off from micro-pillars (h = 35 μm or AR = 3.2).

To gain further insights into the adhesion enhancement, the magnitude of adhesion enhancement was evaluated by the ratio of interfacial energy release rate on the micro-patterned region to that of smooth surface, i.e. $\boldsymbol{G_C/G_0}$. There is an uncertainty of $\boldsymbol{G_0}$ since the peeling force on smooth surface is lower than the force resolution of the load cell. For this, we assume the critical fracture energy release rate of peeling from smooth SU-8 surfaces to have the same value as the effective work of adhesion measured in the indentation test, i.e. $\boldsymbol{G_0}$ = 490m J/m^2. Note that the equivalent force of $\boldsymbol{G_0}$ = 490m J/m^2 is 4.9mN / cm (width of the peeling strip) which is above the force resolution. Thus, this assumption gave use a conservative estimation of the critical energy release rate for peeling from the smooth surfaces even though the contact time in the indentation sample was shorter than that in the conformal samples. Figure 6-10 shows the normalized $\boldsymbol{G_C}$ as a function of normalized surface area $\boldsymbol{A_a/A_0}$. The conformal adhesion enhancement increased by about 550 times as the surface areas increased only by 5 times. The insert plot in Figure 10 shows the adhesion enhancement from the shortest micro-pillars to the tallest micro-pillars. It shows that even though we use the adhesion force from shortest micro-pillars as a reference, the adhesion enhancement is still more than 200 times. This is remarkable. Furthermore, the curve is highly non-linear. This non-linearity between adhesion enhancement and surface area enlargement suggests that the adhesion enhancement is not purely matter of the increases in the physical contact area due to surface roughness.

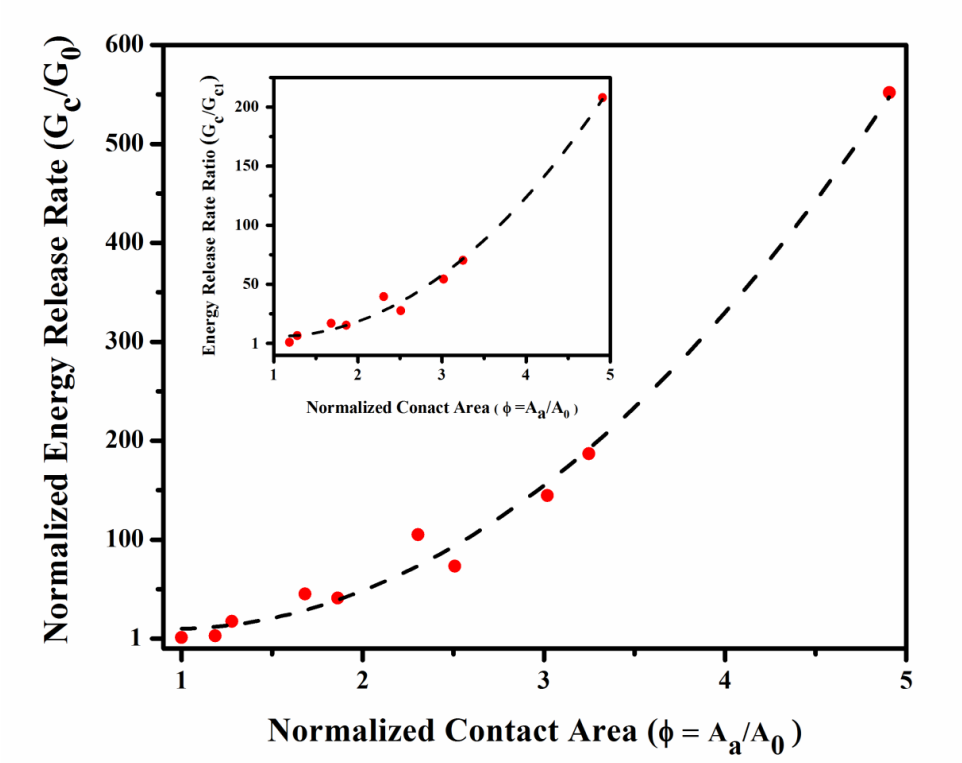

Figure 6-10: Normalized interfacial energy release rate as a function of the normalized contact area. The dotted line is a parabolic curve fitting best to the data points.

6.4 Discussion

Plastic deformation of the peeling strips appears to be related to the adhesion enhancement at the interface. According to Gent and Hamed's theory [165], if the interfacial adhesion between a film and its substrate is sufficiently weak or the adhesive layer is adequately thick or strong, no significant plastic deformation would occur. There was only a slight plastic deformation for the peeling from the smooth surface as shown in Figure 6-7-E. Significant plastic deformations were observed for micro-pillar patterned surfaces in Figure 6-7-F-H, suggesting a significant adhesion enhancement at the interface due to the micro-patterning. From the fracture mechanic point of view, the peeling from the smooth surfaces toward micro-patterned surfaces may involve a transition from a plane-strain condition to a plane-stress condition [72]. This transition may be due to the splitting of the contact surface into many discrete regions in XZ planes. In the other words, the crack plane on the smooth surface is split into many micro-planes having much thinner features with smaller free paths in XZ

plane (Figure 6-11-A). The stressed PDMS material in the XZ plane is much reduced and is prone to yield. This may be one reason for the observed shear-lip for high aspect-ratio pillars. In the Y direction, there is also a reduction in the stressed volume of PDMS and more stress will be able to transfer to the paper strip causing more significant plastic deformations of the peeling strips. According to table 6-1, the variation of the spacing volume V_s or φ_v is notable, i.e. ranging from 6% to 100%. Therefore, yield stress of the peeling strip could be reduced by the micro-patterning. The similar phenomena have been observed by Litteken and Kim and their coworkers [166], [167], showing that the transition from plane-strain to plane-stress fracture increased the fracture energy by 2 times for a ductile polymer embedded into micro-patterned metal surfaces.

Since the conformal contact between the soft elastomer and the micro-patterned substrates involves a 'composite' structured interfacial region or interphase, it may appear to involve the mechanical interlocking effect. However, unlike the removal of solid adhesives from bonded torturous surface cavities, the exit of straight pillars is not blocked by the part of the elastomer matrix. Thus, there is no significant "lock and key" effect for the separation of conformal contact on the regularly-patterned surface. The lack of "lock and key" effect in the 'composite' interphase allows us to examine some details of the debonding processes in terms of the local energy dissipation processes, which could contribute to the observed adhesion enhancement. Figure 6-11-A illustrated individual micro-pillars embedded or in the conformal contact with its elastomer matrix. There are two basic types of contacts: one is the planar contact, and the other is the side-wall contact. In separation, multiple events could happen at the level of micro-pillars, including the mode I (i.e. open mode) failure between the top of the micro-pillars and the PDMS surface, mode I failure between the bottom surface of the micro-pillars and the PDMS protrusions, and mode II (i.e. the shear mode) at the side walls. These local events increased the adhesion at the interface, which subsequently induced significant global plastic deformation on the PDMS tape. In the following, we discussed the local failure events at the level of micro-pillars in terms of their contributions to the adhesion enhancement at the interface.

6.4.1 The planar separation of the micro-pillars from their soft substrate – role of elastic energy dissipation

Although there are significant differences between spatular and conformal contacts on biomimetic micro-patterned surfaces, we may be able to obtain some insights to the conformal adhesion by considering recent understandings of the adhesion enhancement observed on spatular contacts of fibrillar adhesives [64], [71], [72], [109], [115], [141]. The spatular adhesion enhancement of fibrillar adhesives has generally been attributed to the dissipation of stored elastic energy during the deformation and detachment of individual micro-pillars. The deformation could take place in four situations: stretching of the pillars, bending of the pillars, deformation of the backing materials of the pillars, and the deformation of the contact substrate. Lamblet and Hui and their coworkers have applied the Landaus' and Boussenisque's models for the determination of these energetic contributions: the elastic energy stored in stretching of pillars, $\boldsymbol{W_s}$ and in bending pillars, $\boldsymbol{W_b}$; the elastic energy stored in deforming the backing materials and the contact substrate, $\boldsymbol{W_d}$ in the equations 9-11 [109].

$$\boldsymbol{W_s = \frac{F^2 h}{2\pi E_p r^2}}\ (\mathbf{6.9})\ ,\ \boldsymbol{W_b = \frac{2F^2 h^3}{3\pi E_p r^4}}\ (\mathbf{6.10}),\ \text{and}\ \boldsymbol{W_d = \frac{8\pi F^2}{27 E_d r}}\ \ (\mathbf{6.11})$$

where, $\boldsymbol{F}$, $\boldsymbol{h}$, $\boldsymbol{E_p}$ and $\boldsymbol{E_d}$ are the applied force, height of the pillar, and Young's modulus of the pillar and Young's modulus of the substrate/backing, respectively; in the equations 6-9 and 6-10, $\boldsymbol{r}$ is the radius of the pillar; in the equation 9-11, it is the radius of a cylindrical punch indenting into the substrate according to the Boussenisque's problem. Considering the composite nature of the conformal contacts on micro-patterned surfaces, the PDMS penetrated into the SU-8 micro-cavities could be regarded as a network of micron-sized protrusions on the backing layer of the PDMS tape. Therefore, the equations 9-11 might be applicable to both the PDMS micro-protrusions and SU-8 micro-pillars. If we apply these equations to SU-8 pillars, the adhesion enhancement due to the stored elastic energy loss should primarily come from the soft side of the interface because of the high stiffness [169] of the SU-8 micro-pillars ($\boldsymbol{E_p} >> \boldsymbol{E_d}$). That is, the $\boldsymbol{W_d}$ due to the deformation of the PDMS substrate dominates the other two terms. If we apply the above equations to the PDMS protrusions, the SU-8 will be the substrate. In this case, the deformation energy $\boldsymbol{W_d}$ of SU-8 substrate predicted by equation 6-11 is negligible due to its high stiffness; and the deformation of PDMS backing materials is also negligible because the thickness of the PDMS backing layer is larger by at

least one order of magnitude than the height of PDMS protrusions [72]. Assuming these PDMS protrusions as individual features, the equation 9 and 10 suggest that both $\boldsymbol{W_s}$ and $\boldsymbol{W_b}$ increase with the height of the pillars. But the bending of the PDMS protrusions could be dramatically hampered as they are interconnected into a network and laterally confined to the rigid SU-8 pillars. Thus, the elastic energy dissipation due to stretching of the PDMS protrusions W_s would contribute more than the other two terms to the observed adhesion enhancement. From the equation 6-9, the W_s increases linearly with the height of the pillars. Hui's study for the non-conformal contact of soft pillars on rigid substrates, also, shows a linear relationship between pull-off force and pillars height [71].

We may also analyze the conformal contact by considering the soft side as a network of the microscopic holes with finite spacing and depths. The effect of the surface holes on the contact adhesion of the PDMS films was studied using the JKR-type indentation tests by Thomas and Crosby [112]. They suggested the creation of surface micro-holes as a way to control the adhesion of the soft elastomers. Although only a slight adhesion enhancement (less than 2 times) was observed for the multi-holes being in multi-plane contact with a single-asperity indentation probe, they expected a more pronounced adhesion enhancement if the probe was replaced by a multi-asperity surface. The conformal contact on micro-patterned surfaces in our system resembles the situation of multi-asperity contacts. Furthermore, they suggested that the contact mechanical response around a micro-hole is being dictated by the stressed volume of the material, which controls the stiffness of the contact geometry and subsequently alters elastic energy dissipation process. As shown in the Table 6-1, there is a large variation in the stressed volume $\boldsymbol{V_S}$ or $\boldsymbol{\varphi_V}$ in the vicinity of the micro-holes. The stress volume $\boldsymbol{V_S}$ is linearly related to the height of the micro-pillars through equations 6-3 and 6-4. These analyses suggested that the contribution of elastic energy dissipation to the adhesion enhancement linearly increases with the height of micro-pillars. This elastic energy contribution may be responsible to the observed initial linear relationship in Figure 6 between the adhesion and the micro-pillars height.

6.4.2 The side-wall separation of the micro-pillars from their soft substrate - role of local friction

The side-wall separation resembles the "pull-out" of fibres in a composite material. In this case, interfacial separation would happen when the applied force on the fibre overcomes the friction

resistance between fibre walls and encompassing matrix as illustrated in Figure 6-11-A. For two surfaces in an intimate contact, the friction resistance is related to both the load-controlled Coulomb-type friction and the adhesion-controlled intrinsic interfacial shear stress term [120], [123]. Gent expanded the Griffith's energy criterion for pulling out a glass fibre from an elastic PDMS matrix [170]. Presuming the fibre normally stressed by Poissonian contraction of the incompressible elastic matrix (p) as a result of polymer shrinkage during the curing, this friction contribution could be formulated as follow: $\boldsymbol{F_f = 2\pi r(p\mu X + \tau h)}$, where $\boldsymbol{\tau}$ is the interfacial shear stress, $\boldsymbol{\mu}$ is the coefficient of friction, X is the debonded length over which debonding initiates. The process of fibre pull-out usually happens with a critical pull-out force ($\boldsymbol{F_0 = 2\pi r h \tau}$) to initiate the debonding at the end of a rigid fibre embedded is a soft matrix [171], and follows with local stick-slip steps as showed in Figure 6-11-C. In the stick steps, the applied energy is consumed for debonding of interface, and in slip steps the stored energy dissipates in the friction between fibers pulling out of the matrix. Considering multiple micro-pillars involving in the peeling zone as illustrated in Figure 6-11-B, to a first approximation, we may assume the average debonding length is proportional to the fibre length($\overline{\boldsymbol{X}} \propto \boldsymbol{h}$). Thus the pull-out force may linearly increase with the height of the pillars.

$$\sum \boldsymbol{F_f = 2\pi r \tau' h} \qquad (\mathbf{6.11})$$

where $\boldsymbol{F_f}$ is the friction contribution of the pull-off force applied on the peeling front, and $\boldsymbol{\tau'}$ is an average friction stress in the peeling zone. Then, the dissipated work due to the friction force could be

$$\boldsymbol{W_f = \frac{1}{2} h \sum F_f = \pi r \tau' h^2} \qquad (\mathbf{6.12})$$

The total energy dissipation ($\boldsymbol{\Delta G_f}$) per unit apparent area of the micro-patterned surface ($\boldsymbol{A_0}$) of the fibril could be:

$$\boldsymbol{\Delta G_f = \left(\frac{W_f}{A_0} + G_0\right) - G_0 = \frac{W_f}{A_0} = \frac{\pi r \tau' h^2}{\pi r^2} = \frac{\tau' h^2}{r}} \qquad (\mathbf{6.13}).$$

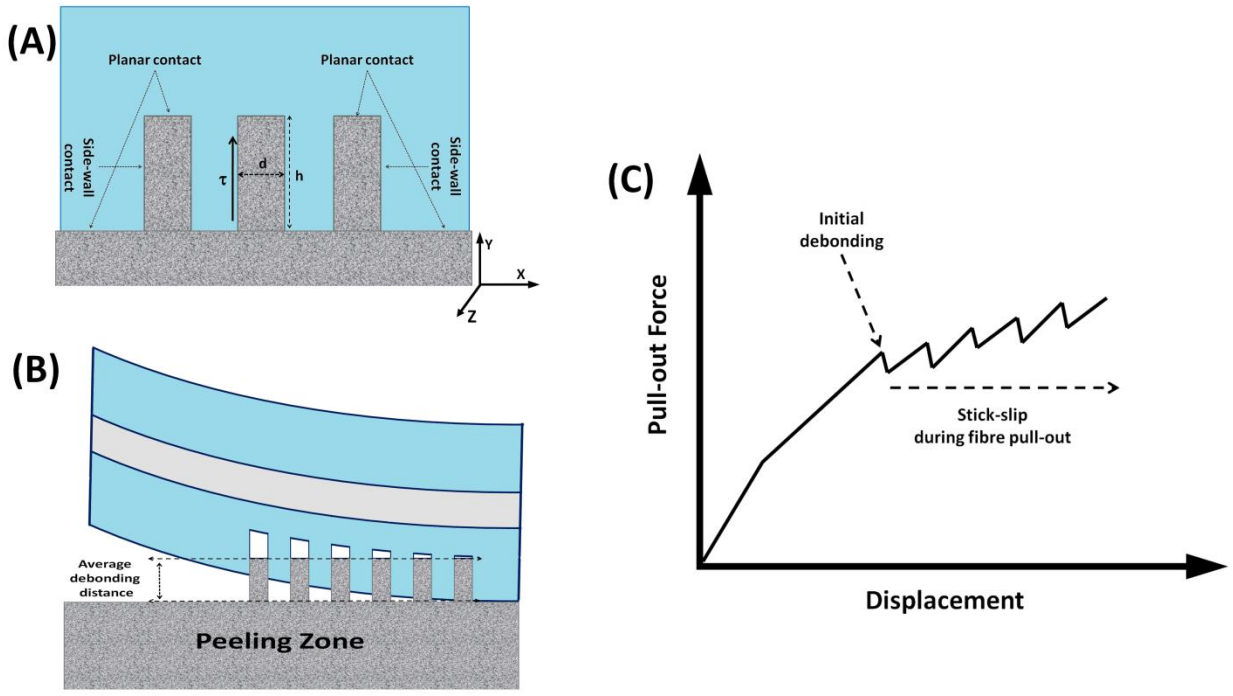

Figure 6-11: Schematic illustration of the peeling zone. (A) front view of the peeling zone showing the micro-pillars embedded into the PDMS tape, (B) side view of the peeling zone showing the decrease in debonded distance from the edge toward the inside of conformal contact, and (C) schematic force vs displacement curve of pulling out individual micro-pillars showing the initial debonding, complete debonding and stick-slip steps.

Therefore, energy dissipation due to the friction could be proportional to square of pillars height. It is interesting to notice in Figure 6-6-A that $\boldsymbol{G_C}$ tends to follow a parabolic relation with the pillars height. This transition takes place in a certain height of the pillars ($\boldsymbol{h \approx 20\mu m}$) at which the curve starts to deviate from the initial linear relation. This transition height seems related to the average debonded length in the pull-out of micro-pillars. That is, for the pillars with heights less than this length scale, they could be pulled out immediately after the debonding; there were no significant stick-slip steps. Once the pillars height exceeded this scale, the stick-slip processes occur and consume a large amount of energy. The local stick-slip events may also contribute to the observed peeling stick-slips as shown in the peeling curve in Figure 6-5. It is also worth to note the occurrence of shear-lip for high aspect-ratio pillars. According to the above friction-based consideration, it is reasonable to attribute this shear-lip to friction-induced local wears. There is a transition from interfacial sliding to friction with wears as the micro-pillar height or the interfacial shear resistance increases [119]. The tip experienced the severest friction since the entire micro-pillar slid through it.

Because the pillars were not pulled out vertically in peeling, the shear lips formed at the same side as the peeling direction. We had no direct information on the wear situation on the side walls but moderate wear was expected. Certainly, the local wearing dissipates the applied energy and contributes the enhanced adhesion strength.

Finally, it might be instructive to compare the possible contributions of the three energy dissipation processes: the global plastic deformation of the peeling strip, local elastic energy dissipation, and local debonding and friction energy dissipation. First, the global plastic contribution is a consequence of the enhanced adhesion at the interface due to micro-patterning. This plastic deformation can arise from both the PDMS coating and the paper strips. However, PDMS is so highly elastic that we can neglect the plastic deformation due to the bending of the PDMS. Thus, the observed plastic deformation could be attributed primarily to the paper strips, which is believed to be larger only by few times than the work of adhesion [172], [173]. Second, from the reported spatular adhesion measurements of biomimetic fibrils similar to our micro-pillars in length scales and geometry, the maximum adhesion enhancements in normal direction were less than 10 times, [64], [71–73], [96], [109], [111], [115], [141], [174]. In addition, most of the fibrillar adhesives are made of soft elastomers while the micro-pillars in our system are rigid. Hence, the contribution of elastic energy dissipation may only be significant for the conformal adhesion on short micro-pillars ($h < 20\ \mu m$). Furthermore, it is not able to explain the non-linear adhesion enhancement by more than two orders of magnitude as shown in Figure 6-6-A. As the height of pillars increases, the friction term become more pronounced. All these information suggests that the friction term plays a primary role in the conformal adhesion behavior of micro-structured surfaces.

6.4.3 Implications for adhesive bonding

The way we performed the experiment of conformal adhesion resembles the bonding process of two surfaces using liquid adhesives; both of them involves the curing or solidification. The initial liquid state makes the conformal contact possible while the solidification renders a cohesive strength to the adhesives. There is little adhesion between PDMS and SU-8 in planar contact as predicted from the calculated thermodynamic work of adhesion. The observed practical adhesion on smooth SU-8 surfaces in peeling experiment are expected larger as indicated by the indentation tests; but they are still too low to be measureable by a load cell with a sensitivity of 1mN. Although it is well known that surface roughness can increase adhesion. Herein, we report the adhesion can be precisely

controlled by surface micro-patterning. Other than the geometrical effect, there is a significant friction-component in the separation. This may suggest an alternative strategy to tune the strength of adhesive bonding of similar or dissimilar materials in contrast to the chemistry-based adhesive bonding, for example, by the use of superglues. As only van der Waals interactions and associated polymer chain diffusion are involved in our system, the proposed strategy may be applicable to all types of polymer surfaces. Just as gecko can climb on both dry and wet surfaces, we expect this micro-patterning based adhesion enhancement will work in both dry and aqueous conditions. The loss of van der Waal force due to the effect of water medium could be compensated by the involvement of friction elements in the adhesive bonding. This is important for the assembling of individual components into functional devices. Other than the application in microelectromechanical system, this strategy may help to meet the requirement of bio-integration in the fabrication and application of biosensor and biomedical devices in which chemical modifications are not always feasible because of the requirement of biocompatibility. For instance, the surface adhesion has recently been utilized in the design of a conformal, bio-interfaced class of silicon electronics [175]. Our studies suggest that the adhesion at interface can be enhanced significantly by creating micro- patterns on the rigid surfaces. A combined use of the micro/nano-structured surfaces with the van der Waals interactions seem to be a potentially more universal solution than the conventional adhesive bonding technology which depends on the chemical and viscoelastic properties of the materials.

6.5 Conclusions

The conformal adhesion on the surfaces patterned with biomimetic micro-pillars was systemically studied by a series of peeling experiment coupled with optical interference imaging. The adhesion enhancement as a function of pillar heights and the associated delamination mechanisms were investigated. The investigations revealed a remarkable conformal adhesion enhancement on the micro-patterned surfaces. The adhesion of a low-surface energy polydimethylsiloxane tape to SU-8 micro-patterned surfaces was found able to increase by 550 folds as the aspect-ratio increases from 0 to 6. A non-linear relationship between adhesion enhancement and surface area enlargement was found, suggesting that the adhesion enhancement is not a purely matter of the increase in the physical contact area due to surface roughness. Furthermore, the different aspects of adhesion enhancement mechanisms – local elastic energy dissipation process, side-wall friction, and plastic deformations – were analyzed and discussed in terms of their contributions to the adhesion enhancement. We conclude that the local adhesion and friction events of pulling micro-pillars out of the embedded

polymer film play a primary role in the observed adhesion enhancement. The local friction-based adhesion enhancement mechanism may have profound implications for effective assembly of similar or dissimilar material components at ever-smaller scales for bio-devices and biomedical applications.

Chapter 7

Conclusions and future recommendations

Propensity of the biomimetic structures in tuning of the adhesion and friction has been studied in this thesis. First, PDMS and SU-8 micropillars with various aspect ratios and geometries were fabricated via soft lithography and UV lithography techniques. PDMS pillars were replicated from Si master molds fabricated by DRIE technique. SU-8 pillars were fabricated in cleanroom area through UV lithography technique. The SEM images showed the straight structure of pillars without any buckling.

Second, micro-indentation tests were carried out on smooth PDMS and micropatterned PDMS. The results showed a remarkable decrease in adhesion. This was attributed to reduction of contact area as the elastic energy dissipation mechanisms taking place during the pull-off are not large enough to compensate this reduction.

Third, various AR micropillars were examined in terms of friction properties and it is concluded that the AR of pillars could act as a friction modulator under different preloads. Especially, in low preloads the sensitivity of the friction force to preload is high. This gives in hand a promising mean to physically tailor the frictional properties of polymers applied in short range small preload applications.

Forth, PDMS micropillars were topped with a terminal thin film. By this the real contact area is preserved while the compliance and proneness of the surface to dissipate elastic energy increases. Thus, the adhesion increases. In the following, viscoelastic thin film terminated biomimetic structures are proposed as a promising pathway to obtain strong adhesion. More than 10 fold increase in pull-off force was attributed to combination of elastic energy dissipation and viscoelastic losses mechanisms.

Fifth, a new generation of use of biomimetic structures was introduced. It is shown that by reaching to a certain AR inter-fibrillar friction would be a promising mechanism of adhesion enhancement. The domain of use of this would be integration of the biomedical rigid or soft devices to soft biointerfaces, where nearly conformal contact between tissue and device is expected. The ongoing research is to

examine or generalize the mechanisms of adhesion enhancement between soft microstructured surfaces and soft adherents.

Recommendations for future work include subtly examining the bottom view imaging to measure the real area of contact. One of the milestones would be distinguishing whether the bending of pillars are responsible for change in friction force or the number of pillars in contact. Moreover, optimization of the microstructures' size and geometry together with durability of the adhesive has not been investigated yet. It is important to explore repetitive adhesion testing on the same spot and washing the adhesive to test durability of the proposed structure.

The overall future trend of the field is utilization of the synthetic structures in different technological applications. For instance, there is a significant demand for biocompatible polymeric tissue adhesives in such medical and biomedical applications as wound dressings, augmentation of suture, reconstructive surgical implantations, and mesh grafts for different healing purposes. These adhesives must retain their anticipated adhesive behaviors to underlying tissue while undergo mechanical deformations and harsh physiological conditions. However, chemical-based conventional adhesives suffer from several inconsistencies in terms of unsuccessful adhesion to tissues, cohesive failure due to detachment, and non-biocompatibility of the common glues.

There are a few reports studying the feasibility of the use of gecko-inspired adhesives in biological applications. A hybrid biologically inspired mechanism of adhesion to bio-surfaces has been proposed by Messersmith's group study [176], in which they have integrated repeatable nature of gecko adhesive and wet adhesive properties of mussels. Moreover, Mahdavi et al. [160] has introduced a biocompatible and biodegradable elastomer coated with a thin tissue-reactive layer exploiting the gecko-inspired surface patterns to tune the adhesion to the underlying tissue. Furthermore, recently, poly(dimethylsiloxane) gecko-inspired surfaces has been applied to skin to examine the performance of adhesion of patterned surfaces as a replacement or refinement of grafts being use in reconstructive surgeries such as tympanoplasty and other applications in this sort [75], [177].

Optimization of several parameters, such as biocompatibility and biodegradability, strong tissue bonding, compliance and conformability of the adhesives to the underlying tissue, is the foremost reason of the complexity of the study of such a system. Also, intrinsic mist and roughness of the bio-

surfaces and strong dependency of the gecko-inspired adhesives to these parameters can complicate the situation. These parameters have opened a challenging horizon of research in the field of biological inspired adhesives.

Permission

Home | Create Account | Help

Title: Conformal Adhesion Enhancement on Biomimetic Microstructured Surfaces
Author: Hamed Shahsavan et al.
Publication: Langmuir
Publisher: American Chemical Society
Date: Jun 1, 2011

User ID
Password
Enable Auto Login
LOGIN
Forgot Password/User ID?
If you're a copyright.com user, you can login to Rightslink using your copyright.com credentials. Already a **Rightslink user** or want to learn more?

PERMISSION/LICENSE IS GRANTED FOR YOUR ORDER AT NO CHARGE

This type of permission/license, instead of the standard Terms & Conditions, is sent to you because no fee is being charged for your order. Please note the following:

- Permission is granted for your request in both print and electronic formats.
- If figures and/or tables were requested, they may be adapted or used in part.
- Please print this page for your records and send a copy of it to your publisher/graduate school.
- Appropriate credit for the requested material should be given as follows: "Reprinted (adapted) with permission from (COMPLETE REFERENCE CITATION). Copyright (YEAR) American Chemical Society." Insert appropriate information in place of the capitalized words.
- One-time permission is granted only for the use specified in your request. No additional uses are granted (such as derivative works or other editions). For any other uses, please submit a new request.

BACK | CLOSE WINDOW

Bibliography

[1] K. Kendall, *Molecular Adhesion and Its Applications The Sticky Universe*, 1st ed. New York: Kluwer Academic/Plenum Publishers, 2001.

[2] J. Colchero, E. Meyer, and O. Marti, "Friction on an Atomic Scale," in *Handbook of Micro/Nanotribology*, 2nd ed., B. Bhushan, Ed. CRC Press LLC, 1999, pp. 273-334.

[3] R. J. Good, "Contact angle, wetting, and adhesion: a critical review," *Journal of Adhesion Science and Technology*, vol. 6, no. 12, pp. 1269-1302, 1992.

[4] J. Berg, "Semi-empirical strategies for predicting adhesion," in *Adhesion Science and Engineering*, vol. 2, A. D. Chaudhury, M. K. and Pocius, Ed. Amsterdam: Elsevier B.V., 2002, pp. 1-73.

[5] D. H. Bangham and R. I. Razouk, "The Swelling of Charcoal. Part V. The Saturation and Immersion Expansions and the Heat of Wetting," *Proc. R. Soc. Lond. A*, vol. 166, p. 572, 1938.

[6] J. N. Israelachvili, *Intermolecular and Surface Forces*, 2nd ed. London: Academic Press, 1992.

[7] K. Kendall, "Adhesion : Molecules and Mechanics Kevin Kendall," *Science*, vol. 263, pp. 1720-1725, 1994.

[8] S. S. Voyutskii and V. L. Vakula, "The role of diffusion phenomena in polymer-to-polymer adhesion," *Journal of Applied Polymer Science*, vol. 7, no. 2, pp. 475-491, Mar. 1963.

[9] C. R. Crick and I. P. Parkin, "Preparation and characterisation of super-hydrophobic surfaces," *Chemistry A Europian Journal*, vol. 16, no. 12, pp. 3568-88, Mar. 2010.

[10] Y. Xiu and C. Wong, "Biomimetic Lotus Effect Surfaces for Nanopackaging," *Nano-Bio-Electronic, Photonic and MEMS Packaging*, p. 47, 2009.

[11] R. N. Wenzel, "Resistance of Solid Surfaces To Wetting By Water," *Industrial & Engineering Chemistry*, vol. 28, no. 8, pp. 988-994, Aug. 1936.

[12] A. Cassie and S. Baxter, "Wettability of porous surfaces," *Transactions of the Faraday Society*, vol. 40, pp. 546–551, 1944.

[13] N. Maeda, N. Chen, M. Tirrell, and J. N. Israelachvili, “Adhesion and friction mechanisms of polymer-on-polymer surfaces.,” *Science*, vol. 297, no. 5580, pp. 379-82, Jul. 2002.

[14] B. V. and Y. P. T. MULLER, V.M., DERJAGUIN, “On two methods of calculation of the forces of sticking of an elastic sphere to a rigid plane,” *Colloids and Surfaces*, vol. 7, pp. 251-259, 1983.

[15] B. Derjaguin, “Effect of contact deformations on the adhesion of particles,” *Journal of Colloid and Interface Science*, vol. 53, no. 2, pp. 314-326, Nov. 1975.

[16] K. Kendall, “Energy analysis of adhesion,” in *Adhesion Science and Engineering Volume 1*, 1st ed., A. V. Dillard, D.A.; Pocius, Ed. Amsterdam: Elsevier, 2002, pp. 77-110.

[17] A. A. Burnham, Nancy. A and Kulik, “Surface Forces and Adhesion,” in *Handbook of Micro/Nanotribology*, 2nd ed., B. Bhushan, Ed. CRC Press LLC, 1999, pp. 247-272.

[18] K. R. Shull, “Contact mechanics,” in *Adhesion Science and Engineering Volume 1*, 1st ed., M. Dillard, D.A.; Pocius, A.V.; Chaudhury, Ed. Amsterdam: Elsevier, 2002, pp. 577-604.

[19] Bradly R. Stevenson, “The cohesion between smoke particles,” *Transactions of the Faraday Society*, vol. 32, pp. 1088-1090, Oct. 1936.

[20] K. L. Johnson, K. Kendall, and a. D. Roberts, “Surface Energy and the Contact of Elastic Solids,” *Proceedings of the Royal Society A*, vol. 324, no. 1558, pp. 301-313, Sep. 1971.

[21] A. A. Griffith, “The phenomenon of rupture and flow in solids,” *Phil Trans R Soc*, vol. 221, p. 163, 1920.

[22] A. N. Gent and A. J. Kinloch, “Adhesion of viscoelastic materials to rigid substrates. III. Energy criterion for failure,” *Journal of Polymer Science Part A-2: Polymer Physics*, vol. 9, no. 4, pp. 659-668, Apr. 1971.

[23] E. H. Andrews and A. J. Kinloch, “Mechanics of Adhesive Failure. I,” *Proceedings of the Royal Society A*, vol. 332, no. 1590, pp. 385-399, 1973.

[24] E. H. Andrews and A. J. Kinloch, “Mechanics of Adhesive Failure. II,” *Proceedings of the Royal Society A*, vol. 332, no. 1590, pp. 401-414, 1973.

[25] D. E. Packham, “Some Contributions of Surface Analysis to the Development of Adhesion Theories,” *The Journal of Adhesion*, vol. 84, no. 3, pp. 240-255, Apr. 2008.

[26] K. R. Shull, D. Ahn, W.-L. Chen, C. M. Flanigan, and A. J. Crosby, "Axisymmetric adhesion tests of soft materials," *Macromolecular Chemistry and Physics*, vol. 199, no. 4, pp. 489-511, Apr. 1998.

[27] B. N. J. Persson, "Biological adhesion for locomotion: basic principles," *Journal of Adhesion Science and Technology*, vol. 21, no. 12, pp. 1145-1173, Oct. 2007.

[28] K. N. G. Fuller and D. Tabor, "The Effect of Surface Roughness on the Adhesion of Elastic Solids," *Proceedings of the Royal Society A*, vol. 345, no. 1642, pp. 327-342, Sep. 1975.

[29] S. N. Gorb, M. Sinha, A. Peressadko, K. a Daltorio, and R. D. Quinn, "Insects did it first: a micropatterned adhesive tape for robotic applications.," *Bioinspiration & biomimetics*, vol. 2, no. 4, pp. S117-25, Dec. 2007.

[30] B. Dean and B. Bhushan, "Shark-skin surfaces for fluid-drag reduction in turbulent flow: a review.," *Philosophical Transactions of the Royal Society - Series A*, vol. 368, no. 1929, pp. 4775-4806, 2010.

[31] Y. Fang, G. Sun, T. Wang, Q. Cong, and L. Ren, "Hydrophobicity mechanism of non-smooth pattern on surface of butterfly wing," *Chinese Science Bulletin*, vol. 52, no. 5, pp. 711-716, Mar. 2007.

[32] G. Xuefeng, "Water-repellent legs of water striders," *Nature*, vol. 432, p. 36, 2004.

[33] K. and L. P. B. Bálint, Zs., Vértesy,Z., Kertész, "Scanning Electron Microscopic Investigations in Butterfly Wings: Detecting Scale Micro- and Nanomorphology and Understanding their Functions," in *Current Issues on Multidisciplinary Microscopy Research and Education*, A. M.-V. and L.Labajos-Broncano, Ed. FORMATEX Microscopy Book Series, 1999.

[34] C. Neinhuis, "Characterization and Distribution of Water-repellent, Self-cleaning Plant Surfaces," *Annals of Botany*, vol. 79, no. 6, pp. 667-677, Jun. 1997.

[35] W. Federle, "Why are so many adhesive pads hairy?," *The Journal of Experimental Biology*, vol. 209, no. 14, pp. 2611-21, Jul. 2006.

[36] E. Arzt, S. Gorb, and R. Spolenak, "From micro to nano contacts in biological attachment devices.," *Proceedings of the National Academy of Sciences of the United States of America*, vol. 100, no. 19, pp. 10603-6, Sep. 2003.

[37] K. Autumn et al., "Adhesive force of a single gecko foot-hair.," *Nature*, vol. 405, no. 6787, pp. 681-5, Jun. 2000.

[38] K. Autumn et al., “Evidence for van der Waals adhesion in gecko setae.,” *Proceedings of the National Academy of Sciences of the United States of America*, vol. 99, no. 19, pp. 12252-6, Sep. 2002.

[39] K. Autumn, “Properties, principles, and parameters of the gecko adhesive system,” in *Biological adhesives*, S. A. M. and C. J.A., Ed. Berlin Heidelberg: Springer Verlag, 2006, pp. 225-256.

[40] B. Bhushan, “Adhesion of multi-level hierarchical attachment systems in gecko feet,” *Journal of Adhesion Science and Technology*, vol. 21, no. 12, pp. 1213-1258, Oct. 2007.

[41] K. Autumn and N. Gravish, “Gecko adhesion: evolutionary nanotechnology.,” *Philosophical Transactions Series A*, vol. 366, no. 1870, pp. 1575-90, May 2008.

[42] J.-S. Kwak and T.-W. Kim, “A review of adhesion and friction models for gecko feet,” *International Journal of Precision Engineering and Manufacturing*, vol. 11, no. 1, pp. 171-186, Apr. 2010.

[43] W. R. Hansen and K. Autumn, “Evidence for self-cleaning in gecko setae.,” *Proceedings of the National Academy of Sciences of the United States of America*, vol. 102, no. 2, pp. 385-9, Jan. 2005.

[44] K. Autumn and W. Hansen, “Ultrahydrophobicity indicates a non-adhesive default state in gecko setae.,” *Journal of comparative physiology. A, Neuroethology, sensory, neural, and behavioral physiology*, vol. 192, no. 11, pp. 1205-12, Nov. 2006.

[45] K. Autumn, S. T. Hsieh, D. M. Dudek, J. Chen, C. Chitaphan, and R. J. Full, “Dynamics of geckos running vertically.,” *The Journal of Experimental Biology*, vol. 209, no. 2, pp. 260-72, Jan. 2006.

[46] A. Haase, “Untersuchungen über den Bau und die Entwicklung der Haftlappen bei den Geckotiden,” *Archiv f Naturgesch*, vol. 66, no. 3, pp. 321-345, 1900.

[47] W. D. Dellit, “Zur Anatomie und Physiologie der Geckozehe,” *Jena Z Naturw*, vol. 68, pp. 613-656, 1934.

[48] P. F. A. Maderson, “Keratinized epidermal derivatives as an aid to climbing in gekkonid lizards,” *Nature*, vol. 203, pp. 780-781, 1964.

[49] U. Hiller, “Untersuchungen zum Feinbau und zur Funktion der Haftborsten von Reptilien,” *Zoomorphology*, vol. 62, pp. 307-362, 1968.

[50] U. Hiller, “Correlation between Corona-Discharge of Polyethylene-Films and the adhering Power of Tarentola m. mauritanica (Rept.),” *forma et functio*, vol. 1, pp. 350-352, 1969.

[51] U. Hiller, “Comparative studies on the functional morphology of two gekkonid lizards,” *J Bombay Nat Hist Soc*, vol. 73, pp. 278-282, 1975.

[52] K. Autumn and A. M. Peattie, “Mechanisms of adhesion in geckos.,” *Integrative and Comparative Biology*, vol. 42, no. 6, pp. 1081-90, Dec. 2002.

[53] G. Huber et al., “Evidence for capillarity contributions to gecko adhesion from single spatula nanomechanical measurements.,” *Proceedings of the National Academy of Sciences of the United States of America*, vol. 102, no. 45, pp. 16293-6, Nov. 2005.

[54] W. Sun, P. Neuzil, T. S. Kustandi, S. Oh, and V. D. Samper, “The nature of the gecko lizard adhesive force.,” *Biophysical journal*, vol. 89, no. 2, pp. L14-7, Aug. 2005.

[55] N. S. Pesika et al., “Gecko adhesion pad: a smart surface?,” *Journal of physics. Condensed Matter*, vol. 21, no. 46, p. 464132, Nov. 2009.

[56] H. E. Jeong and K. Y. Suh, “Nanohairs and nanotubes: Efficient structural elements for gecko-inspired artificial dry adhesives,” *Nano Today*, vol. 4, no. 4, pp. 335-346, Aug. 2009.

[57] Y. Zhao, T. Tong, L. Delzeit, A. Kashani, M. Meyyappan, and A. Majumdar, “Interfacial energy and strength of multiwalled-carbon-nanotube-based dry adhesive,” *Journal of Vacuum Science & Technology B: Microelectronics and Nanometer Structures*, vol. 24, no. 1, p. 331, 2006.

[58] L. Ge, S. Sethi, L. Ci, P. M. Ajayan, and A. Dhinojwala, “Carbon nanotube-based synthetic gecko tapes.,” *Proceedings of the National Academy of Sciences of the United States of America*, vol. 104, no. 26, pp. 10792-5, Jun. 2007.

[59] L. Qu, L. Dai, M. Stone, Z. Xia, and Z. L. Wang, “Carbon nanotube arrays with strong shear binding-on and easy normal lifting-off.,” *Science*, vol. 322, no. 5899, pp. 238-42, Oct. 2008.

[60] L. Ge et al., “Cooperative Adhesion and Friction of Compliant Nanohairs.,” *Nano Letters*, vol. 90, pp. 4509-4513, Oct. 2010.

[61] M. Northen and K. Turner, “Meso-scale adhesion testing of integrated micro- and nano-scale structures,” *Sensors and Actuators A: Physical*, vol. 130-131, pp. 583-587, Aug. 2006.

[62] M. T. Northen and K. L. Turner, “A batch fabricated biomimetic dry adhesive,” *Nanotechnology*, vol. 16, no. 8, pp. 1159-1166, Aug. 2005.

[63] M. T. Northen, C. Greiner, E. Arzt, and K. L. Turner, “A Gecko-Inspired Reversible Adhesive,” *Advanced Materials*, vol. 20, no. 20, pp. 3905-3909, Oct. 2008.

[64] A. K. Geim, S. V. Dubonos, I. . V. Grigorieva, K. S. Novoselov, A. A. Zhukov, and S. Y. Shapoval, “Microfabricated adhesive mimicking gecko foot-hair,” *Nature Materials*, vol. 2, no. 7, pp. 461-3, Jul. 2003.

[65] M. Sitti and R. S. Fearing, “Synthetic gecko foot-hair micro/nano-structures as dry adhesives,” *Journal of Adhesion Science and Technology*, vol. 17, no. 8, pp. 1055-1073, Aug. 2003.

[66] C. Majidi et al., “High Friction from a Stiff Polymer Using Microfiber Arrays,” *Physical Review Letters*, vol. 97, no. 7, pp. 18-21, Aug. 2006.

[67] B. Schubert et al., “Towards friction and adhesion from high modulus microfiber arrays,” *Journal of Adhesion Science and Technology*, vol. 21, no. 12, pp. 1297-1315, Oct. 2007.

[68] J. Lee, C. Majidi, B. Schubert, and R. S. Fearing, “Sliding-induced adhesion of stiff polymer microfibre arrays. I. Macroscale behaviour.,” *Journal of the Royal Society, Interface*, vol. 5, no. 25, pp. 835-44, Aug. 2008.

[69] J. Lee and R. S. Fearing, “Contact self-cleaning of synthetic gecko adhesive from polymer microfibers,” *Langmuir*, vol. 24, no. 19, pp. 10587-91, Oct. 2008.

[70] J. Lee, B. Bush, R. Maboudian, and R. S. Fearing, “Gecko-inspired combined lamellar and nanofibrillar array for adhesion on nonplanar surface,” *Langmuir*, vol. 25, no. 21, pp. 12449-53, Nov. 2009.

[71] N. J. Glassmaker, T. Himeno, C.-Y. Hui, and J. Kim, “Design of biomimetic fibrillar interfaces: 1. Making contact,” *Journal of the Royal Society, Interface*, vol. 1, no. 1, pp. 23-33, Nov. 2004.

[72] C.-Y. Hui, N. J. Glassmaker, T. Tang, and A. Jagota, “Design of biomimetic fibrillar interfaces: 2. Mechanics of enhanced adhesion.,” *Journal of the Royal Society, Interface*, vol. 1, no. 1, pp. 35-48, Nov. 2004.

[73] S. Kim and M. Sitti, “Biologically inspired polymer microfibers with spatulate tips as repeatable fibrillar adhesives,” *Applied Physics Letters*, vol. 89, no. 26, p. 261911, 2006.

[74] M. K. Kwak, H. E. Jeong, W. G. Bae, H.-S. Jung, and K. Y. Suh, "Anisotropic Adhesion Properties of Triangular-Tip-Shaped Micropillars.," *Small*, vol. 7, no. 16, p. 2266, Jun. 2011.

[75] M. K. Kwak, H.-E. Jeong, and K. Y. Suh, "Rational Design and Enhanced Biocompatibility of a Dry Adhesive Medical Skin Patch," *Advanced Materials*, vol. 23, no. 34, pp. 3949-3953, Jul. 2011.

[76] J. Yu et al., "Gecko-Inspired Dry Adhesive for Robotic Applications," *Advanced Functional Materials*, vol. 21, no. 16, pp. 3010-3018, May 2011.

[77] A. del Campo and E. Arzt, "Fabrication approaches for generating complex micro- and nanopatterns on polymeric surfaces.," *Chemical Reviews*, vol. 108, no. 3, pp. 911-45, Mar. 2008.

[78] C. Greiner, A. D. Campo, and E. Arzt, "Adhesion of bioinspired micropatterned surfaces: effects of pillar radius, aspect ratio, and preload," *Langmuir*, vol. 23, no. 7, pp. 3495-502, Mar. 2007.

[79] C. Greiner, S. Buhl, A. del Campo, and E. Arzt, "Experimental Parameters Controlling Adhesion of Biomimetic Fibrillar Surfaces," *The Journal of Adhesion*, vol. 85, no. 9, pp. 646-661, Sep. 2009.

[80] S. Reddy, E. Arzt, and a. del Campo, "Bioinspired Surfaces with Switchable Adhesion," *Advanced Materials*, vol. 19, no. 22, pp. 3833-3837, Nov. 2007.

[81] J. Kwon, E. Cheung, S. Park, and M. Sitti, "Friction enhancement via micro-patterned wet elastomer adhesives on small intestinal surfaces.," *Biomedical Materials*, vol. 1, no. 4, pp. 216-20, Dec. 2006.

[82] H. Shahsavan and B. Zhao, "Conformal adhesion enhancement on biomimetic microstructured surfaces," *Langmuir*, vol. 27, no. 12, pp. 7732-42, Jun. 2011.

[83] A. del Campo, I. Álvarez, S. Filipe, and M. Wilhelm, "3D Microstructured Surfaces Obtained by Soft-Lithography Using Fast-Crosslinking Elastomeric Precursors and 2D Masters," *Advanced Functional Materials*, vol. 17, no. 17, pp. 3590-3597, Nov. 2007.

[84] B. Aksak, M. P. Murphy, and M. Sitti, "Adhesion of biologically inspired vertical and angled polymer microfiber arrays.," *Langmuir*, vol. 23, no. 6, pp. 3322-32, Mar. 2007.

[85] G. Castellanos, E. Arzt, and M. Kamperman, "Effect of viscoelasticity on adhesion of bioinspired micropatterned epoxy surfaces," *Langmuir*, vol. 27, no. 12, pp. 7752-9, Jun. 2011.

[86] D. Suh, S.-J. Choi, and H. H. Lee, "Rigiflex Lithography for Nanostructure Transfer," *Advanced Materials*, vol. 17, no. 12, pp. 1554-1560, Jun. 2005.

[87] H. E. Jeong, S. H. Lee, P. Kim, and K. Y. Suh, "Stretched polymer nanohairs by nanodrawing.," *Nano Letters*, vol. 6, no. 7, pp. 1508-13, Jul. 2006.

[88] H. E. Jeong, S. H. Lee, P. Kim, and K. Y. Suh, "High aspect-ratio polymer nanostructures by tailored capillarity and adhesive force," *Colloids and Surfaces A*, vol. 313-314, pp. 359-364, Feb. 2008.

[89] S. Kim, M. Sitti, C.-Y. Hui, R. Long, and A. Jagota, "Effect of backing layer thickness on adhesion of single-level elastomer fiber arrays," *Applied Physics Letters*, vol. 91, no. 16, p. 161905, 2007.

[90] R. Long, C.-Y. Hui, S. Kim, and M. Sitti, "Modeling the soft backing layer thickness effect on adhesion of elastic microfiber arrays," *Journal of Applied Physics*, vol. 104, no. 4, p. 044301, 2008.

[91] D. Sameoto and C. Menon, "Direct molding of dry adhesives with anisotropic peel strength using an offset lift-off photoresist mold," *Journal of Micromechanics and Microengineering*, vol. 19, no. 11, p. 115026, Nov. 2009.

[92] D. Sameoto and C. Menon, "A low-cost, high-yield fabrication method for producing optimized biomimetic dry adhesives," *Journal of Micromechanics and Microengineering*, vol. 19, no. 11, p. 115002, Nov. 2009.

[93] D. Sameoto and C. Menon, "Deep UV patterning of acrylic masters for molding biomimetic dry adhesives," *Journal of Micromechanics and Microengineering*, vol. 20, no. 11, p. 115037, Nov. 2010.

[94] A. del Campo, C. Greiner, I. Álvarez, and E. Arzt, "Patterned Surfaces with Pillars with Controlled 3D Tip Geometry Mimicking Bioattachment Devices," *Advanced Materials*, vol. 19, no. 15, pp. 1973-1977, Aug. 2007.

[95] A. del Campo, C. Greiner, and E. Arzt, "Contact shape controls adhesion of bioinspired fibrillar surfaces.," *Langmuir*, vol. 23, no. 20, pp. 10235-43, Sep. 2007.

[96] M. P. Murphy, B. Aksak, and M. Sitti, "Gecko-inspired directional and controllable adhesion.," *Small*, vol. 5, no. 2, pp. 170-5, Feb. 2009.

[97] M. P. Murphy, B. Aksak, and M. Sitti, "Adhesion and anisotropic friction enhancements of angled heterogeneous micro-fiber arrays with spherical and spatula tips," *Journal of Adhesion Science and Technology*, vol. 21, no. 12, pp. 1281-1296, Oct. 2007.

[98] C. Greiner, E. Arzt, and A. del Campo, "Hierarchical Gecko-Like Adhesives," *Advanced Materials*, vol. 21, no. 4, pp. 479-482, Jan. 2009.

[99] H. E. Jeong, J.-K. Lee, H. N. Kim, S. H. Moon, and K. Y. Suh, "A nontransferring dry adhesive with hierarchical polymer nanohairs.," *Proceedings of the National Academy of Sciences of the United States of America*, vol. 106, no. 14, pp. 5639-44, Apr. 2009.

[100] M. P. Murphy, S. Kim, and M. Sitti, "Enhanced adhesion by gecko-inspired hierarchical fibrillar adhesives.," *ACS Applied Materials & Interfaces*, vol. 1, no. 4, pp. 849-55, Apr. 2009.

[101] Y. Zhang, C.-T. Lin, and S. Yang, "Fabrication of hierarchical pillar arrays from thermoplastic and photosensitive SU-8.," *Small*, vol. 6, no. 6, pp. 768-75, Mar. 2010.

[102] R. Spolenak, S. Gorb, H. Gao, and E. Arzt, "Effects of contact shape on the scaling of biological attachments," *Proceedings of the Royal Society A*, vol. 461, no. 2054, pp. 305-319, Feb. 2005.

[103] B. N. J. Persson, "On the mechanism of adhesion in biological systems," *The Journal of Chemical Physics*, vol. 118, no. 16, p. 7614, 2003.

[104] C.-Y. Hui, N. J. Glassmaker, and a. Jagota, "How Compliance Compensates for Surface Roughness in Fibrillar Adhesion," *The Journal of Adhesion*, vol. 81, no. 7-8, pp. 699-721, Jul. 2005.

[105] B. Bhushan, A. G. Peressadko, and T.-W. Kim, "Adhesion analysis of two-level hierarchical morphology in natural attachment systems for 'smart adhesion'," *Journal of Adhesion Science and Technology*, vol. 20, no. 13, pp. 1475-1491, Oct. 2006.

[106] H. Yao and H. Gao, "Mechanics of robust and releasable adhesion in biology: Bottom–up designed hierarchical structures of gecko," *Journal of the Mechanics and Physics of Solids*, vol. 54, no. 6, pp. 1120-1146, Jun. 2006.

[107] M. Schargott, V. L. Popov, and S. Gorb, "Spring model of biological attachment pads.," *Journal of Theoretical Biology*, vol. 243, no. 1, pp. 48-53, Nov. 2006.

[108] A. Jagota and S. J. Bennison, "Mechanics of adhesion through a fibrillar microstructure.," *Integrative and Comparative Biology*, vol. 42, no. 6, pp. 1140-5, Dec. 2002.

[109] M. Lamblet, E. Verneuil, T. Vilmin, A. Buguin, P. Silberzan, and L. Léger, "Adhesion enhancement through micropatterning at polydimethylsiloxane-acrylic adhesive interfaces," *Langmuir*, vol. 23, no. 13, pp. 6966-74, Jun. 2007.

[110] K. Kendall, “Thin-film peeling-the elastic term,” *Journal of Physics D: Applied Physics*, vol. 8, p. 1449, 1975.

[111] N. J. Glassmaker, A. Jagota, C.-Y. Hui, W. L. Noderer, and M. K. Chaudhury, “Biologically inspired crack trapping for enhanced adhesion.,” *Proceedings of the National Academy of Sciences of the United States of America*, vol. 104, no. 26, pp. 10786-91, Jun. 2007.

[112] T. Thomas and A. J. Crosby, “Controlling Adhesion with Surface Hole Patterns,” *The Journal of Adhesion*, vol. 82, no. 3, pp. 311-329, Apr. 2006.

[113] D. Maugis, “Fracture mechanics and the adherence of viscoelastic bodies,” *Journal of Physics D: Applied Physics*, vol. 11, no. 14, pp. 1989-2023, Jan. 2001.

[114] E. P. Chan, D. Ahn, and A. J. Crosby, “Adhesion of Patterned Reactive Interfaces,” *The Journal of Adhesion*, vol. 83, no. 5, pp. 473-489, May 2007.

[115] A. J. Crosby, M. Hageman, and A. Duncan, “Controlling polymer adhesion with ‘pancakes’,” *Langmuir*, vol. 21, no. 25, pp. 11738-43, Dec. 2005.

[116] W. Ashurst, W., Carraro, C., Maboudian, R., Frey, “Wafer level anti-stiction coatings for MEMS,” *Sensors and Actuators A: Physical*, vol. 104, no. 3, pp. 213-221, May 2003.

[117] J. Liu, C. Y. Hui, and A. Jagota, “Effect of fibril arrangement on crack trapping in a film-terminated fibrillar interface,” *Journal of Polymer Science Part B: Polymer Physics*, vol. 47, no. 23, pp. 2368–2384, 2009.

[118] L. Shen, N. J. Glassmaker, A. Jagota, and C.-Y. Hui, “Strongly enhanced static friction using a film-terminated fibrillar interface,” *Soft Matter*, vol. 4, no. 3, p. 618, 2008.

[119] A. M. Homola, J. N. Israelachvili, P. M. Mcguiggan, and M. L. Gee, “Fundamental experimental studies in tribology: the transition from ‘interfacial’ friction of undamaged molecularly smooth surfaces to “normal’’ friction with wear,” *Wear*, vol. 136, pp. 65 - 83, 1990.

[120] A. Berman and C. Drummond, “Amontons law at the molecular level,” *Tribology letters*, vol. 4, no. 2, pp. 95–101, 1998.

[121] G. Adams, “Contact modeling — forces,” *Tribology International*, vol. 33, no. 5-6, pp. 431-442, May 2000.

[122] Y. Mo, K. T. Turner, and I. Szlufarska, "Friction laws at the nanoscale.," *Nature*, vol. 457, no. 7233, pp. 1116-9, Feb. 2009.

[123] J. Gao, W. D. Luedtke, D. Gourdon, M. Ruths, J. N. Israelachvili, and U. Landman, "Frictional Forces and Amontons' Law: From the Molecular to the Macroscopic Scale," *The Journal of Physical Chemistry B*, vol. 108, no. 11, pp. 3410-3425, Mar. 2004.

[124] M. Nosonovsky and B. Bhushan, "Multiscale friction mechanisms and hierarchical surfaces in nano- and bio-tribology," *Materials Science and Engineering: R: Reports*, vol. 58, no. 3-5, pp. 162-193, Nov. 2007.

[125] F. Wu-Bavouzet, J. Cayer-Barrioz, A. Le Bot, F. Brochard-Wyart, and A. Buguin, "Effect of surface pattern on the adhesive friction of elastomers," *Physical Review E*, vol. 82, no. 3, pp. 1-9, Sep. 2010.

[126] E.-S. Yoon et al., "Tribological properties of bio-mimetic nano-patterned polymeric surfaces on silicon wafer," *Tribology Letters*, vol. 21, no. 1, pp. 31-37, Jan. 2006.

[127] Y. Okamoto, K. Nishio, J.-ichi Sugiura, M. Hirano, and T. Nitta, "Friction of elastomer-on-glass system and direct observation of its frictional interface," *Journal of Physics: Conference Series*, vol. 89, p. 012011, Nov. 2007.

[128] M. Varenberg and S. Gorb, "Shearing of fibrillar adhesive microstructure: friction and shear-related changes in pull-off force," *Journal of The Royal Society, Interface*, vol. 4, no. 15, pp. 721-725, Aug. 2007.

[129] H. Yao, G. D. Rocca, P. R. Guduru, and H. Gao, "Adhesion and sliding response of a biologically inspired fibrillar surface: experimental observations.," *Journal of the Royal Society, Interface*, vol. 5, no. 24, pp. 723-33, Jul. 2008.

[130] B. He, W. Chen, and Q. Jane Wang, "Surface Texture Effect on Friction of a Microtextured Poly(dimethylsiloxane) (PDMS)," *Tribology Letters*, vol. 31, no. 3, pp. 187-197, Aug. 2008.

[131] S. Vajpayee, R. Long, L. Shen, A. Jagota, and C.-Y. Hui, "Effect of rate on adhesion and static friction of a film-terminated fibrillar interface.," *Langmuir*, vol. 25, no. 5, pp. 2765-71, Mar. 2009.

[132] M. Varenberg and S. N. Gorb, "Hexagonal Surface Micropattern for Dry and Wet Friction," *Advanced Materials*, vol. 21, no. 4, pp. 483-486, Jan. 2009.

[133] C. J. Rand and A. J. Crosby, "Friction of soft elastomeric wrinkled surfaces," *Journal of Applied Physics*, vol. 106, no. 6, p. 064913, 2009.

[134] N. Gravish et al., “Rate-dependent frictional adhesion in natural and synthetic gecko setae.,” *Journal of the Royal Society, Interface*, vol. 7, no. 43, pp. 259-69, Feb. 2010.

[135] R. K. Kramer, C. Majidi, and R. J. Wood, “Shear-mode contact splitting for a microtextured elastomer film.,” *Advanced Materials*, vol. 22, no. 33, pp. 3700-3, Sep. 2010.

[136] E. Buselli, V. Pensabene, P. Castrataro, P. Valdastri, A. Menciassi, and P. Dario, “Evaluation of friction enhancement through soft polymer micro-patterns in active capsule endoscopy,” *Measurement Science and Technology*, vol. 21, no. 10, p. 105802, Oct. 2010.

[137] B. Aksak, C.-yuen Hui, and M. Sitti, “The effect of aspect ratio on adhesion and stiffness for soft elastic fibres,” *Journal of the Royal Society, Interface*, vol. 8, no. 61, pp. 1166-75, Aug. 2011.

[138] B. Bhushan and R. a. Sayer, “Surface characterization and friction of a bio-inspired reversible adhesive tape,” *Microsystem Technologies*, vol. 13, no. 1, pp. 71-78, Sep. 2006.

[139] M. P. Murphy, B. Aksak, and M. Sitti, “Adhesion and anisotropic friction enhancements of angled heterogeneous micro-fiber arrays with spherical and spatula tips,” *Journal of Adhesion Science and Technology*, vol. 21, no. 12, pp. 1281-1296, Oct. 2007.

[140] E. Verneuil, B. Ladoux, A. Buguin, and P. Silberzan, “Adhesion on Microstructured Surfaces,” *The Journal of Adhesion*, vol. 83, no. 5, pp. 449-472, May 2007.

[141] C. Greiner, R. Spolenak, and E. Arzt, “Adhesion design maps for fibrillar adhesives: the effect of shape.,” *Acta biomaterialia*, vol. 5, no. 2, pp. 597-606, Feb. 2009.

[142] A. Chateauminois and C. Fretigny, “Local friction at a sliding interface between an elastomer and a rigid spherical probe,” *The European Physical Journal. E, Soft matter*, vol. 27, no. 2, pp. 221-7, Oct. 2008.

[143] A. P. Russell, “Integrative functional morphology of the gekkotan adhesive system (reptilia: gekkota).,” *Integrative and Comparative Biology*, vol. 42, no. 6, pp. 1154-1163, 2002.

[144] A. P. Russell, “A contribution to the functional morphology of the foot of the tokay, Gekko gecko (Reptilia, Gekkonidae),” *Journal of Zoology London*, vol. 176, pp. 437-476, 1975.

[145] R. Ruibal and V. Ernst, "The structure of the digital setae of lizards," *Journal of Morphology*, vol. 117, no. 3, pp. 271-294, 1965.

[146] Y. Tian et al., "Adhesion and friction in gecko toe attachment and detachment.," *Proceedings of the National Academy of Sciences of the United States of America*, vol. 103, no. 51, pp. 19320-5, Dec. 2006.

[147] B. Zhao et al., "Adhesion and friction force coupling of gecko setal arrays: implications for structured adhesive surfaces," *Langmuir*, vol. 24, no. 4, pp. 1517-24, Feb. 2008.

[148] B. Zhao et al., "Role of tilted adhesion fibrils (setae) in the adhesion and locomotion of gecko-like systems.," *The Journal of Physical Chemistry B*, vol. 113, no. 12, pp. 3615-3621, 2009.

[149] H. Zeng et al., "Frictional adhesion of patterned surfaces and implications for gecko and biomimetic systems," *Langmuir*, vol. 25, no. 13, pp. 7486-95, Jul. 2009.

[150] N. Pesika et al., "Peel-Zone Model of Tape Peeling Based on the Gecko Adhesive System," *The Journal of Adhesion*, vol. 83, no. 4, pp. 383-401, 2007.

[151] S. Chen and H. Gao, "Bio-inspired mechanics of reversible adhesion: Orientation-dependent adhesion strength for non-slipping adhesive contact with transversely isotropic elastic materials," *Journal of the Mechanics and Physics of Solids*, vol. 55, no. 5, pp. 1001-1015, 2007.

[152] K. Takahashi, J. Berengueres, K. Obata, and S. Saito, "Geckos' foot hair structure and their ability to hang from rough surfaces and move quickly," *International Journal of Adhesion and Adhesives*, vol. 26, no. 8, pp. 639-643, 2006.

[153] N. Gravish, M. Wilkinson, and K. Autumn, "Frictional and elastic energy in gecko adhesive detachment," *Journal of the Royal Society, Interface*, vol. 5, no. 20, pp. 339-348, 2008.

[154] E. P. Chan, C. Greiner, E. Arzt, and A. J. Crosby, "Designing Model Systems for Enhanced Adhesion," *MRS Bulletin*, vol. 32, no. June, pp. 496-503, 2007.

[155] a. Ghatak, L. Mahadevan, J. Y. Chung, M. K. Chaudhury, and V. Shenoy, "Peeling from a biomimetically patterned thin elastic film," *Proceedings of the Royal Society A*, vol. 460, no. 2049, pp. 2725-2735, Sep. 2004.

[156] J. Y. Chung and M. K. Chaudhury, "Roles of discontinuities in bio-inspired adhesive pads.," *Journal of the Royal Society, Interface*, vol. 2, no. 2, pp. 55-61, Mar. 2005.

[157] A. Majumder, A. Ghatak, and A. Sharma, "Microfluidic adhesion induced by subsurface microstructures.," *Science*, vol. 318, no. 5848, pp. 258-61, Oct. 2007.

[158] D. E. Packham, "Discontinuities at the Interface and Adhesion," *The Journal of Adhesion*, vol. 86, no. 12, pp. 1231-1243, Nov. 2010.

[159] G. Y. Lee, K. Cheung, W. Chang, and L. P. Lee, "Mechanical interlocking with precisely controlled nano-and microscale geometries for implantable microdevices," in *1st Annual International IEEE-EMBS Special Topic Conference on Microtechnologies in Medicine & Biology 1*, 2000, no. 1, pp. 1-5.

[160] A. Mahdavi et al., "A biodegradable and biocompatible gecko-inspired tissue adhesive.," *Proceedings of the National Academy of Sciences of the United States of America*, vol. 105, no. 7, pp. 2307-12, Feb. 2008.

[161] P. B. Aaron, Lau. K. H. and Messersmith, "Wet Performance of Biomimetic Fibrillar Adhesives," in *Biological Adhesive Systems*, Janek von Byern and Ingo Grunwald, Ed. Springer, 2010, pp. 285–294.

[162] S. Vajpayee, K. Khare, S. Yang, C.-Y. Hui, and A. Jagota, "Adhesion Selectivity Using Rippled Surfaces," *Advanced Functional Materials*, vol. 21, no. 3, p. n/a-n/a, 2010.

[163] S. Wu, "Calculation of interfacial tension in polymer systems," *Journal of Polymer Science Part C: Polymer Symposia*, vol. 34, pp. 19-30, Mar. 1971.

[164] H. H. Kausch and M. Tirrell, "Polymer Interdiffusion," *Annual Review of Materials Science*, vol. 19, no. 1, pp. 341-377, Aug. 1989.

[165] A. N. Gent and G. R. Hamed, "Peel mechanics for an elastic-plastic adherend," *Journal of Applied Polymer Science*, vol. 21, no. 10, pp. 2817-2831, Oct. 1977.

[166] C. S. Litteken and R. H. Dauskardt, "Adhesion of polymer thin-films and patterned lines," *International Journal of Fracture*, vol. 119/120, no. 4-2, pp. 475-485, 2003.

[167] W.-S. Kim, I.-H. Yun, J.-J. Lee, and H.-T. Jung, "Evaluation of mechanical interlock effect on adhesion strength of polymer–metal interfaces using micro-patterned surface topography," *International Journal of Adhesion and Adhesives*, vol. 30, no. 6, pp. 408-417, Sep. 2010.

[168] C.-Y. Hui, N. J. Glassmaker, T. Tang, and A. Jagota, "Design of biomimetic fibrillar interfaces: 2. Mechanics of enhanced adhesion," *Journal of The Royal Society, Interface*, vol. 1, no. 1, pp. 35-48, Nov. 2004.

[169] A. Del Campo and C. Greiner, “SU-8: a photoresist for high-aspect-ratio and 3D submicron lithography,” *Journal of Micromechanics and Microengineering*, vol. 17, no. 6, p. R81-R95, 2007.

[170] a. N. Gent and G. L. Liu, “Pull-out and fragmentation in model fibre composites,” *Journal of Materials Science*, vol. 26, no. 9, pp. 2467-2476, 1991.

[171] C. Wang, “Fracture mechanics of single-fibre pull-out test,” *Journal of materials science*, vol. 32, no. 2, pp. 483–490, 1997.

[172] A. El Maachi, A., Sapieha, S., Yelon, “No,” *Nord. Pulp Pap. Res. J.*, vol. 14, pp. 17-22, 1999.

[173] A. El Maachi, A., Sapieha, S., Yelon, “No Title,” *J. Pulp Pap. Sci.*, vol. 21, p. J362-J366, 1995.

[174] E. Cheung and M. Sitti, “Adhesion of biologically inspired polymer microfibers on soft surfaces.,” *Langmuir*, vol. 25, no. 12, pp. 6613-6, Jun. 2009.

[175] J. Viventi et al., “A conformal, bio-interfaced class of silicon electronics for mapping cardiac electrophysiology.,” *Science translational medicine*, vol. 2, no. 24, p. 24ra22, 2010.

[176] H. Lee, B. P. Lee, and P. B. Messersmith, “A reversible wet/dry adhesive inspired by mussels and geckos.,” *Nature*, vol. 448, no. 7151, pp. 338-41, Jul. 2007.

[177] E. J. De Souza et al., “In vitro adhesion measurements between skin and micropatterned poly(dimethylsiloxane) surfaces.,” *Conference Proceedings of the International Conference of IEEE Engineering in Medicine and Biology Society*, vol. 2009, no. 0, pp. 6018-6021, 2009.